CATION DIFFUSION IN FLUORITE LATTICES

A thesis
presented for the degree of

DOCTOR OF PHILOSOPHY

in

THE UNIVERSITY OF LONDON

by

RICHARD JOHN HAWKINS B.A.(Cantab.)

Ceramic and Nuclear Materials Group,
Royal School of Mines,
Imperial College of Science and Technology.

February 1967.

Abstract

Volume diffusion coefficients have been determined for uranium -233 self-diffusion in stoichiometric and non-stoichiometric uranium dioxide, and for thorium -230 self-diffusion in thoria. Concentration profiles were determined by α-ray spectrometry. This method gave a point on the concentration curve every 0.1micron Thus it was possible to measure diffusion coefficients between about 10^{-15} and 10^{-12} $cm.^2 sec.^{-1}$ The effect of instrumental error on the concentration profile determined by α-ray spectrometry was investigated analytically.

A comparison of concentration profiles in single crystal and polycrystalline urania showed that grain-boundary diffusion occurred. An analysis of the poly-crystalline profiles in terms of a volume and grain-boundary diffusion part gave values for volume diffusion coefficients which agreed well with the single crystal results.

Pure, dry hydrogen or CO/CO_2 mixtures were used to maintain the composition of the urania. For U^{233} self-diffusion in urania;

UO_2(stoichiometric) (1477 - 1720°C)

$$D_{2.0} = 6.06 \times 10^{-7} \exp(-70{,}000/RT)\ cm^2 sec^{-1}$$

$UO_{2.01}$ (1400 - 1650°C)

$$D_{2.01} = 2.04 \times 10^{-3} \exp(-88{,}900/RT)\ cm^2 sec^{-1}$$

$UO_{2.03}$ (1400 - 1600°C)

$$D_{2.03} = 2.79 \times 10^{-2} \exp(-94{,}900/RT)\ cm^2 sec^{-1}$$

$UO_{2.10}$ (1400 - 1650°C)

$$D_{2.10} = 1.09 \exp(-105{,}000/RT)\ cm^2 sec^{-1}$$

$UO_{2.15}$ (1350 - 1550°C)

$$D_{2.15} = 6.79 \times 10^{-3} \exp(-80{,}900/RT)\ cm^2 sec^{-1}$$

The ratio of the grain-boundary coefficient to the volume diffusion coefficient was about 10^5 for all compositions.

The diffusion of uranium increased very rapidly for small departures from the stoichiometric composition

For x less than 0.1, at 1400°C,

$$\log D = 0.434 \log x - 13.31$$

The activation energy increased with increasing x (in UO_{2+x}) up to x = 0.1 after which it decreased again.

Thorium diffusion in thoria was measured in vacuo, hydrogen and air, but the partial pressure of oxygen had little effect on the cation diffusion. For Th^{230} volume diffusion in thoria, (1600°C to 2100°C)

$$D_{Th} = 1.25 \times 10^{-7} \exp(-58{,}800/RT) \text{ cm}^2\text{sec}^{-1}$$

Models for cation diffusion in urania and thoria were investigated and experimental observations could be explained quite well.

An attempt to correlate physical properties with self-diffusion coefficients in urania suggested that sintering and fission-gas release are closely related to oxygen diffusion rather than uranium diffusion.

List of Contents

		Page
1.	Introduction	8
1.1	General introduction	9
1.2	Thermodynamics and structure of UO_2, UO_{2+x} and ThO_2	10
1.3	Models for diffusion processes	20
1.4	Previous work on UO_2 and UO_{2+x}	25
1.5	Previous work on Th self-diffusion in ThO_2	33
2.	Alpha-ray spectrometry	34
2.1	Introduction	35
2.2	Alpha-ray spectrometry	36.
2.3	Calibration of the spectrometer	43
2.4	Check on the calibration	46
2.5	Effect of instrumental error on the concentration profile	51
3.	Experimental	54
3.1	Materials	55
3.2	Polishing	59
3.3	Cleaning the surface of the pellets	60
3.4	Plating the tracer	60
3.5	Diffusion anneals	65

		Page
4.	Analysis of results	77
4.1	Resolution of the spectrometer	78
4.2	The bound surface layer	79
4.3	Single crystal concentration profile	80
4.4	Polycrystal concentration profile	80
5.	Results	89
5.1	Stoichiometric UO_2	90
5.2	Polycrystal results	93
5.3	D_o and the activation energy	114
5.4	Dependence of D on p_{O_2} and x	115
5.5	D.S.A. results	119
5.6	Discussion of results and errors	119
5.7	Grain-boundary diffusion	126
5.8	Decrease in Surface Activity results	129
6.	General discussion	130
6.1	Other work on U self-diffusion in UO_2	131
6.2	Theories for cation diffusion in UO_{2+x} and ThO_2	139
6.3	Cation diffusion in UO_2 solid solutions	163
6.4	Self-diffusion in fluorite lattices and other oxides	165
7.	Relationship of diffusion to other physical properties in UO_2	170
7.1	Sintering	171
7.2	Creep	177

		Page
7.3	Grain growth in urania	178
7.4	Fission gas release from UO_2	180
7.5	Physical properties of ThO_2	183
8.	Conclusions	185
Appendix 1.	Grain-boundary diffusion	188
Appendix 2.	Range-energy relationship for α-particles in UO_2	191
Appendix 3.	Effect of instrumental error on the diffusion profile	197
Appendix 4.	Results	202
References		232
Acknowledgements		239

INTRODUCTION

1. INTRODUCTION

1.1.1 General Introduction Several determinations of cation diffusion in fluorite-type lattices have been made, viz. uranium dioxide,[1-5] calcia-stabilised zirconia[6-7] and calcium fluoride.[8,9] The fluorite-type oxides chosen for this study were UO_2, UO_{2+x} and ThO_2. The chemical and physical properties of uranium dioxide have been studied extensively,[10,11] but fewer measurements have been made on thoria.[12,13,14] Some of these properties such as creep, sinterability, grain growth and fission gas release may be related to diffusional processes within the solid.[15-21] A knowledge of both anion and cation diffusion in these oxides and their correlation with relevant physical properties could lead to a deeper understanding of the processes involved.

1.1.2 Uranium Dioxide Uranium dioxide is the most widely used uranium compound in the nuclear power field today, and is likely to be used in more and more reactors because of its good resistance to irradiation damage and its high melting point. A thorough knowledge of the chemical and physical properties of urania is essential for good reactor design. The fabrication of the fuel requires the sintering of a powder to form pellets. Creep, grain growth and the diffusion of

fission products are important factors in determining the life of a fuel element. Slight deviations from the stoichiometric composition in uranium dioxide can cause large changes in these physical properties[10,22-27] and the determination of diffusion coefficients in both stoichiometric and non-stoichiometric urania is essential.

1.1.3 Thoria Thoria, or a solid solution with UO_2, is used in nuclear reactors; the thorium being a fertile material. It is also used as a refractory material and as a solid state electrolyte when a few per cent of a second oxide is added to increase the ionic conductivity

1.2 Thermodynamics and Structure of UO_2, UO_{2+x} and ThO_2

A review of the crystal structure is presented in this section in order to define the system in which diffusion is occurring.

1.2.1 Phase diagram fro UO_2-Oxygen the range of non-stoichiometry of Uranium dioxide has been carefully studied over the past few years and the most probable phase diagram is given by Roberts[10,28] (Fig 1) for the hyperstoichiometric oxide. More recent work

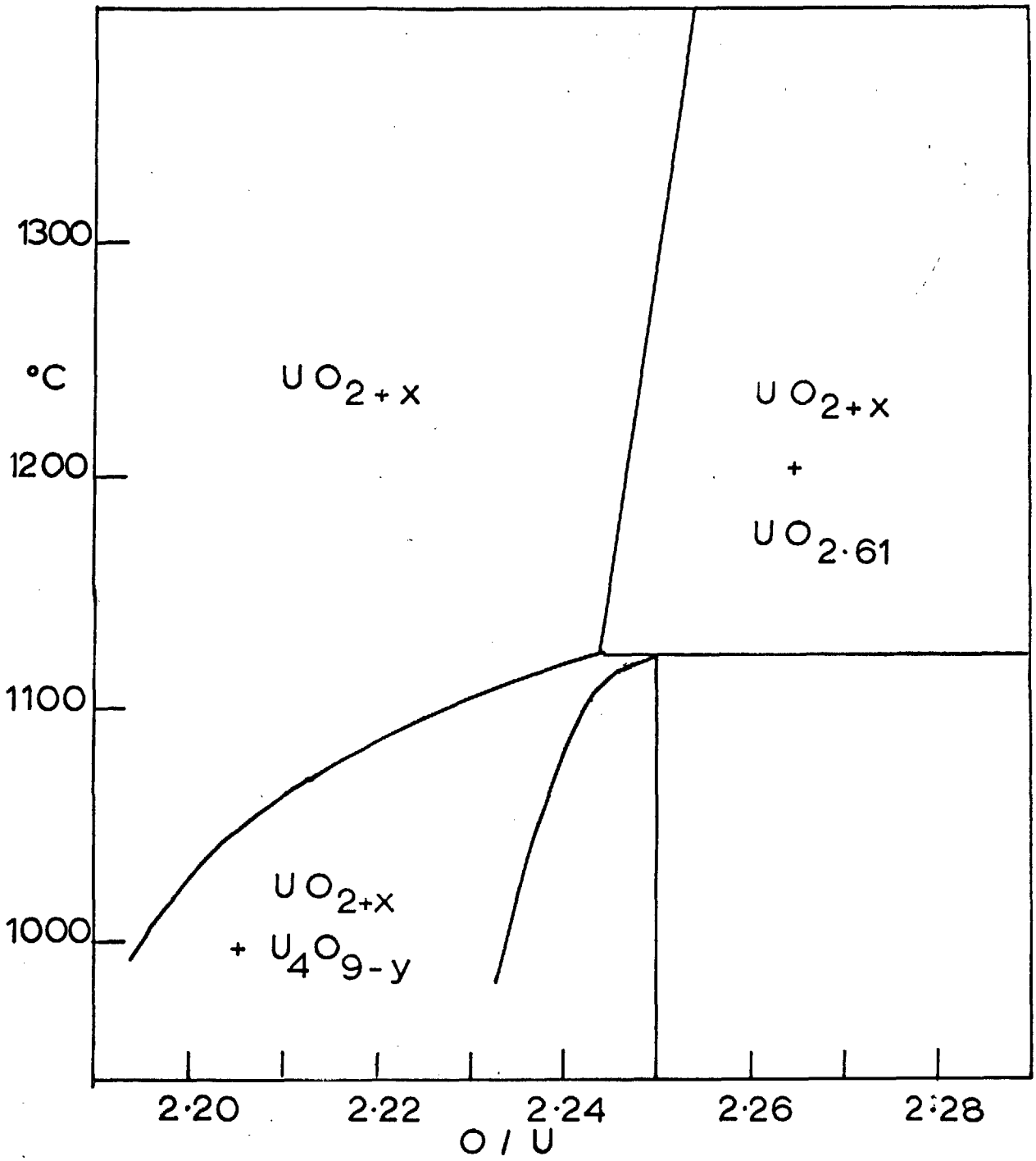


Fig. 1. Portion of UO_2-O_2 phase diagram showing limit of UO_{2+x} phase.[28]

has shown the existence of hypostoichiometric UO_{2-y}[29,30] but Amato et al.[31] have shown that organic additions (as binders) may determine whether or not there is excess uranium metal on quenching, so the position of the phase boundary is not yet clear.

1.2.2 Phase diagram for ThO_2-oxygen It is not certain whether thoria shows a range of composition or not. It has been reported that it may become slightly substoichiometric, but the analysis was of insufficient accuracy. Cohen et al.[32] maintain that hyperstoichiometric thoria does not exist. The Th^{4+} ion is very stable and compounds with thorium in a higher valence state are not known,[33] so the absence of hyperstoichiometric thoria is not surprising. However, Th^{3+} is known to exist and the possibility of a range of sub-stoichiometric thoria cannot be discounted.

1.2.3 Structure of UO_2 and ThO_2[11] The structure of UO_2 and ThO_2 has been confirmed by neutron diffraction studies at room temperature to be fluorite-type, (Fig 2), with isotropic thermal motion of the oxygen and metal ions. The rms displacements are 0.056Å for uranium and 0.074Å for oxygen. At higher temperatures the intensities of the neutron reflections deviate from those calculated for the fluorite arrangement assuming

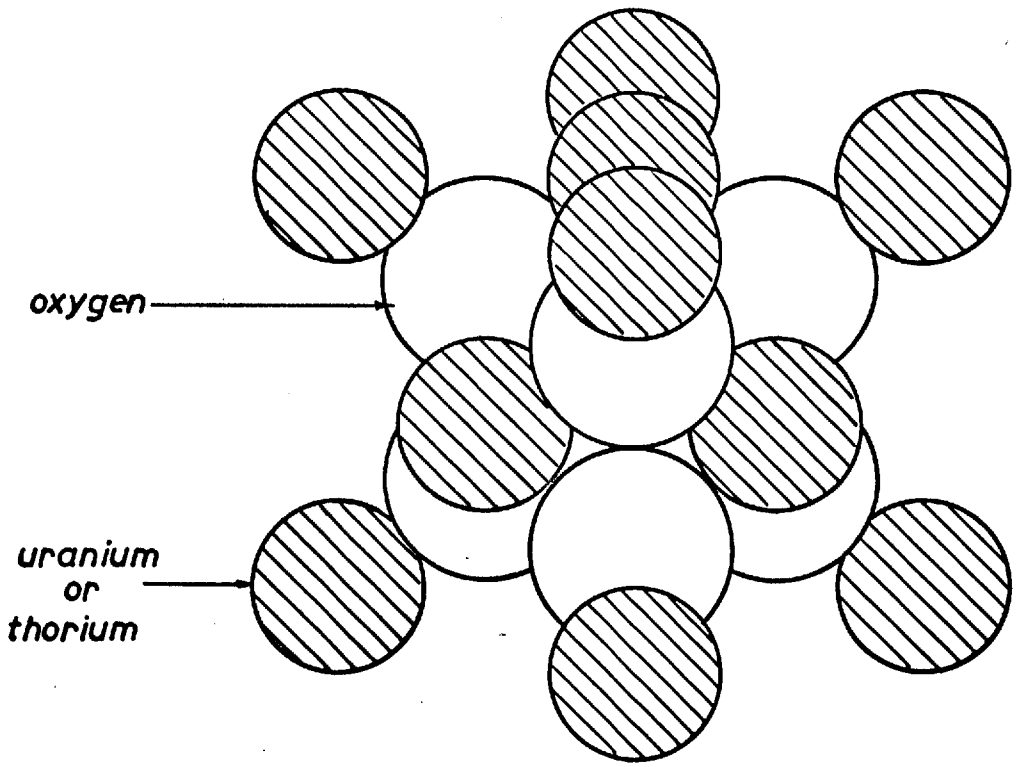


FIG. 2 THE FLUORITE STRUCTURE

isotropic thermal motion.[34] The differences can be allowed for by displacing the oxygen ions at random along the <111> directions to give a disordered structure or by allowing the oxygen to vibrate anisotropically across the normal fluorite position. At 1000°C Willis[34] gives the positions of oxygen as $(\frac{1}{4}+\delta, \frac{1}{4}+\delta, \frac{1}{4}+\delta)$, where $\delta = 0.016$ for UO_2 and $\delta = 0.014$ for ThO_2, with the uranium and thorium on normal sites. More recent work on CaF_2 by Willis and supporting work by Dolling et al., favours the interpretation in terms of anisotropic vibrations. The structure of UO_2 is considered to be uranium on normal lattice sites executing isotropic thermal motion with a mean-square amplitude given by

$$\overline{u_S^2} = 1.33 \times 10^{-5} T \ (\text{Å}^2) \text{ (above } 400^\circ\text{C)}$$

and the anisotropic vibration of the oxygen described roughly by four spheres which begin to separate along <111> as the temperature rises. At 1000°C the displacement of the spheres is about 0.15Å. In ThO_2 the displacement is slightly less.

1.2.4 Structure of UO_{2+x}[11] When oxygen dissolves in UO_2 to form UO_{2+x} the symmetry elements of the 'statistical cell' are the same as for UO_2. The extra atoms are distributed randomly and although some short range ordering may occur, no long range ordering

is possible. Neutron diffraction studies on $UO_{2.13}$ at 800°C[41] have yielded the atomic positions in the statistical cell and their occupation numbers (table 1).

Table 1

Crystal structure of $UO_{2.13}$ at 800°C[34]

Atom	Unit cell coordinates	Contribution to formula unit U_mO_n	Temperature factor B(Å)
U	000	m=1.00(0.01)	1.18(0.06)
O	uuu	n=1.82(0.02)	1.45(0.08)
O'	0.5vv	n=0.08(0.05)	1.8 (1.6)
O"	www	n=0.23(0.11)	7.5 (2.7)

u = 0.267 (0.001), v = 0.39 (0.01), w = 0.38(0.01)

Standard deviations of parameters in brackets.

$B = 8\pi^2 \overline{U_s^2} = \frac{8\pi^2}{3} \overline{U^2}$

where $\overline{U_s^2}$ = mean square displacement and $\overline{U^2}$ is <u>total</u> mean square displacement.

Models for the structure of UO_{2+x} have the U ions fixed at normal fluorite positions. Actually, the total rms displacement of the uranium ions is about 0.212Å in $UO_{2.12}$ at 800°C which is slightly greater than that (0.185Å) for UO_2 at the same temperature. This difference can be accounted for either by a random displacement of the U ions of about 0.1Å from

their normal positions, or by displacing a few ions large distances to give an average displacement of 0.212Å. So far, all attempts to produce a model for the structure of UO_{2+x} with the U ions displaced have been unsuccessful.

There are three types of defects in the oxygen sublattice; normal lattice sites, O, with an apparent displacement to $(\frac{1}{4}+\delta, \frac{1}{4}+\delta, \frac{1}{4}+\delta)$ ($\delta = 0.017$) of which probably five to eight per cent are empty (c.f. UO_2 where all are occupied); interstitial oxygen, O' and O". The hole at $(\frac{1}{2},\frac{1}{2},\frac{1}{2})$ is not occupied; instead two kinds of interstitial site exist. One (O') is half-way along the line joining $(\frac{1}{2},\frac{1}{2},\frac{1}{2})$ to the centre of the line joining two nearest normal oxygen lattice sites, and the other (O") is half-way along the line joining $(\frac{1}{2},\frac{1}{2},\frac{1}{2})$ to a normal oxygen. The interstitial atoms are about 1Å from the nearest hole. These three defects cannot be distributed completely at random as this would inevitably bring some oxygens too close together, so the results in Table 1 are interpreted in terms of the formation of defect zones.[35] The relative concentrations, normal O vacancies: O' ions: O" atoms is given experimentally as 13: 8: 16: An idealized model considers the ratios as 2: 1: 2 where an oxygen ion enters the lattice at an O' site ejecting two normal oxygens to O" sites. However, this model does not give

the correct absolute concentrations of the defects. For $UO_{2.12}$ this model predicts $UO_{1.76}$ $O'_{0.12}$ $O''_{0.24}$ whereas Table 1 gives $UO_{1.87\pm0.03}$ $O'_{0.08\pm0.04}$ $O''_{0.16\pm0.06}$. The errors in the occupation numbers are high but the discrepancy between 1.76 and 1.87 for normal oxygen vacancies cannot be explained in this way.

Figure 3 shows a 2:2:2 model where an extra O' oxygen is included in the lattice. The predicted formula $UO_{1.88}$ $O'_{0.12}$ $O''_{0.12}$ is in good agreement with the observed formula.

Roberts and Markin consider the structure of UO_{2+x} to consist of small zones of U_4O_9, the model being essentially the same as that shown in Figure 3.

This has some support through electron diffraction work by Steeb et al.,[35] which established a unit cell of $U_{64}O_{140}$ in $UO_{2.19}$ single crystal material in the temperature range 250 - 600°C. Nagels et al.,[36] found evidence of U_4O_9 in $UO_{2.007}$ to $UO_{2.17}$, but this work was at room temperature and U_4O_9 would have precipitated out. They found the solubility limit of oxygen in UO_2 at room temperature to be $UO_{2.001}$, but there was no evidence of U_4O_9 zones. Further support for U_4O_9 zones arises from neutron diffraction studies on U_4O_{9-y}.[37]

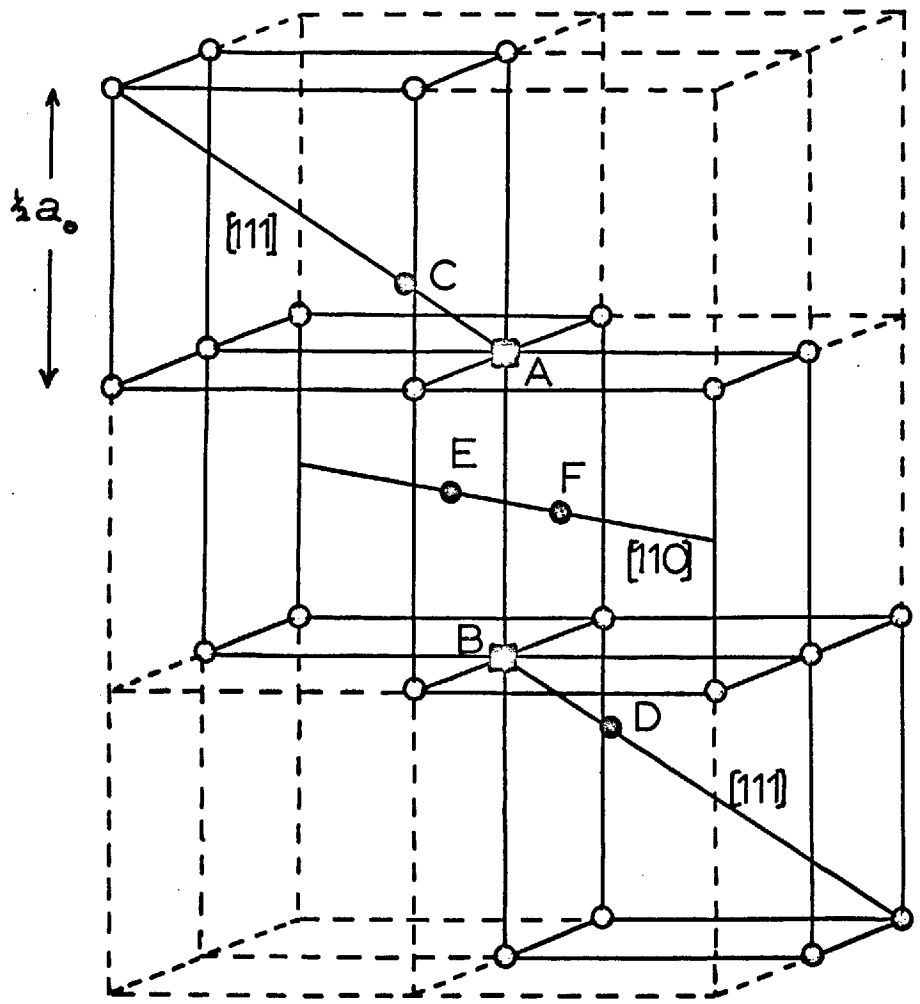


Fig. 3. Structure of UO_{2+x}

2:1:2 model. Interstitial O′, enters at E displacing normal oxygen at A and B along [111] to O″ positions, C and D.

2:2:2 model. O′ at E and F, O″ at C and D.

The oxygens in the composite cell occupy exactly the same kinds of position as oxygen in the UO_{2+x} statistical cell.

Besides the fundamental reflections for the composite cell, there are also superlattice reflections on X-ray, electron and neutron diffraction patterns which indicate that displacements of uranium, and probably oxygen too, take place. These displacements have not yet been determined.

1.2.5 Defects on the cation sublattice in UO_{2+x}

The exact nature of the defects on the cation sublattice needs to be known in order to obtain a model for the diffusion process. Dawson et al.,[38] and Arrott et al.,[39] reported U^{6+} ions in UO_{2+x} from magnetic susceptibility measurements. Using the same method, Haraldsen et al.,[40] reported U^{5+}. Roberts et al.,[41] postulated U^{5+} for the zones of U_4O_9 in UO_{2+x} which is well supported in that a U^{6+} - O distance would be 2.07 to 1.9Å. Aronson[910] required U^{5+} ions for a good fit of electrical conductivity measurements with theory and this is supported by Roberts et al.,[41] and Hoch[42]. Thus, it is probable that U^{5+} exists in UO_{2+x}, but the exact positions of these ions are not known.

The defects on the cation sublattice in ThO_2 are probably interstitials and vacancies defined by Frenkel and Schottky products.[43]

1.3 Models for diffusion processes The driving force for diffusional processes is a decrease in chemical potential, the direction of movement being down the activity gradient. In self-diffusion studies the movement can be described by Fick's first law:

$$J = -D \frac{\partial c}{\partial x} \quad \text{(for steady-state conditions)}$$

D = diffusion coefficient;

J = flux;

$\frac{\partial c}{\partial x}$ = concentration gradient

and for non-steady-state conditions Fick's second law applies:

$$\frac{\partial c}{\partial t} = D \frac{\partial^2 c}{\partial x^2}$$

1.3.1 Solutions of the diffusion equation

Solutions of Fick's equations are readily available for various boundary conditions.[44-47] The conditions obtaining in this series of experiments approximate to diffusion from an instantaneous source into a semi-infinite medium. For these boundary conditions the concentration at a depth x after a time t, is given by

the well-known equation,

$$C(x,t) = \frac{C_o}{\sqrt{\pi Dt}} \exp\left(\frac{-x^2}{4Dt}\right) \qquad -(1)$$

(C_o = initial concentration in the layer)

This equation applies only to a single mechanism of diffusion.

In polycrystalline material some account must be taken of diffusion down grain boundaries. Several solutions, with various approximations, for diffusion into a polycrystal from a surface layer maintained at a constant composition are available,[48-51] but only one solution for diffusion from an instantaneous source into an idealized polycrystal has been found (Suzuoka[52]). The average concentration at a depth x is given by,

$$c(x,t) = \frac{K}{\sqrt{\pi Dt}} \exp\left(\frac{-\eta^2}{4}\right) + \frac{K}{b\sqrt{\pi}} \int_1^{\Delta} \left((\eta^2/\sigma)-2\right) \times \left(\exp\left(\frac{-\eta^2}{4\sigma}\right)\right) \sqrt{(\Delta-\sigma)/(\Delta-1)} \left(\frac{-X^2}{\sqrt{\pi}} - X \operatorname{erfc} X\right) \frac{d\sigma}{\sigma^{3/2}} \qquad -(2)$$

(where $X = \sqrt{\frac{\Delta-1}{\Delta-\sigma}} \cdot \frac{\sigma-1}{\beta}$;

K = amount of diffusant per unit area in instantaneous source;

$\eta = x/\sqrt{Dt}$;

$2b$ = mean linear dimension of grain;

$\Delta = D_b/D$;

$\beta = 2a(\Delta-1)/\sqrt{Dt}$;

$2a$ = thickness of grain boundary, assumed to be 5Å).

Another solution, which appears to be slightly more complicated than Suzuoka's, is shortly to be published by Wuttig et al.[53]

1.3.2 Determination of diffusion coefficients

A review of methods for determining diffusion coefficients when diffusion is taking place from an instantaneous source into a semi-infinite medium is given here. Cation diffusion coefficients are known to be small in UO_2[1-5] so that the method must be applicable to small penetration depths.

1.3.3 Decrease in Surface Activity method[54] (D.S.A)

This is only applicable if there is no grain boundary diffusion. The relative activities (concentrations) down to a fixed depth are measured before and after a diffusion anneal and, depending on the counting geometry, the results are expressed as in equations 3 and 4, (derived from equation 1).

For '2π' counting [1]

$$\frac{A}{A_o} = \text{erf } E - \frac{1}{E\sqrt{\pi}}\left(1 - \exp\left(-E^2\right)\right) \qquad (3)$$

($E = R/2\sqrt{Dt}$, where R = range of α-particles)

Collimated count,

$$\frac{A}{A_o} = \operatorname{erf}\frac{R}{2\sqrt{Dt}} \qquad (4)$$

The method is applicable to very small diffusion coefficients and is non-destructive, but very large errors can result from loss of tracer by evaporation or from the effects of a bound surface layer.[55]

1.3.4 Determination of the concentration profile

The advantage of defining the concentration profile is that both volume and grain boundary diffusion can be detected.

a) Sectioning This method is only good when the penetration depth is large compared to the slices which are removed. This is not the case in UO_2[2,3,5] where it is very difficult to remove thin parallel slices. The method is destructive.

b) Alpha-ray spectrometry Alpha-particles have a limited range in matter[56] and the residual energy of an α-particle emitted from a solid can be related to its depth of origin within the solid.

McNamara[1] used a '2 π' counting geometry in his α-ray spectrometer, but the spectrum did not give the concentration profile directly. An equation (equation 1) had to be assumed for the diffusion process and the

α-particle spectrum was calculated for various values of Dt.

In later work McNamara made collimated counts on diffused samples to obtain the concentration profile directly. Alcock et al.,[57] including some of the work from this thesis, and Schmitz[58] have also used α-ray spectrometry to determine concentration profiles in UO_2.

The effective "slice thickness" in α-ray spectrometry can be made extremely small (e.g. 0.03 to 0.1μ) depending on the amplification of the spectrometer and the activity of the tracer. The method is non-destructive, so complete concentration profiles can be obtained for different times of diffusion anneal with the same specimen.

1.3.5 Determination of D and D_b from the concentration profile

For single crystal material only volume diffusion is expected and a plot of 'log (activity)' versus 'x^2' will give D from equation 1.

Suzuoka's model for diffusion in polycrystals shows that near the surface the grain boundaries can act as sinks, and at large penetrations 'log (concentration)' versus '$x^{6/5}$' is linear. Tables of values for the grain boundary contribution to the diffusion process are available,[52, Appendix 1] and for the range of grain

sizes and expected D_b (grain boundary diffusion coefficient) in polycrystalline UO_2 and ThO_2 the gradient of 'log C' versus 'x^2' down to a depth of $3\sqrt{Dt}$ should give D (volume diffusion) to 10-15%[52]

D_b is found in the equation,

$$0.973 \log (\Delta - 1) = 6.567 - 1.644 \log \gamma - \log \sqrt{Dt} \quad (5)$$

(where $\Delta = D_b/D$;

$\gamma = -\partial \log C / \partial (x^{6/5})$)

1.4 Previous work on UO_2 and UO_{2+x} A full critical analysis of previous results is being witheld until values for volume and grain boundary diffusion have been established.

The methods used by previous workers include the decrease in surface activity method (D.S.A.), sectioning and α-ray spectrometry. In no instance is there good agreement between different sets of results.

1.4.1 D.S.A. method The decrease in surface activity method has been used by McNamara,[1] Auskern and Belle,[2] and Lindner and Schmitz[3] for cation self-diffusion in urania under a hydrogen atmosphere

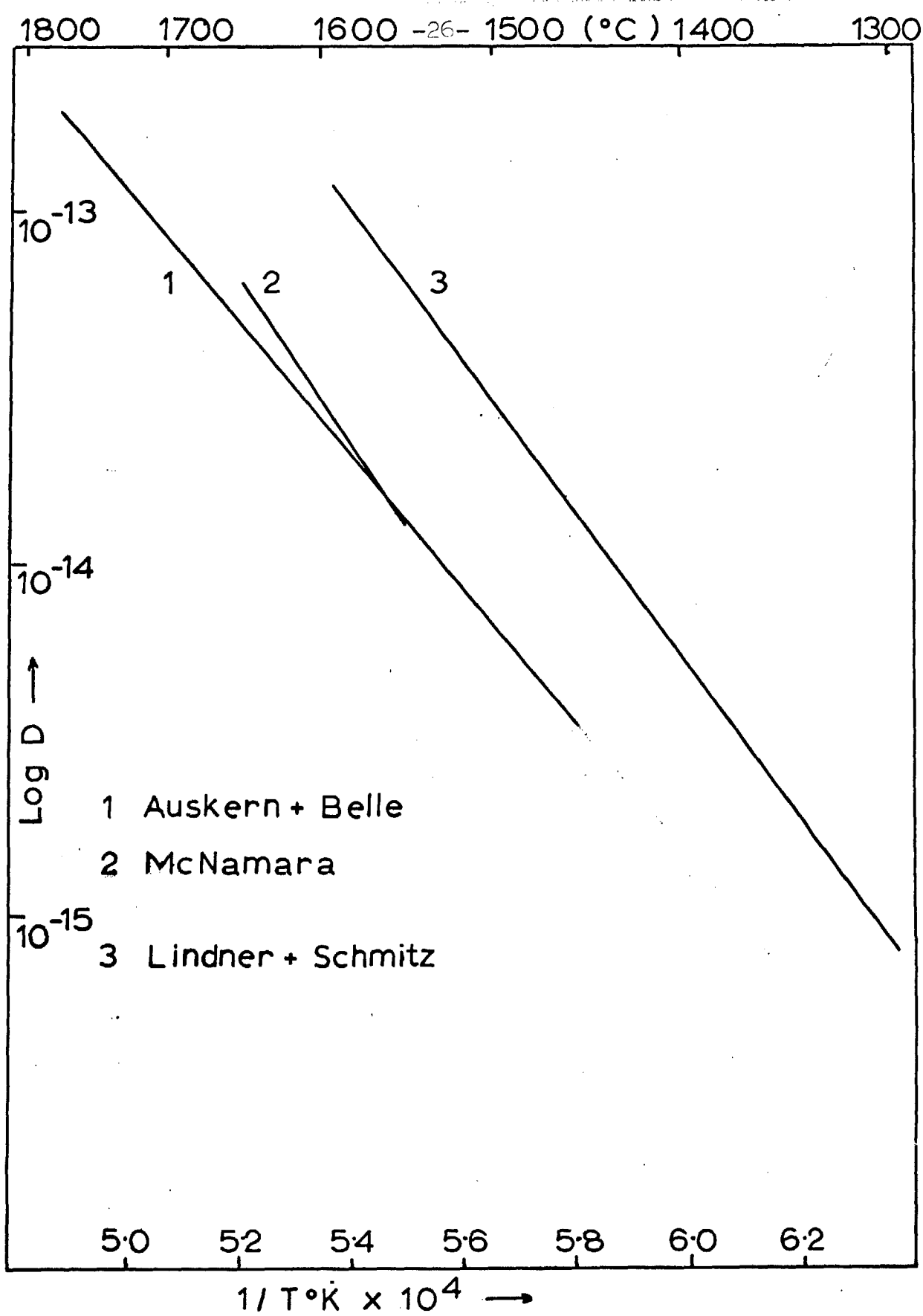


Fig. 4. Decrease in Surface Activity results for U-diffusion in stoichiometric UO_2.

These results are shown in Figure 4. It can be seen that there is only fair agreement between the three sets of measurements. Both Auskern and Belle, and McNamara, used diffusion couples, whereas Lindner and Schmitz did not use pellets face to face. The higher results of the latter workers could be explained by higher evaporation losses. All three sets of experiments were performed on polycrystalline material and grain-boundary diffusion could explain the scatter in the results. A decrease in the value of D with time would be expected if grain boundary diffusion were present and Auskern and Belle showed a slight decrease in their experiments, but because of a large experimental error this was not taken to be significant.

Equations for D are,

McNamara, $D = 0.12 \exp(-108{,}000/RT)\ cm^2.sec.^{-1}$

(the pre-exponential factor is 1.2 in reference 1 but this should be 0.12 to give a better fit with experimental results.)

Auskern and Belle,

$$D = 4.3 \times 10^{-4} \exp(-88{,}000/RT)\ cm^2.sec.^{-1}$$

$$(Q = -88 \text{ kcal } \pm 11)$$

Lindner and Schmitz,

$$D = 0.23 \exp(-104{,}000/RT)\ cm^2.sec.^{-1}$$

$$(Q = -104 \text{ kcal } \pm 7)$$

Because of the many sources of error these results must be used with caution. Little significance can be attached to the pre-exponential factor and the activation energy if two mechanisms of diffusion are responsible for movement of the tracer. However, the value of D obtained from these equations can be useful if considered as an 'effective' diffusion coefficient in that particular polycrystalline sample.

1.4.2 Sectioning Methods Auskern and Belle, Lindner and Schmitz, and recently Yajima et al,[59] performed sectioning experiments to find concentration profiles in polycrystals of UO_2. Lindner and Schmitz claimed good agreement with the D.S.A. diffusion coefficient. This could be explained either by a large error in the range of the α-particles or by grain-boundary diffusion.

Nagels et al.,[5] recently published results on sectioning experiments in single crystals UO_2. Any sectioning experiment is difficult in UO_2 when such thin layers have to be removed and this work is probably the most significant. However, the diffusion anneals were carried out in a vacuum furnace and there is some possibility that the material was not at the stoichiometric composition. A further discussion of this work will be made in the light of the present work on UO_{2+x}.

Yajima et al.,perfommed experiments at very high temperatures in order to obtain a large penetration of the tracer. In this instance, the sectioning work can be quite accurate, but the stoichiometry of the urania was not fixed in these experiments (see Discussion).

1.4.3 Alpha-ray spectrometry results McNamara and Schmitz have determined concentration profiles in polycrystalline UO_2. The slope of 'log C' versus 'x^2' (equation 1) well away from the surface of the pellets, gave results in agreement with D.S.A. measurements. However, McNamara also determined the concentration profile after diffusion into a single crystal and this led to a diffusion coefficient 10 times smaller than that in polycrystalline material at the same temperature. All the concentration profiles in polycrystals showed a steep section near the surface. An analysis of this part of the profile gave a value of D close to the single crystal value. The fact that 'log C' versus 'x^2' is a straight line is not indicative of the absence of grain boundary diffusion.[1,52,61,62]

Marin and Michaud[63] used α-ray spectrometry for diffusion in UO_2 and they reported a value of D of about $5 \times 10^{-16} cm^2.sec.^{-1}$ at 1700°C (c.f.D.S.A. work gives about $10^{-13} cm^2.sec.^{-1}$). This result will be discussed in the light of the present work.

1.4.4 Evidence for grain boundary diffusion in UO_2

a) McNamara showed direct evidence of grain boundary diffusion in stoichiometric UO_2 and an analysis following Fisher's model gave $D_b/D = 10^5$ (McNamara gave $D_b/D = 20$; but this was due to an error in measuring the slope of 'log C' versus 'x').

b) Belle and Lustman's sectioning experiment showed a tail probably due to grain boundary diffusion (Fig.5). Again $D_b/D = 20$ was given, but the analysis was wrong. It appears that the diffusion coefficients were calculated from the two portions of the 'log C' versus 'x^2' plot, D being determined from the steep slope near the surface and D_b from the shallower slope using equation 1. This assumes two completely independent mechanisms for two diffusion processes from an instantaneous source into a semi-infinite medium.

If the two processes did follow the same equations as apply to purely volume diffusion[64] then the problem would be one of diffusion into a composite medium.[44] On the other hand, if the second section of the concentration profile is taken to be grain-boundary diffusion and Fisher's model is assumed then, $D_b/D = 5 \times 10^6$ approximately (at 1615°C).

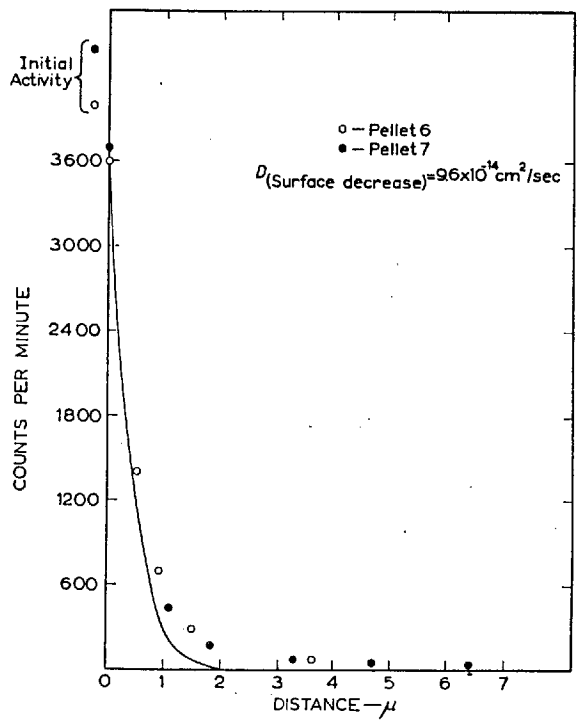


Fig. 6. Activity profile. The solid line is the calculated profile based on the surface decrease D.

Auskern and Belle[2]

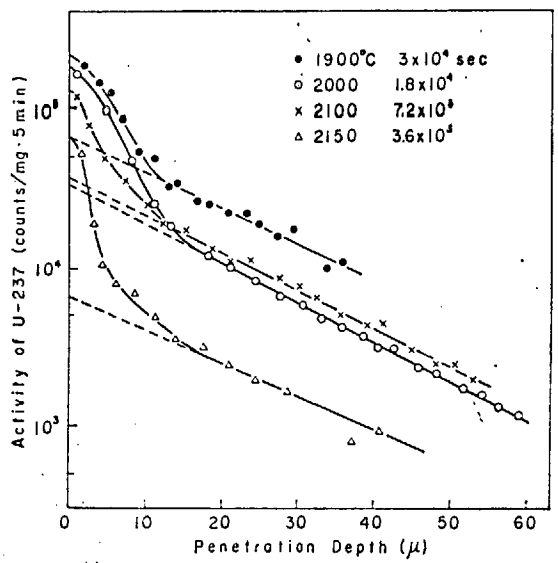


Fig. 5. Penetration curve.

Yajima et al.[59]

Fig. 5. Grain-boundary diffusion in UO_2.

c) Yajima et al.,[59] interpreted their concentration profiles in terms of a volume diffusion part near the surface and a grain-boundary diffusion part farther in (Fig.5). These results give strong support to the existence of U grain-boundary diffusion in UO_2.

d) Schmitz[58] reports that the grain boundaries quickly fill up with tracer and remain at a constant concentration. This would only be correct if the initial surface layer were so anisotropic that no surface diffusion or volume diffusion could take place to fill up the boundaries as they gradually became depleted by diffusion of the tracer away into the grains.

1.4.5 Cation diffusion in UO_{2+x} Marin and Michaud[65] show that diffusion is probably enhanced in non-stoichiometric urania. The only values of D reported for cation diffusion in non-stoichiometric urania are those of Lindner and Schmitz[3]. However, the diffusion anneals were carried out under an argon atmosphere, and assuming this to have the same oxygen content at all temperatures, the value of x in UO_{2+x} would change depending on which non-stoichiometric composition was in equilibrium with the fixed oxygen partial pressure at the temperature of the anneal.

(A D.S.A. method was used to measure D). The significance of this work is to demonstrate an increase in D when urania becomes non-stoichiometric.

1.5 Previous work on Th self-diffusion in ThO_2

Tentative results have been reported for Th^{230} diffusion in $Th^{232}O_2$.[12] Diffusion anncals were performed on polycrystalline material with a grain size about 10 to 20 microns. The results showed considerable scatter, giving an activation energy of 37.8 kcal.mole^{-1}; $D = 10^{-11} cm^2 sec^{-1}$ at 1400°C in air. Considerable grain-boundary diffusion was indicated.

ALPHA-RAY SPECTROMETRY

2 ALPHA-RAY SPECTROMETRY

2.1 Introduction It can be assumed that α-ray particles emitted from the surface of UO_2 with the same residual energy have originated at the same depth below the surface.[1] For a collimated count, all α-particles with residual energies between E and E+ ΔE will have originated in a slice of thickness Δr at a depth r below the surface (Figure 6). The number of α-particles with energies E to E+ ΔE will be proportional to the concentration of the tracer in the slice. If the α-particle energies are sorted with a multichannel pulse analyser then the count in successive channels will give a concentration profile since this corresponds to counts from successive slices in the pellet.

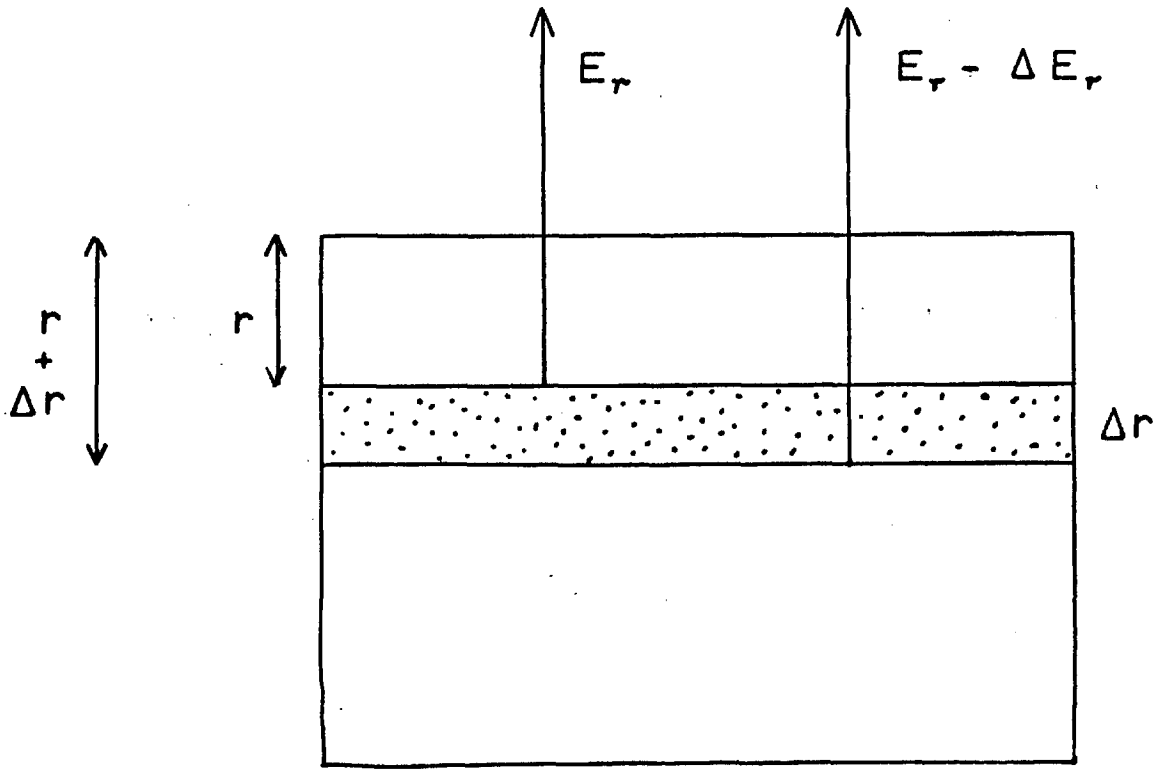
An empirical method of calibration was established which was independent of the α-particle range-energy relationship in matter. Several checks on the calibration were possible.

The effect of "instrumental error" on the concentration profile was investigated analytically. The instrumental error in the α-ray spectrometer produced a Gaussian spread for a monoenergetic source instead of a count in one channel only.

2.2 Alpha-ray spectrometer It is difficult to obtain a good collimated count with an ionisation chamber, since a micro-mesh grid must be placed over the sample to achieve collimation so cutting down the activity.[1] The use of a solid-state detector[65,66] enables the whole of the surface of the diffused sample to contribute to a collimated count. The counting apparatus (Figure 7) consists of a solid-state detector, at a fixed distance from the radioactive source, contained in a light-proof, vacuum-tight chamber. The detector is sensitive to light, and a vacuum is required because of the limited range of α-particles in air. A vacuum of 50 microns is adequate for a source to detector distance of about 3 cm., the pressure limit depending on the amplification of the spectrometer and the energy change per channel. An oil vapour trap consisting of copper gauze in a U-tube[67] was found to be adequate to prevent contamination of the sensitive surface of the detector.

The solid-state detector consisted of a single crystal of n-type silicon on which had been formed a p-type surface layer. A very thin gold film formed an electrical contact to the p-type layer and a second contact was made to the back of the slice. The application of an e.m.f. across the p-n junction causes

Concentration in a slice of a pellet:



Display on 100-channel pulse analyser:

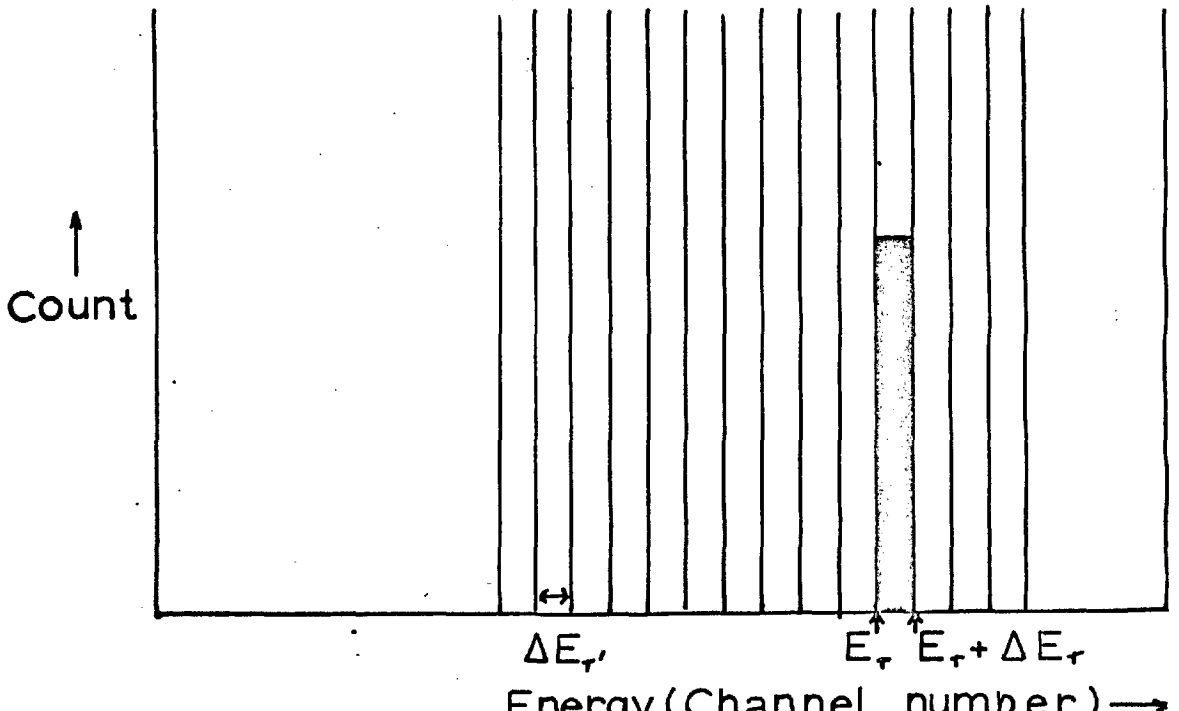


Fig. 6. Alpha-ray spectrometry.

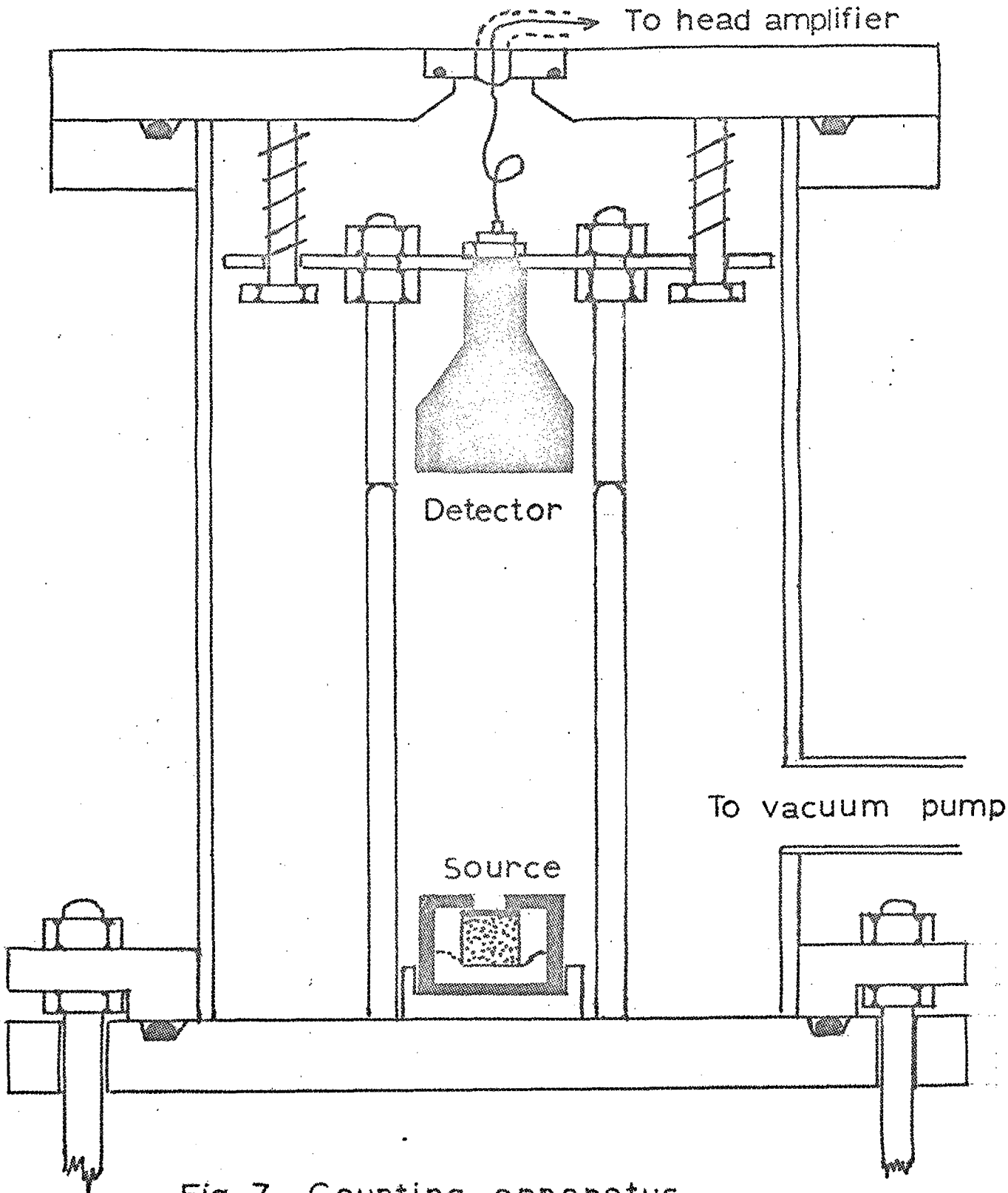


Fig. 7. Counting apparatus.

the charge carriers to separate forming a depleted zone. The passage of ionising radiation through this depleted region forms electron-hole pairs which are collected under the influence of the electrical field and produces a pulse proportional to the energy of the incident radiation. This pulse can be amplified and fed to a 100 channel pulse analyser.

The detector used for this work was an Elliot type SRD 1. This was operated at 100 V bias from a 1786 D power unit. The pulses from the detector were fed into a pre-amplifier (I.D.L.type 652; Rise time = Fall time = 1 μsec; Attenuation = 22db) and eventually to a multichannel pulse analyser (1363D) (normal settings: Back-bias = 22V; Channel width = 0.33 V). A standard weightless U-233 source (4.816 MeV (83.5%); 4.773 MeV (14.9%)) was used to measure the resolution of the spectrometer. The width of half the peak height was 80 keV. (The resolution was nominally 50 keV for an SRD 1 type detector).

2.2.1 The counting geometry The sensitive area of the detector was about 0.6 inches in diameter and the diameter of the largest diffused samples counted was about 0.25 inches.

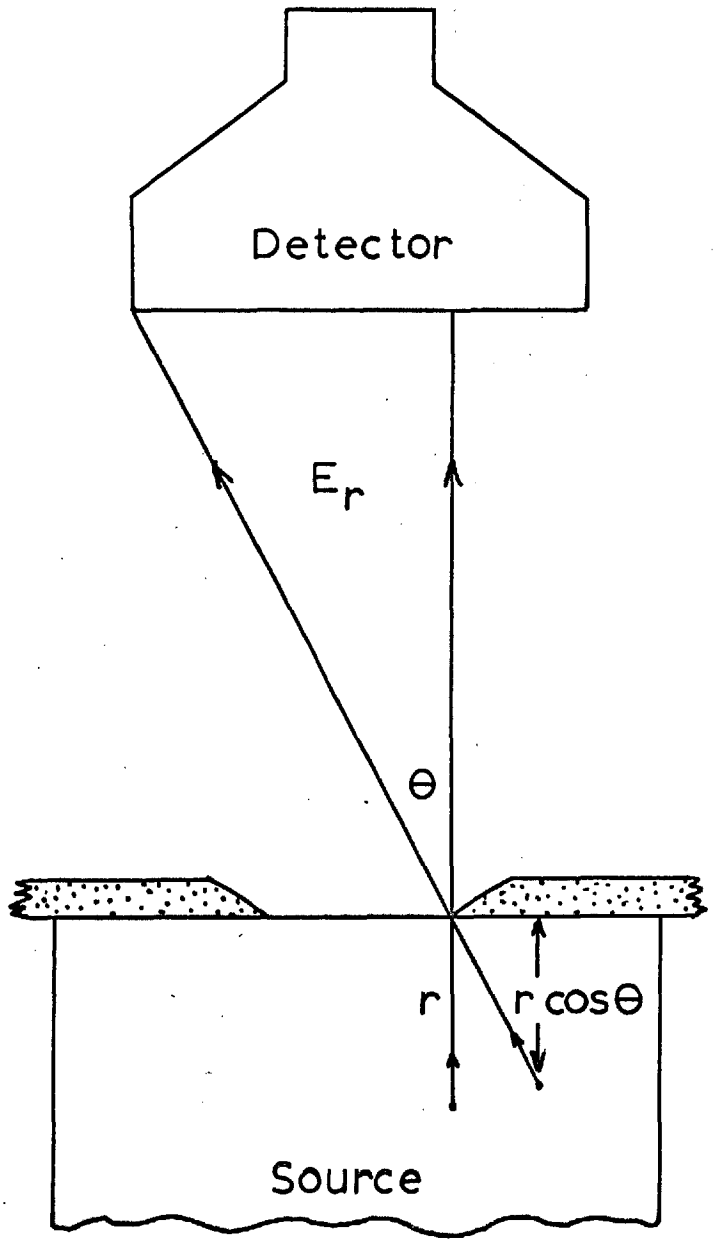


Fig. 8. Variation in depth for an α-particle of energy E_r.

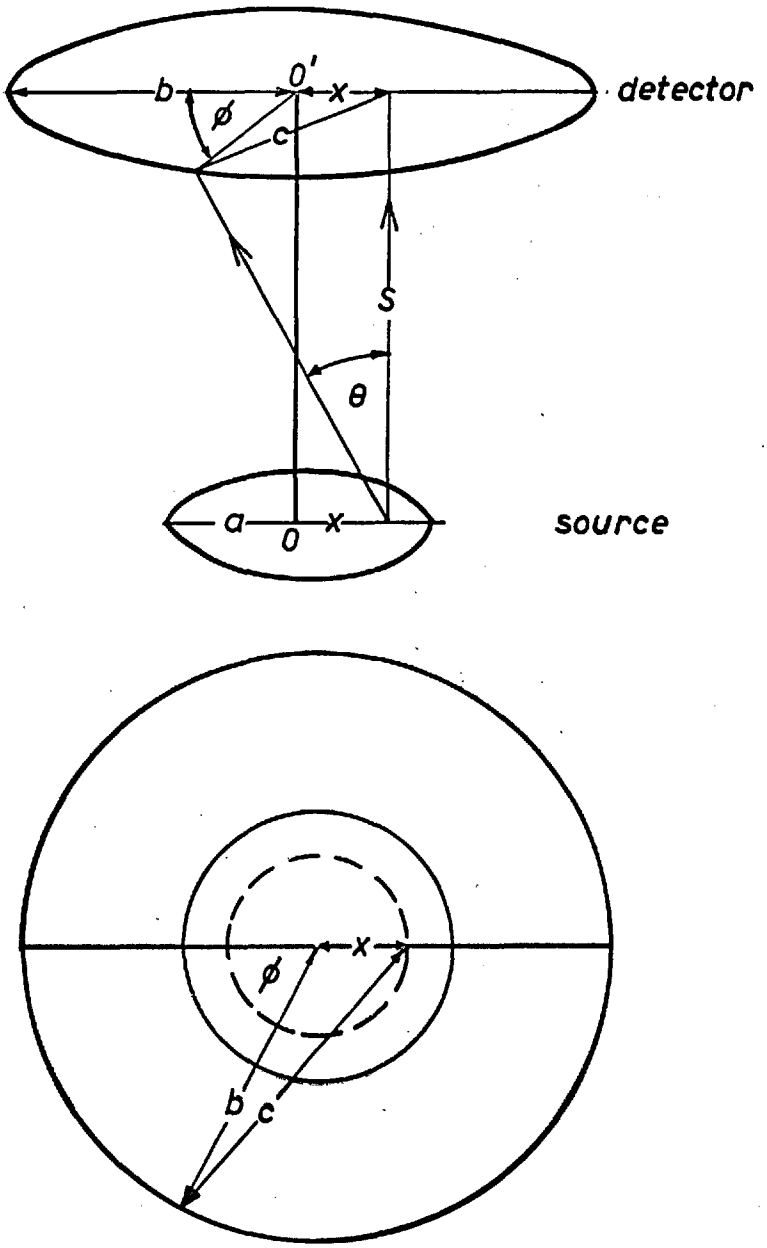


FIG. 9 DETERMINATION OF AVERAGE VALUE OF cos θ

Consider Figure 8. The greatest difference in depth of origin for α-particles with the same energy impinging on the detector is $r - r \cos\Theta_x$. For this difference to be 5% of r, d = 1.31 inches. For a 1% difference d = 3.02 inches. When d = 3 inches the activity was very low because of the severe collimation, so a position of d = 1.4 inches was used most often for counting.

Since the α-particles are not perfectly collimated, the depth below the surface of the source corresponding to a certain energy will in most cases be smaller than that for a collimated count (Fig.8). For the standard counting position this difference could be as much as 5%, so the average depth of origin for an α-particle of energy E_r was worked out.

From Figure 8 the depth of origin of an α-particle is,

$$r \cos\Theta$$

The average depth of origin for energy E_r is,

$$r \overline{\cos\Theta}$$

where $\overline{\cos\Theta}$ is the average value of $\cos\Theta$ for all α-particles with energy E_r.

Consider Figure 9, $\overline{\cos\Theta}$ is given by,

$$\overline{\cos\theta} = \frac{\int_0^a 2\pi x.2.\int_0^{\pi}\int_0^{\theta^{max}} \cos\theta\, d\theta\, .d\phi\, .dx}{\int_0^a 2\pi x.2.\int_0^{\pi}\int_0^{\theta^{max}} d\theta\, .d\phi\, .dx}$$

4π cancels in the numerator and denomiinator, and we have on integrating once,

$$\overline{\cos\theta} = \frac{\int_0^a x.\int_0^{\pi} \sin\theta^{max}\, d\phi\, dx}{\int_0^a x.\int_0^{\pi} \theta^{max}\, d\phi\, dx}$$

$$\overline{\cos\theta} = \frac{\int_0^a x.\int_0^{\pi}\sqrt{\frac{b^2+x^2+2bx\cos\phi}{b^2+x^2+S^2+2bx\cos\phi}}\, d\phi\, dx}{\int_0^a x.\int_0^{\pi} \tan^{-1}\left(\frac{\sqrt{b^2+x^2+2bx\cos\phi}}{S}\right) d\phi\, dx}$$

This was evaluated graphically by plotting

"$\sqrt{\frac{b^2+x^2+2bx\cos\phi}{b^2+x^2+S^2+2bx\cos\phi}}$" vs. "$\phi$" (0 to π) for various x (0 to a), finding the area A_x, and plotting "xA_x" vs. "x" to give the double integral in the numerator; and similarly for the denominator, (a = 0.125; b = 0.3; S = 1.4 in.).

Thus, $\overline{\cos\theta} = 0.995$

giving that the average value of the depth for an α-particle energy E_r is 0.995r.

The error in r is only important when the collimation is not good. Here, the error introduced into D is about 1% which is negligible compared to other sources of error.

2.3 Calibration of the spectrometer Previous workers[1,58] have assumed a linear range-energy relationship for α-particles in UO_2, and linear amplification of the pulses. An empirical method of calibration has been developed which is applicable to any range-energy (energy-channel number) relationship for α-particles in matter.

2.3.1 Calibration For a homogeneous source with a constant concentration of an α-emitter, N atoms per cc., the total count from the surface down to a depth r within the source must be,

$$C_r = \frac{\omega}{4\pi} Ar \quad N \lambda t \qquad -⑥$$

where ω = solid angle (small) over which the count is taken;

t = time of counting;

A = area of source;

λ = radioactive constant.

Re-arranging equation 6;

$$r = \frac{4\pi}{\omega} \frac{C_r}{AtN\lambda} \qquad -⑦$$

For a standard weightless source of the same area as the homogeneous source we have,

$$\frac{C_\omega}{C_{4\pi}} = \frac{\omega}{4\pi} \qquad -⑧$$

(where $C_{4\pi}$ is the '4 π' count for the standard source and C_{ω} is the count over a solid angle ω, i.e. in the fixed position in the counting chamber.)

Knowing A, t, N and λ and using equations 7 and 8, values of C_r, corresponding to channel K_r, can be determined to give r. A graph of 'r' versus 'channel number' can be plotted.

This method of calibration automatically allows for the efficiency of the detector (normally 98%[68]), and other effects, such as back-scatter, which are assumed to be the same for a homogeneous and a weightless source. The value of 'r' is the average value as obtained in section 2.2.2.

2.3.2 A simplification in the calibration for UO_2

Consider two homogeneous sources, one consisting of U^{238} and U^{234} in radioactive equilibrium and one enriched with U^{233} (0.1% was actually used). Let the counts from these two sources be $C_{238/234}$ and $C_{238/234/233}$ in the same time and for the same area. Then, from equation 6;

$$\frac{C_{233}}{C_{238/234}} = \frac{(N\lambda)_{233}}{2(N\lambda)_{238}}$$

(where $C_{233} = C_{238/234/233} - C_{238/234}$)

$$\text{so } (N\lambda)_{233} = \frac{C_{233}}{C_{238/234}} \times 2(N\lambda)_{238} \qquad (9)$$

N_{238} can be calculated from the density of the pellets and λ_{238} is known. Thus $(N\lambda)_{233}$ can be found and used directly in equation 7. This was found to agree exactly with the enrichment figure, and the known value of λ_{233}.

2.3.3 Calibration for ThO_2 The calibration for thoria was taken directly from the calibration for urania. Values for the change in energy with distance in UO_2 and ThO_2 were available for several α-particle energies[58] giving,

$$\left(\frac{dE}{dx}\right)_{UO_2} = 1.13 \times \left(\frac{dE}{dx}\right)_{ThO_2}$$

Thus, $$x_{ThO_2} = 1.13\, x_{UO_2}$$

and, $$x^2_{ThO_2} = 1.28\, x^2_{UO_2}\text{ , etc.}$$

2.3.4 Correction factor for low energy α-particles

A homogeneous source should give the same count in all channels of the pulse analyser (equation 6). This was not found, (Fig.10) (see ref.58 and section 3.5), and an empirical correction was made to a constant channel width to give the concentration (activity) in the same units in all channels. For example, the 'slice-thickness' at a depth of about 7.5 microns was about 77% of that near the surface, requiring a correction factor of about 1.3 to give the concentration in the correct units.

2.4 Check on the calibration Checks on the calibration method could be made in part and in toto. The solid angle of counting could be estimated from the geometry of the counting chamber; and a complete calibration could be carried out by the methods of McNamara and Schmitz assuming a linear range-energy relationship for α-particles in UO_2. A second independent check was obtained by calibrating the spectrometer in terms of energy using a monoenergetic source and varying the energy of the α-particles arriving at the detector by changing the gas pressure in the chamber.

2.4.1 Solid angle of counting An estimate of $\omega/4\pi$ (equation 8) could be made by considering the geometry of counting.

The solid angle subtended by the detector at A (Figure 11) is very close to that subtended at O for small values of x, and is given by,

$$\omega = 2\pi(1 - \cos\theta)$$

therefore,

$$\frac{\omega}{4\pi} = \frac{1}{2} - \frac{d}{2\sqrt{d^2+b^2}} \qquad (10)$$

Substituting values for b and d in equation 10 gives $\omega/4\pi$, but the error is large in measuring b, the radius of the detector.

$$d = 1.4 \pm 0.02 \text{ in.},$$

$$b = 0.3 \pm 0.03 \text{ in.}$$

Equation 10 gives $\omega/4\pi = 0.010 \ (^{+0.007}_{-0.001})$

This agrees well with the empirical value of 0.010 ± 0.001

2.4.2 Calibration assuming linear range-channel number relationship

Schmitz[58] gives values of dE/dx (keV/μ) calculated from a theoretical equation for the energy loss of charged particles moving through matter.[69]

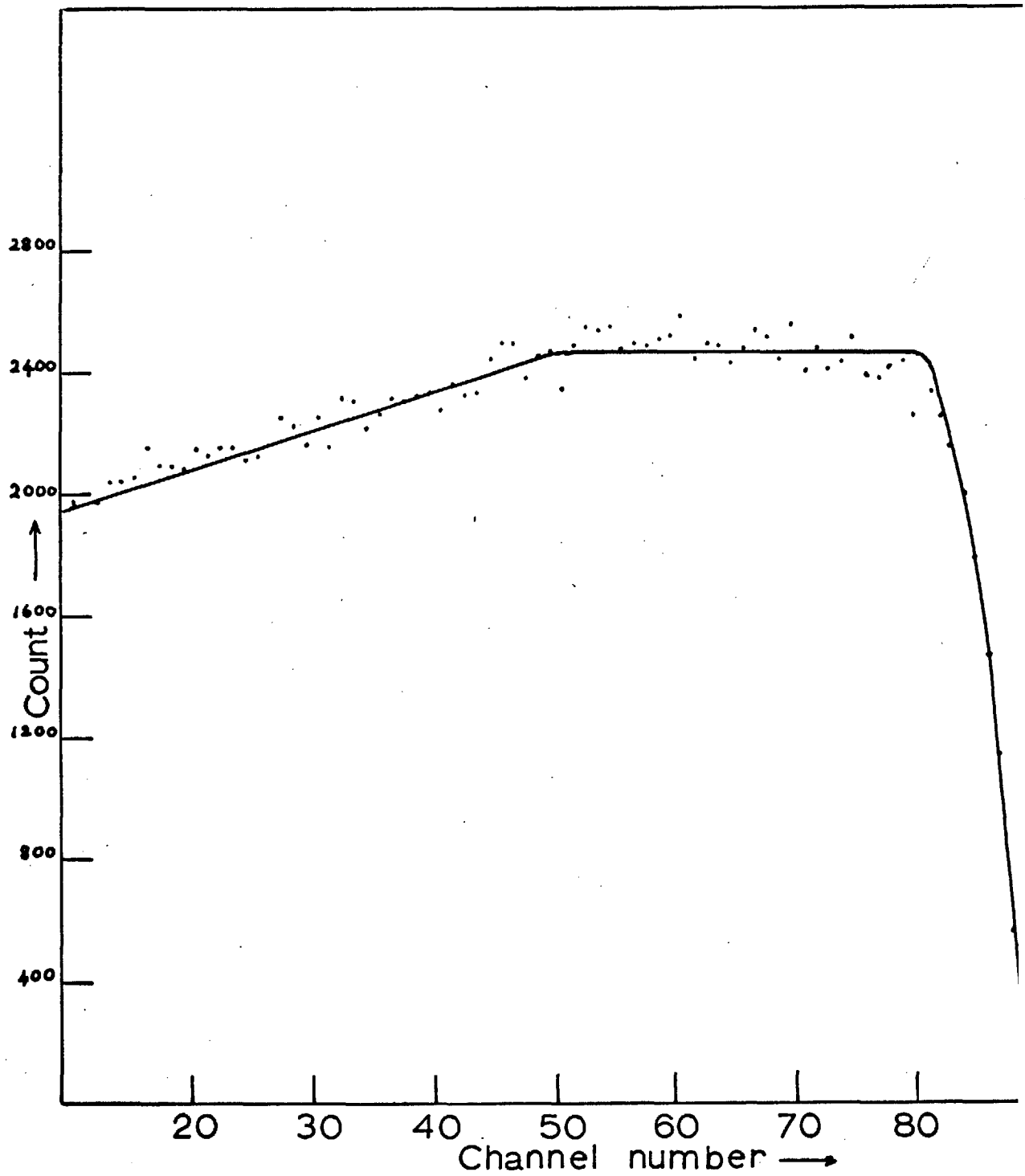


Fig. 10. Count for homogeneous source showing fall-off towards lower energies.

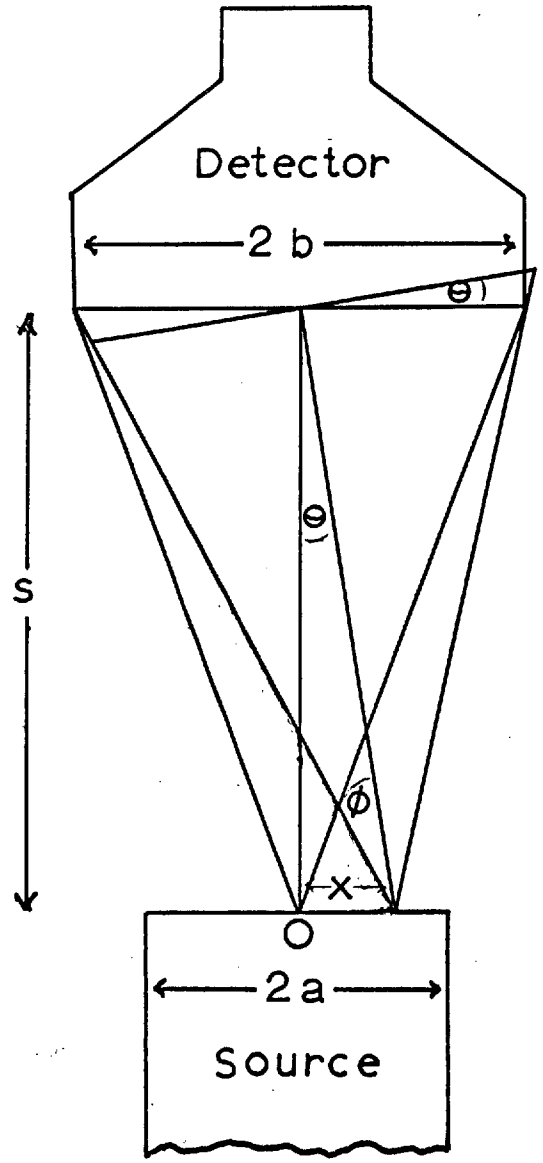


Fig.11. Solid angle of count.

dE/dx changes slightly with energy, but it is assumed to be constant over the range of energies considered. So, using a multi-standard source with peaks of known energy the number of keV per channel can be found, and using the values of dE/dx the number of microns per channel can be obtained.

For energies about 4.8 MeV a multi-standard source (U^{233}, Pu^{239}, Am^{241}, Pu^{238}, Cm^{242}) gave 30keV per channel. Schmitz gives 283 keV per micron, so 1 channel width = 0106 micron which was in fair agreement with the empirical calibration.

2.4.3 Range-energy relationship for α-particles in UO_2

Equation 6 (section 2.3.1) predicts that the same count should be obtained in all channels of the multi-channel pulse - analyser for a homogeneous source (with a linear range-energy relationship and linear amplification in the spectrometer). This was not found to be so, (Fig.10). A calibration of the spectrometer in terms of energies of the α-particles was made and it was found that a plot of 'energy' versus 'channel number' was not linear, (appendix 2). This, together with changing dE/dx[58] (section 2.4.2) explained the fall-off in count towards lower energies. The fall-off does not affect the calibration in section 2.3.1.

2.5 Effect of Instrumental Error on the concentration profile

The count from a weightless source should be registered in one channel of the pulse analyser. This is not obtained; instead a spread, close to a Gaussian distribution, is found (Figure 12). This spread would modify the concentration profile and a solution was obtained for a Gaussian spread applied to the case of diffusion from an instantaneous source into a semi-infinite medium (appendix 3). The concentration at x is given by,

$$C_x = \frac{\beta' C_o}{2\sqrt{2\pi\sigma^2(D^{*2}+1)}} \cdot \exp\left(\frac{-(x^*)^2}{D^{*2}+1}\right) \cdot \operatorname{erfc}\left(\frac{-x^* D^*}{D^{*2}+1}\right) \quad -(13)$$

(where $x^* = x/\sqrt{2\sigma^2}$

$D^* = 2Dt/\sqrt{2\sigma^2}$;

σ = standard deviation of the Gaussian.)

For the range of D's and diffusion times for UO_2 UO_{2+x} and ThO_2, "log C_x" versus "x^2" becomes a straight line after $x^* = 4$ with a gradient,

$$G = \frac{-1}{2.303\,(4Dt+2\sigma^2)}$$

(c.f. $-1/9.212\,Dt$ with no spread)

i.e. $$D = \frac{-1}{9.212\,Gt} - \frac{2\sigma^2}{4t} \quad -(14)$$

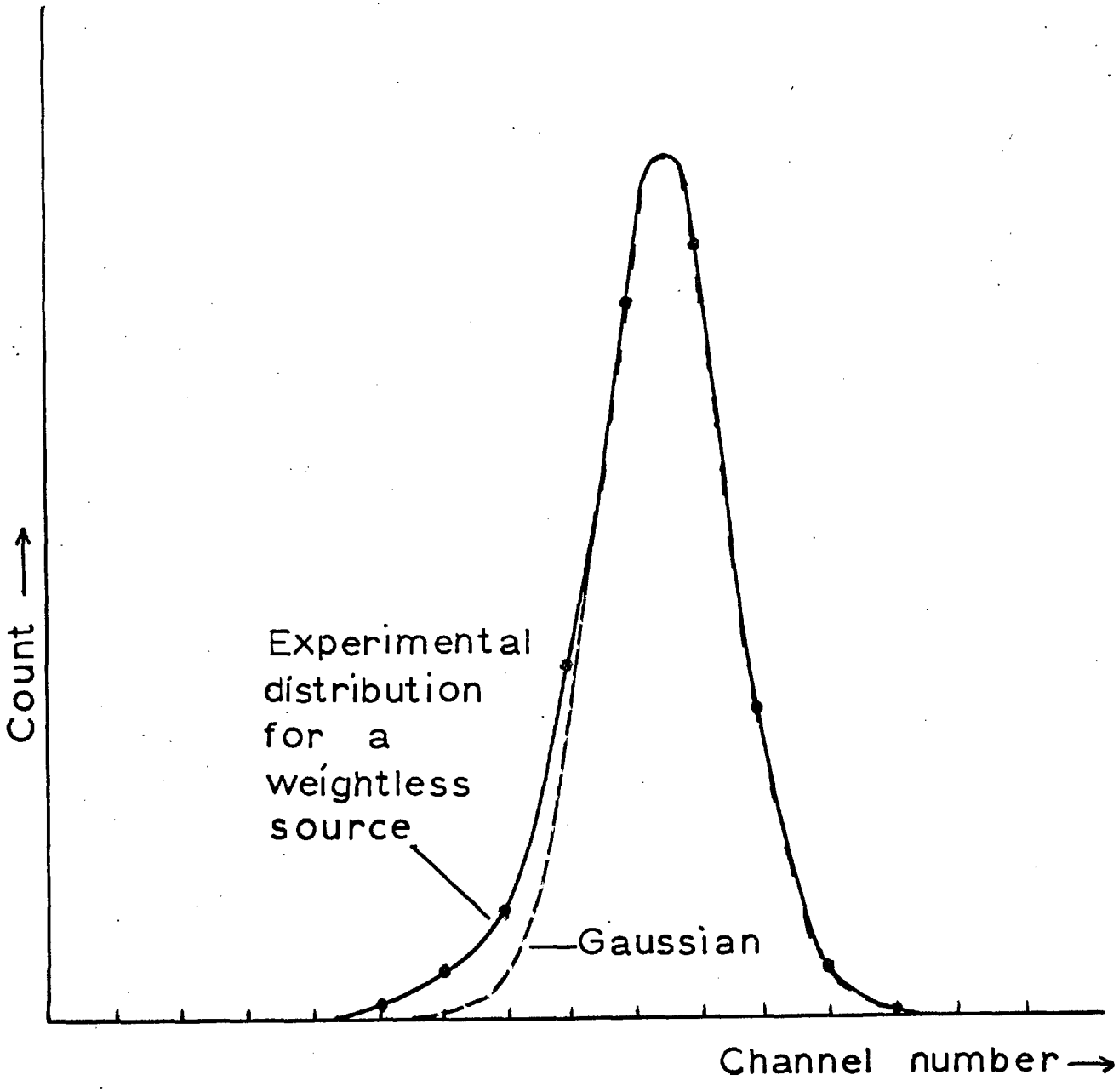


Fig. 12..Gaussian spread.

The correction term only becomes important for large spreads, short diffusion times, and small values of Dt. Generally, the correction was about 1% with a maximum of about 2% for a diffusion run of 8 days in $UO_{2.00}$ at 1477°C.

EXPERIMENTAL

3 EXPERIMENTAL

3.1 Materials The polycrystalline UO_2 was the same as that used by McNamara[1] and the single crystal UO_2 came from the same source as that used by Nagels et al.[5] The thoria pellets were made in the laboratory.

3.1.1 Stoichiometric UO_2 The pellets were supplied by the Chemistry Division, A.E.R.E., Harwell, and were made by sintering cold compacted UO_2 powder in cracked ammonia at 1750°C. This material had a grain size of about 12 μ.

The single crystal UO_2 was made at Mol, Belgium, and was grown from the vapour.[70]

3.1.2 Preparations of UO_{2+x} Non-stoichiometric urania was prepared by two methods: 1) Oxidation using U_3O_8 at 1100°C[71] in an evacuated silica tube.

2) Oxidation at 1600°C using CO/CO_2.

Due to miscalculations method 1) was used for most samples. Fortunately, the mistakes were not important as will be shown later. The first wrong assumption was

that the supply of oxygen from CO/CO_2 was severely limited by the flow of gas and its low oxygen partial pressure. Although the equilibration in the solid state would have been faster at higher temperatures, this method was rejected because of the supposed paucity of oxygen. In fact, the supply of oxygen would be very large since the CO/CO_2 ratio would adjust as the oxygen was removed into the urania, e.g. 5 gm.$UO_{2.0}$ requires about 2×10^{-3} mole oxygen to form $UO_{2.1}$. This could be supplied by 90 ml of CO_2 forming $CO+\frac{1}{2}O_2$. The CO/CO_2 mixture in equilibrium with $UO_{2.1}$ at 1400°C has a ratio 1/53, so there is ample CO_2 in the system to provide oxygen for the formation of $UO_{2.1}$, (pure CO would be required over stoichiometric UO_2). In the first part of the oxidation probably most of the CO_2 would dissociate. At flow rates of about 100 ml/min., the supply of oxygen from the CO/CO_2 is adequate. The ability of the CO/CO_2 mixtures to supply and remove oxygen quickly at the temperatures of the diffusion anneals (the rate depending on solid state diffusion) ensured that the samples were at the correct composition.

The second error which led to the low temperature oxidation process being used was a miscalculation of the oxygen diffusion coefficient. Darken and Gurry[118] state that diffusion into a slab is 93% complete when,

$$\frac{Dt}{L^2} = 1.0$$

(L = half-thickness.)

This would be a slight overestimate for a pellet. Use of the wrong value of the oxygen diffusion coefficient predicted complete homogenisation within a time of 2 days. However, useof the correct values (Auskern and Belle[72] $D_{2.002}$ is 10 times too big) required about 30 days for $UO_{2.06}$ and several months for $UO_{2.002}$ at 1000°C. Thus oxidation at about 1000°C does not achieve homogenisation with the treatment given in this work, although several days at 1600°C, as used in the second method, would be sufficient.

As an empirical check on the reduction of UO_{2+x} by the CO/CO_2 mixture two single crystals, $UO_{2.01}$ and $UO_{2.1}$, were annealed in an atmosphere in equilibrium with $UO_{2.01}$. Both gave similar concentration profiles and diffusion coefficients for U; indicating that the $UO_{2.1}$ had been quickly reduced to $UO_{2.01}$. This is understandable from equations in Darken and Gurry's book for diffusion into a slab for the surface held at constant composition, c_s. If c is the [illegible] composition at depth x after time t, then for $c = 0.95c_s$, $x/\sqrt{Dt} = 0.1$. Using the lowest estimate of D at the lowest temperature of the

diffusion anneals, it is found that the first micron reaches a composition higher than $0.95c_s$ in 25 secs. and first 10μ in 2,500 sec. Since the uranium diffuses much more slowly than oxygen, the composition is established well before the U tracer diffuses in. However, the flux of oxygen could affect the diffusion coefficient of the uranium[73] but no difference in D_u was observed in fully homogenised pellets and those prepared by method 1.

Thus, even without prior oxidation, provided that the gas has access to the activd surface, diffusion of the cation into urania of known composition can be studied. Oxidation effects should show up in D calculated for different times in the same sample. D was found to be constant with time (see Fig.40).

3.1.3 Thoria Experiments were performed on commercially available thoria and pellets prepared from reactor grade thorium nitrate.

The preparation of the pellets was as follows[74,75] $Th(NO_3)_4.10H_2O$ was dissolved in de-ionised water. This solution was made acid and the oxalate was precipitated by the dropwise addition of excess oxalic acid. The precipitate was filtered, washed with alcohol, and left to dry. The oxalate was transferred to an alumina boat

and heated slowly to about 350°C and left overnight when most of the water would be evolved. The final calcination treatment was to raise the temperature to 900°C for a few hours. The oxide was stored in a desiccator and before pressing pellets the powder was pre-sintered at 1200°C, cooled, mixed with about 1% binder (Cranco, 10 vol% methyl methacrylate in benzene) and dried under an infra-red lamp. Pellets were pressed with a 1 cm. diameter steel ram and die at a pressure of 40 t.s.i. Any discolouration on the pellets after pressing was removed with 500 grade emery paper. The binder was burnt off by heating to 600 - 700°C for about 5 hours in air. The final sinter was performed in a vacuum furnace at a temperature of about 1900°C for 5 hours. This produced white translucent pellets with a grain size of about 30μ, which subsequently increased to about 100μ after being heated to about 2000°C.

3.2 Polishing Both single and polycrystalline samples of UO_2, UO_{2+x} and ThO_2 were roughly polished using silicon carbide paper (under water) down to 600 grade. The fine polishing was performed with diamond paste (Dialap - 14, 8, 3 and 4 micron), on cartridge paper on plate glass. An excellent mirror-like finish was obtained. The technique of using a fibrous paper, with

the abrading particles embedded in it should ensure that no really deep scratches appear on the surface; and very few were observed. It was felt that absolute flatness of the surface was not necessary since a collimated count of the surface was taken to determine the concentration profile and, provided that the undulations of the surface were small, and that most of the tracer made contact, then the conditions would not be too far removed from the theoretical model for diffusion from a plane source. Some pellets were annealed after polishing, usually for about 1 day under the conditions of the subsequent diffusion anneal, before the tracer was deposited.

3.3 Cleaning the surface of the pellets Most of the urania pellets were cleaned by washing in carbon tetra-chloride and then in alcohol. However, when work was started on thoria it was found essential to clean the surface thoroughly. Warm alcoholic KOH was used to remove grease and after rinsing with water, perchloric acid was swabbed over the pellet surface. Finally the pellets were washed with alcohol.

3.4 Plating the tracer Several different methods of deposition of the tracer were tried. The best method for $U^{233}O_2$ was vacuum sublimation and a quick

method for both U^{233} and Th^{230} was developed by Mr D.Sood at Imperial College using an alcoholic solution of the perchlorate of the tracer cation.

3.4.1 Plating Stoichiometric UO_2 The tracer used for diffusion studies in urania was supplied as a solution of 2 mg. of U-233 metal dissolved in 1 ml. of nitric acid, and was subsequently made up to 10 ml. with distilled water.

Several methods were used to deposit the active layer on to the polished surface of the diffusion specimen

i) Using tetraethylene glycol as a wetting agent This method required some skill and patience. The best results were obtained by evaporating down the aqueous solution of U-233 nitrate to a small bulk and then adding one drop of T.E.G. just before the deposition occurred. In this way attack on the retaining ring of Zapon varnish was reduced to a minimum. The varnish was removed by heating in vacuo at about 1000°C. Quite a high activity could be obtained without serious impurity contamination, but this method was tedious and unreliable in that autoradiographic evidence often showed very uneven deposits. This was superseded by vacuum sublimation and was not used for UO_{2+x}.

ii) Vacuum sublimation The aqueous solution was evaporated to dryness on the heating filament of the vacuum sublimation appartus. Two types of heating elements were used,

(1) Tungsten spiral. The vapour pressure of UO_2 is quite high at 2000°C[77] being about 7 x 10^{-5}mm. The oxide evaporates congruently[78] and so deposition by sublimation in vacuo was possible.

(2) Tantalum strip. The use of tantalum would probably mean that the UO_2 was reduced and U-233 metal was deposited[79] However, the small amount of metal involved would rapidly be oxidised in air or in the subsequent diffusion anneal. This method was chosen since higher activities could be put down due to the higher vapour pressure of the uranium metal. Typical conditions for sublimations from the tantalum strip were 10 sec. at a very bright white heat (~2000°C) and a vacuum of about 5 μ.

3.4.2 Plating UO_{2+x} i) Vacuum sublimation All vacuum sublimations for the non-stoichiometric UO_{2+x} were from a molybdenum filament. Firing took place at about 3 μ pressure for 30 sec. at about 2000°C.

ii) Deposition from an alcoholic solution of U-233 perchlorate (80)

This method required that the solution contained no water whatsoever so that the evaporation of the whole of a film of the alcoholic solution of the tracer took place simultaneously to give an even deposit of the tracer. There was no need to convert the perchlorate to the oxide, as this would occur very quickly, when beginning the diffusion anneal.

The preparation of the solution was parallel to that for thorium perchlorate (section 3.4.4)

3.4.3 The U-233 dioxide layer A number of α-ray spectra of deposited sources have shown the layers to have about the same spread as a weightless source (Fig.13). Any crystallites present must be less than about 0.1μ high (one channel width).

The thickness estimated from the amount of active material used, assuming an even layer, was in all cases less than 0.1μ.

Although the tracer may be deposited as small crystallites rather than a plane source, it is likely, in view of the high vapour pressure of UO_2 and UO_{2+x} and the fact that etching takes place at grain boundaries, (81)

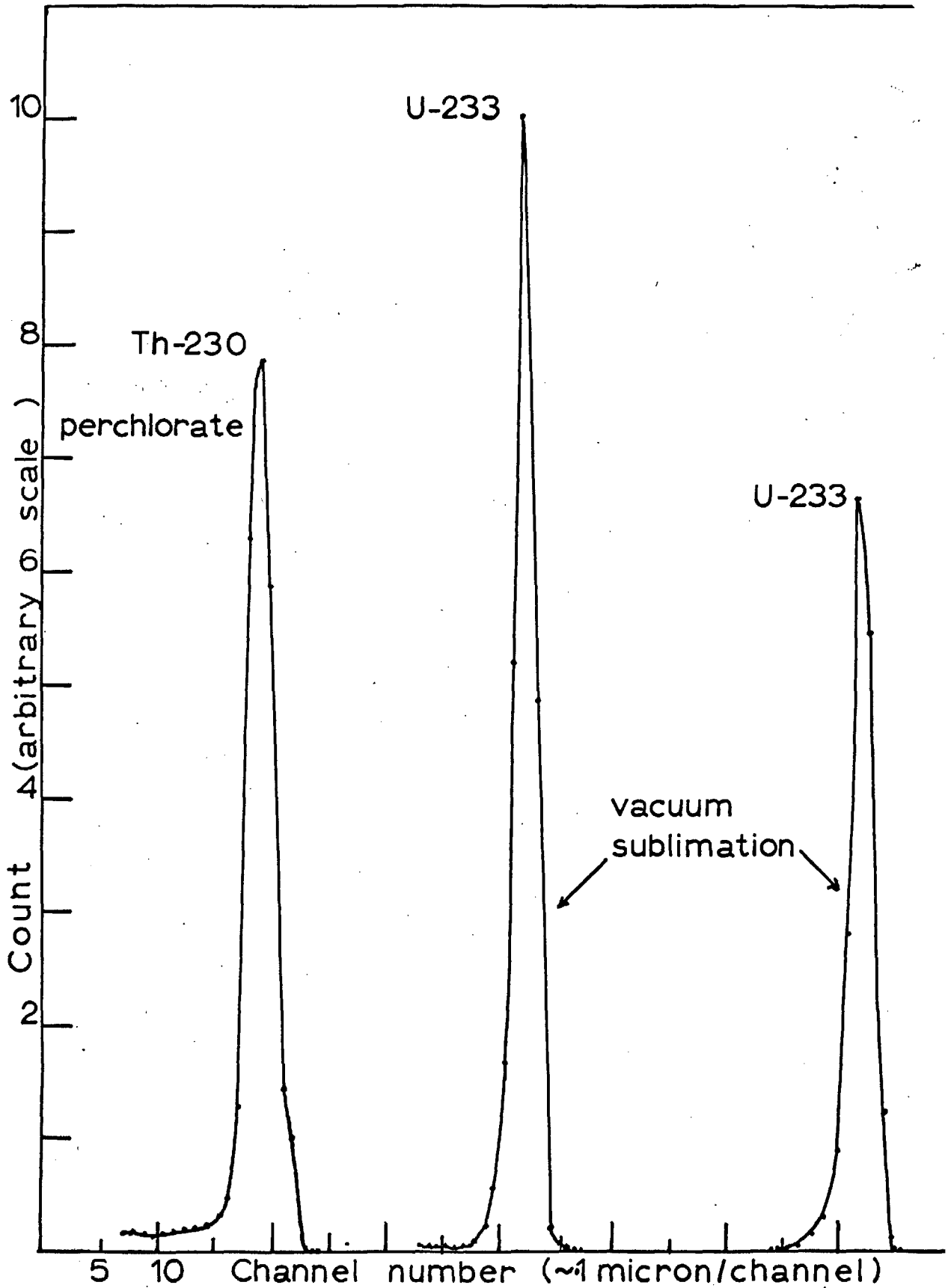


Fig. 13. Plated tracer layers.

that they would rapidly disappear forming a plane source because of the relative ease of removing molecules of UO_2 from the sharp edges and corners of the crystallites.

3.4.4 ThO_2 The tracer was supplied as a solution of 1 mg. of 12% Th-230/88%Th-232 in 1 ml. of nitric acid.

The method of deposition of the tracer layer was from an alcoholic solution of thorium perchlorate.(80) The solution was prepared by adding excess perchloric acid to the solution of Th-230 in nitric acid and evaporating to dryness. Pure, dry ethanol was added to the residue to form a solution of the tracer and kept well stoppered to prevent the uptake of the water from the atmosphere.

The perchlorate was usually converted to the oxide by heating to $1000^{0}C$ in air for a few minutes before the diffusion anneal to ensure that the tracer was not rubbed off in the subsequent handling of the pellets.

3.5 Diffusion Anneals The experimental assembly for the diffusion anneals is shown in Figure 14. A molybdenum furnace was used, its windings being protected by cracked ammonia. A Pt/13% Rh-Pt control thermocouple, well protected with alumina cement, fed a Kent controller

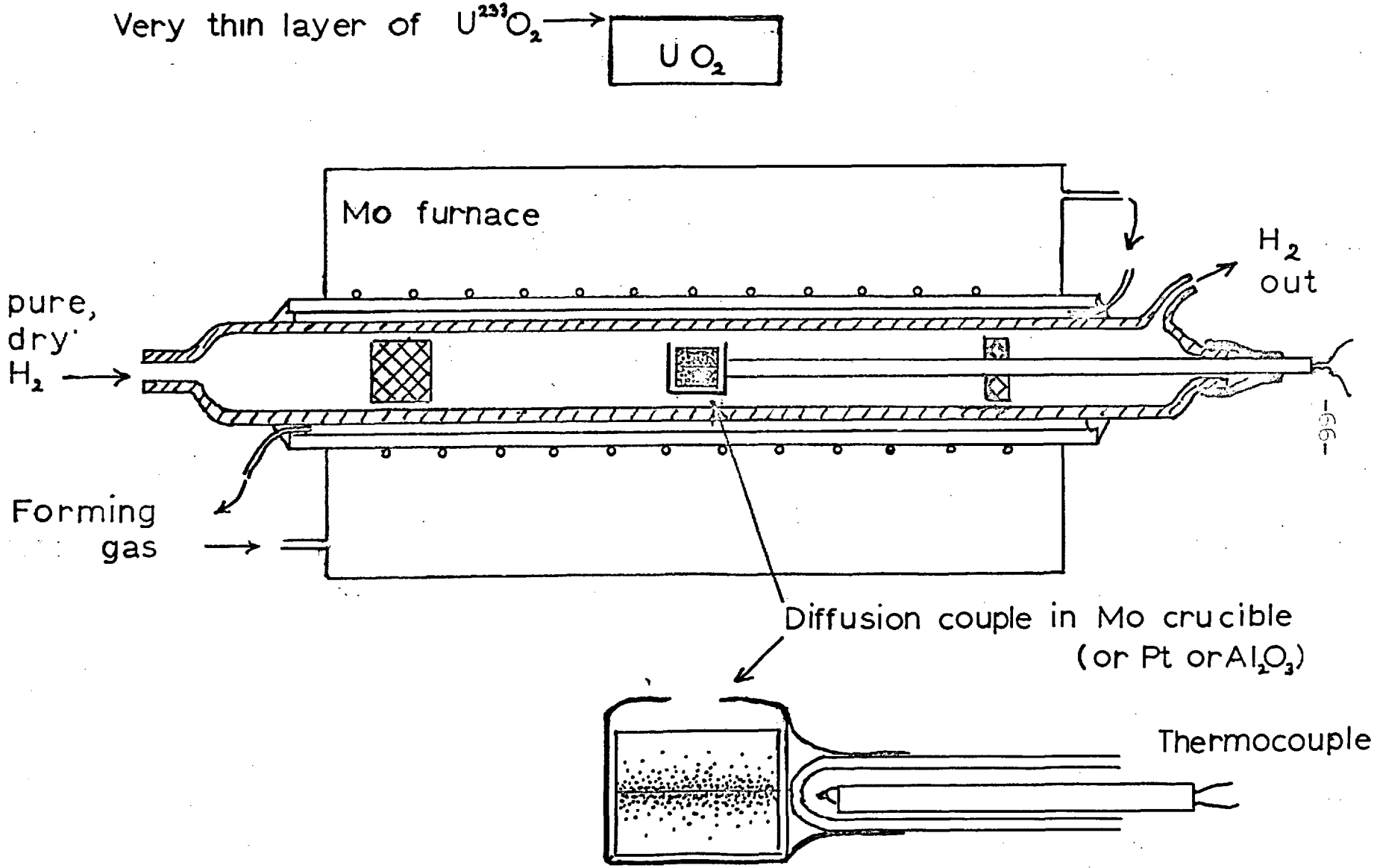


Fig. 14. Diffusion anneals.

(eventually replaced by a Smith's controller) which kept the temperature constant to $\pm$ 5°C at all temperatures. The reaction tube was made of recrystallised alumina with B34 cones araldited to both ends. The diffusion couple was placed in a crucible at the end of a long thermocouple sheath which could be pushed through a sliding seal made from rubber pressure tubing. The control atmosphere entered at one end of the reaction tube and the exit, to a dibutyl phthalate bubbler, was at the same end as the sliding seal. The temperature was measured with either a Pt/13% Rh/Pt or 5% Rh-Pt/20% Rh-Pt thermocouple.

For ThO_2 diffusion anneals in vacuo, a conventional vacuum furnace with a tungsten heating coil was used.

3.5.1 Stoichiometric UO_2 The stoichiometric urania diffusion couples were mounted either in an alumina or a molybdenum crucible.[82] At the start of the diffusion anneal dry argon was passed through the furnace for about half an hour to expel any air. Then whilst the diffusion sample was still in the cold part of the furnace the atmosphere was changed to high purity hydrogen. The hydrogen was taken from a cylinder (high purity) and dried by passing through an all-glass apparatus containing magnesium perchlorate and silica gel.

An estimate of the oxygen partial pressure was obtained using an oxygen meter (section 3.5.3). This gave a value of about $10^{-14.6}$ for p_{O_2} at 1400°C, assuming a H_2/H_2O mixture.

In the final arrangement for the diffusion anneals P_2O_5 was used for drying the hydrogen. An estimate of p_{O_2} was made using a long alumina boat containing ZnO. With the centre of the furnace at 1600°C the oxide was fully reduced at 420°C (the melting point of zinc) and a discolouration was observed down to 350°C. This indicated that p_{O_2} at 1600°C was at the most 10^{-18} atm., and possibly as low as 10^{-20}. Only one stoichiometric UO_2 sample was annealed in this atmosphere (single crystal 1670°C).

The temperature of the diffusion couple was changed slowly to avoid thermal shock. On average about 40 minutes were taken to reach the temperature of the diffusion anneal. An allowance of half the time spent between 0.8T and the diffusion anneal temperature, T, was given in order to correct the time of the diffusion anneal for slow heating and cooling.

3.5.2 UO_{2+x} In order to maintain the composition of the non-stoichiometric urania CO/CO_2 gas

mixtures were used. A conventional gas-train was used employing capillary flow meters. The CO_2 was purified by passing it over moist KOH pellets, and both gases were dried with magnesium perchlorate and silica gel.

The data used for the oxygen partial pressure in equilibrium with UO_{2+x} were taken from two sources[83,84] (Figures 15,16) but there was not total agreement in these measurements.[28,83-86]

The e.m.f. data of Markin and Bones agreed very well with the data of Aukrust et al., if the deviation of the latter workers' results at lower temperatures is attributed to non-attainment of equilibrium conditions in the $UO_{2+x}/CO/CO_2$ system which they used.

Diffusion couples were not used for the non-stoichiometric urania runs because of the enhanced sintering characteristics of this material.[10,24] Instead, the pellets were placed active face downwards in a platinum crucible. The single crystals were wrapped in Pt foil to prevent excessive evaporation of the urania. Although etching in the vicinity of the grain boundaries was observed in the highly non-stoichiometric urania only a small depth of material would be lost from the surface of the grains and the boundary conditions for the volume diffusion process would probably not be changed very much.

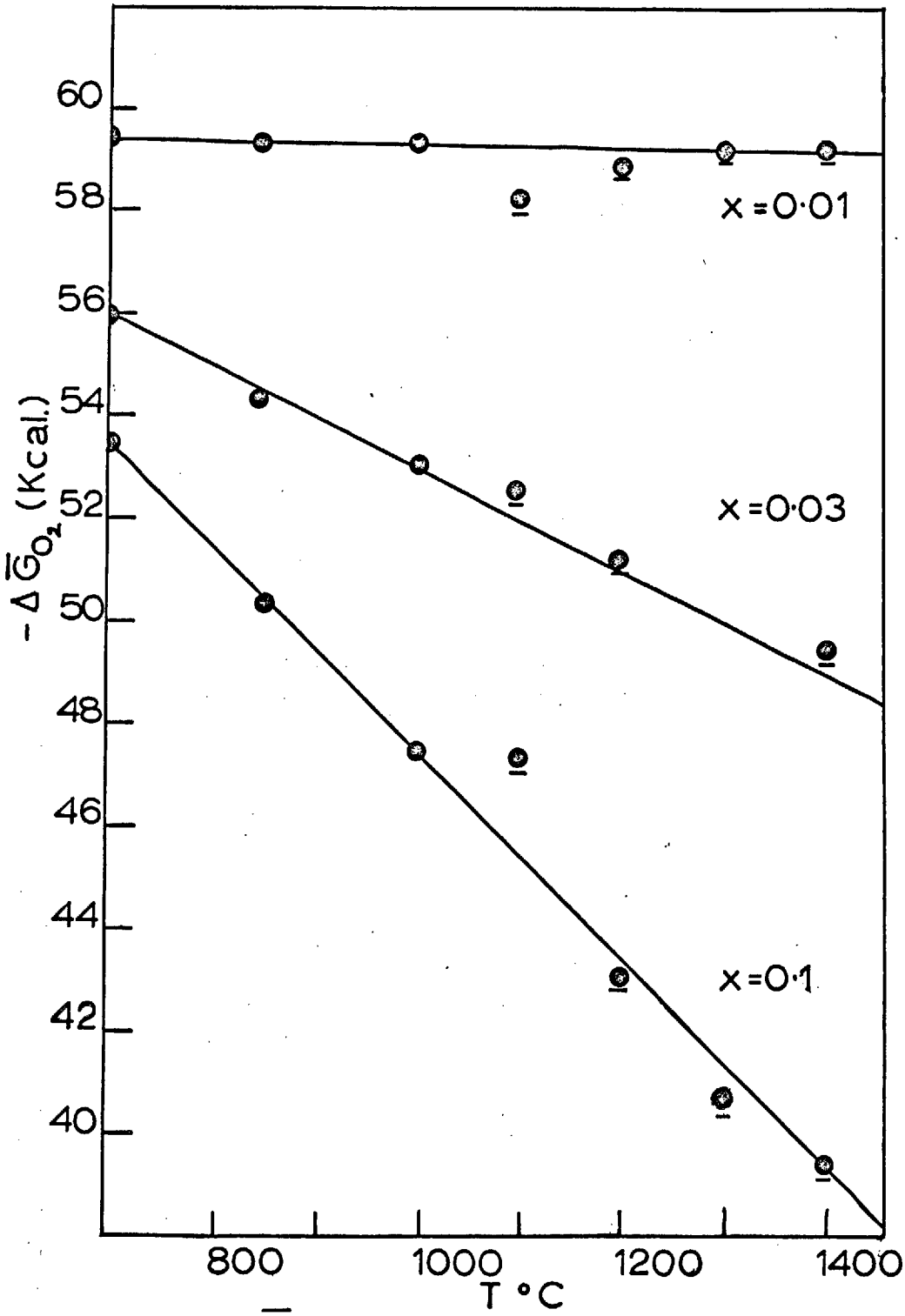


Fig. 15. $\Delta\bar{G}_{O_2}$ vs. temperature for UO_{2+x}

● ref. 83 ⊜ ref. 84

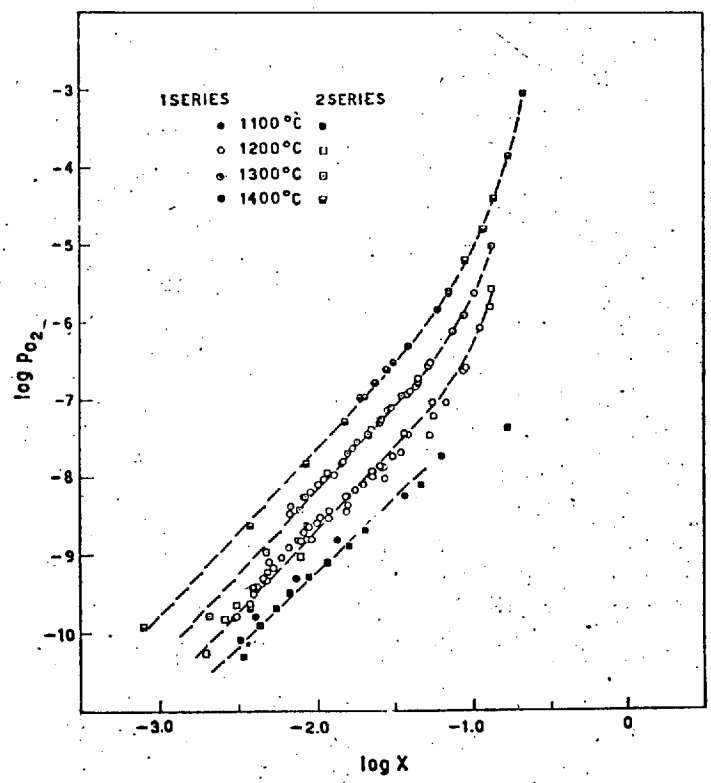


Fig. 16. Log p_{O_2} vs. log x (Aukrust et al.[84])

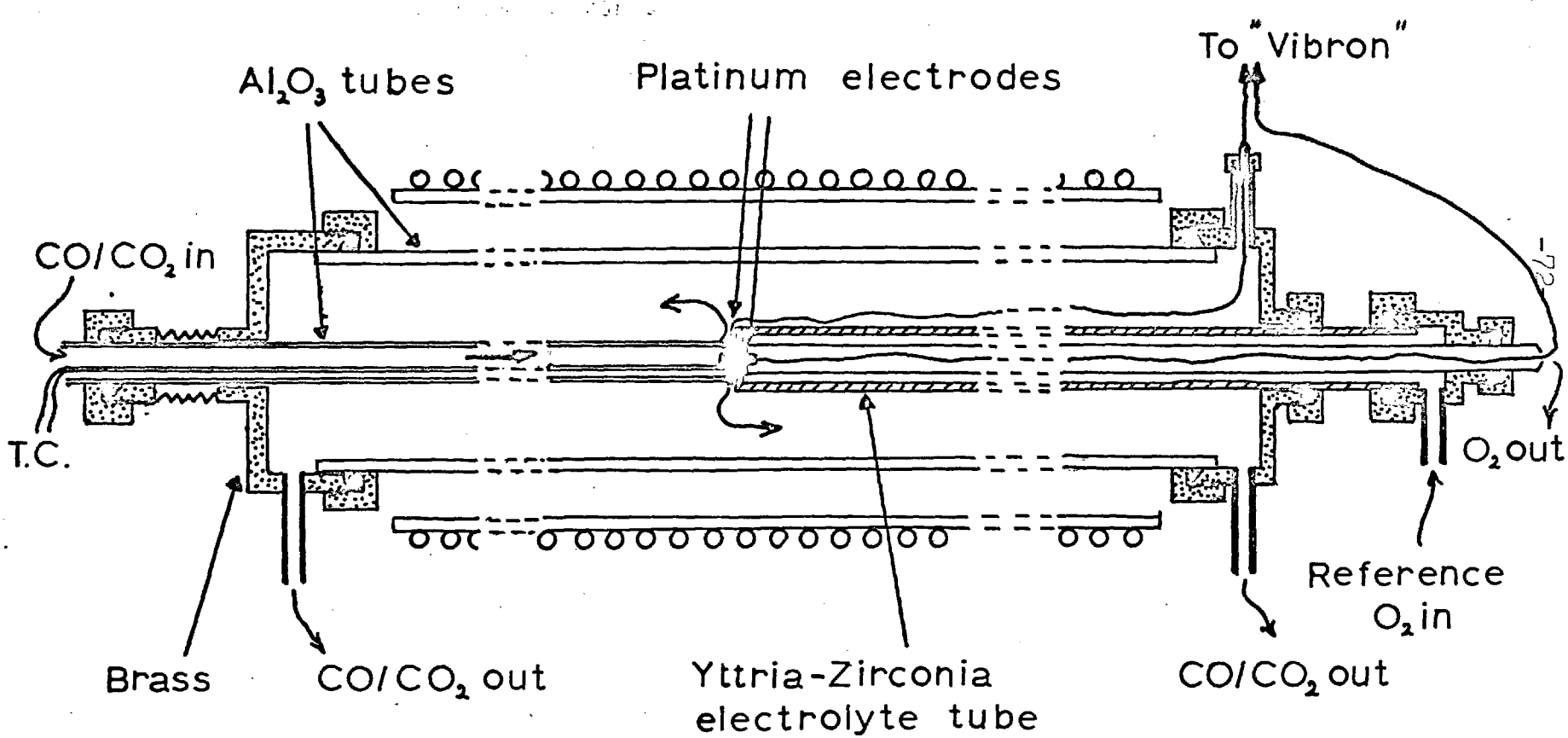


Fig. 17. Oxygen meter.

This is supported by the general reproducibility of the results despite the fact that the protection of the active surface was sometimes less good than at other times.

3.5.3 Oxygen meter As a check on the CO/CO_2 ratio and on hydrogen pick-up in the molybdenum furnace the exit gases were passed to an oxygen meter. The oxygen meter[87-90] (Figure 17) consisted of an yttria-stabilised zirconia flat-ended tube with two Pt electrodes, one in the CO/CO_2 mixture, and the other, a reference electrode, in pure O_2 at 1 atmosphere pressure. The meter operated at a temperature of 1250°K and the e.m.f. was measured with a potentiometer or a Vibron electrometer. An initial calibration by passing CO/CO_2 mixtures directly from the flow-meters to the oxygen meter gave e.m.f's to within about 0.3% of the calculated value for a range of flow rates (167 to 240 $ml.min^{-1}$) and CO/CO_2 ratios (1/1 to 1/36) One composition, CO/CO_2 1/1, was also checked by gas chromatography and found to be correct.

An estimate of the allowable error in the e.m.f was made so that a good check on the value of x in UO_{2+x} could be made. For the oxygen meter operating at 1250°K it is found that since,[91]

$$\log \frac{p_{CO_2}}{p_{CO}} = \frac{14,550}{T} - 4.404 + \tfrac{1}{2} \log p_{O_2}$$

and p_{CO_2}/p_{CO} is fixed,

then,

$$\log p_{O_{2(1250^\circ K)}} = 29,100 \left(\frac{1}{T} - \frac{1}{1250}\right) + \log p_{O_{2(T)}} \quad (15)$$

(T = temperature of diffusion anneal)

and, $$E = \frac{RT}{4F} \ln \frac{p_{O_2}\ (gas)}{p_{O_2}\ (pure\ O_2)}$$

so we have,

$$E = 62.21 \log p_{O_{2(1250^\circ K)}} \text{ mv.} \quad (16)$$

E is measured directly (equation 16) so $\log p_{O_{2(T)}}$ (equation 15) can be found.

As can be seen in Figure 16, a small change in $\log p_{O_2}$ (or E) can produce a large change in x. For $UO_{2.01}$ $\log p_{O_2}$ should be within 0.1 of the required value, and this corresponds to a change in e.m.f. of about 6mV.

3.5.4 ThO_2 diffusion anneals Diffusion anneals were performed in vacuo, air and CO/CO_2 mixtures to ascertain the effect of the oxygen partial pressure on the cation diffusion coefficient. For the runs in vacuo

diffusion couples were made by holding the pellets face to face, but separated with a wire loop, of either tungsten or molybdenum wire. The pellets were suspended inside the tungsten heating coil of a vacuum furnace. Runs in air were in the molybdenum furnace with the ends of the reaction tube left open. The pellets were contained in an alumina boat with no protection of the active face. For diffusion anneals in CO/CO_2 the pellets were wrapped in Pt foil.

3.5.5 Complicating factors in ThO_2 diffusion runs

i) Vacuum anneals. When ThO_2 is heated for a long time at high temperatures under a high vacuum there is a possibility of reducing ThO_2 to Th and the pellet becomes grey as the metal separates out. This was observed after 4 days at 1800°C although a few hours at 2000°C did not produce this effect - probably because a high vacuum had not been established. Any runs in which the material had become black were rejected.

ii) Many ThO_2 runs in vacuo were unsuccessful in that the tracer did not diffuse in, but remained bound at the surface. To overcome this problem the pellets were very carefully cleaned, (section 3.3). The perchlorate layer was usually fired for a few minutes in air to form the

oxide so that the pellets could be handled without the tracer layer being destroyed by uptake of moisture from the air. For most hydrogen runs the plated pellets were kept warm so that the perchlorate layer did not pick up moisture and the conversion to the oxide took place in the furnace, but some were fired to the oxide before the run. Similar results were obtained with both methods.

iii) Anneals in air. Thoria pellets from three different sources were heated in air at 1000°C inside a silica tube, and at 1600°C inside an alumina tube. All of the pellets became orange-brown in colour. This effect was also noticed when ThO_2 was heated at 1600°C in (wet) H_2 direct from a cylinder. When heated in H_2 at 1000°C the pellets reverted to their original white colour. This suggests that thoria may take up some excess oxygen, either by oxidising impurities in the pellet, or perhaps by forming non-stoichiometric thoria with interstitial oxygen ions acting as donors or vacant cation sites acting as acceptors with the formation of colour centres. However, the colour did not fade after prolonged exposure to ultra-violet light as might have expected if colour centres were formed.

ANALYSIS OF RESULTS

4. ANALYSIS OF RESULTS

The solution of the diffusion equation for diffusion from an instantaneous source into a semi-infinite medium (equation 1) can be applied directly to the case of diffusion into a single crystal. The model for diffusion into a polycrystal which best fits the experimental conditions, is due to Suzuoka. Allowing for the possibility of a bound surface layer and using Suzuoka's model the theoretical concentration profiles can be compared with the experimental profiles and also aid interpretation of the tracer distribution.

Since the spectrometer had a finite resolution and there was a possibility of a bound surface layer, the magnitude of the effect from these two causes was evaluated.

4.1 Resolution of the spectrometer The effect of instrumental error (section 2.6) is small except near the surface. The spread for a standard weightless source must be determined so that the penetration depth beyond which the effect is small can be determined (equation 13). Typical spreads from a weightless source and plated layers are shown in Figure 13. The spread was close to a Gaussian (Figure 12),

$$I = I_0 \exp\left(\frac{-(x - \bar{x})^2}{2\sigma^2}\right)$$

where $\sqrt{2}\sigma$ was about 0.08 microns.

$x^* = 4$ at about 0.6 to 0.7 micron (section 2.6) and so a straight line is expected on a "log activity" versus "x^2" plot after $0.5\mu^2$.

4.2 The bound surface layer Some of the plated layer may not diffuse in. It must be assumed that the part of the layer which takes part in the diffusion process does so from $t = 0$ onwards, and that part which is bound at $t = 0$ is still bound at the end of the diffusion anneal. This assumption may not be valid and low diffusion coefficients could result from the slow release of tracer from the surface. However, measurements in single crystals and polycrystals for different times should give the same volume diffusion coefficient, if the effect of the bound surface layer is small.

From Figure 13 it can be seen that the activity due to a bound surface layer would be 1/100 times the peak value at $0.5\mu^2$. So from the height of the peak at the surface after an anneal the contribution at $x^2 = 0.5\mu^2$ could be estimated and in all cases was found to be negligible.

4.3 Single crystal concentration profile Here the diffusion process was expected to be by volume diffusion alone and the concentration profile was expected to follow equation 1 for sufficiently large x since the effects of instrumental error (equation 14) were small away from the surface of the sample.

A bound surface layer would give a sharp peak at the surface like a plated layer.

The general form of the expected profiles is shown in Figure 18 for Dt = $3 \times 10^{-9} cm^2$. This is the smallest 'Dt' value expected, when the instrumental error has the largest effect.

4.4.1 Polycrystal concentration profiles If the diffusion follows Suzuoka's model, then the useful parts of the profile can be predicted. Approximate values of D for UO_2 were already known[1-5] (including the low-valued single-crystal result) so the range of Dt values were known. The grain size of the pellets was known and the ratio D_b/D was re-calculated from refs. 1 and 60. Figure 19 shows the error in determining D from the slope of 'log (activity)' versus 'x^2' from 0 to $3\sqrt{Dt}$

($\beta = 2a(\Delta - 1)/\sqrt{Dt}$;

$2a$ = g.b. width = 5Å;

$n = b/\sqrt{Dt}$; b = mean linear dimension of the grains.)

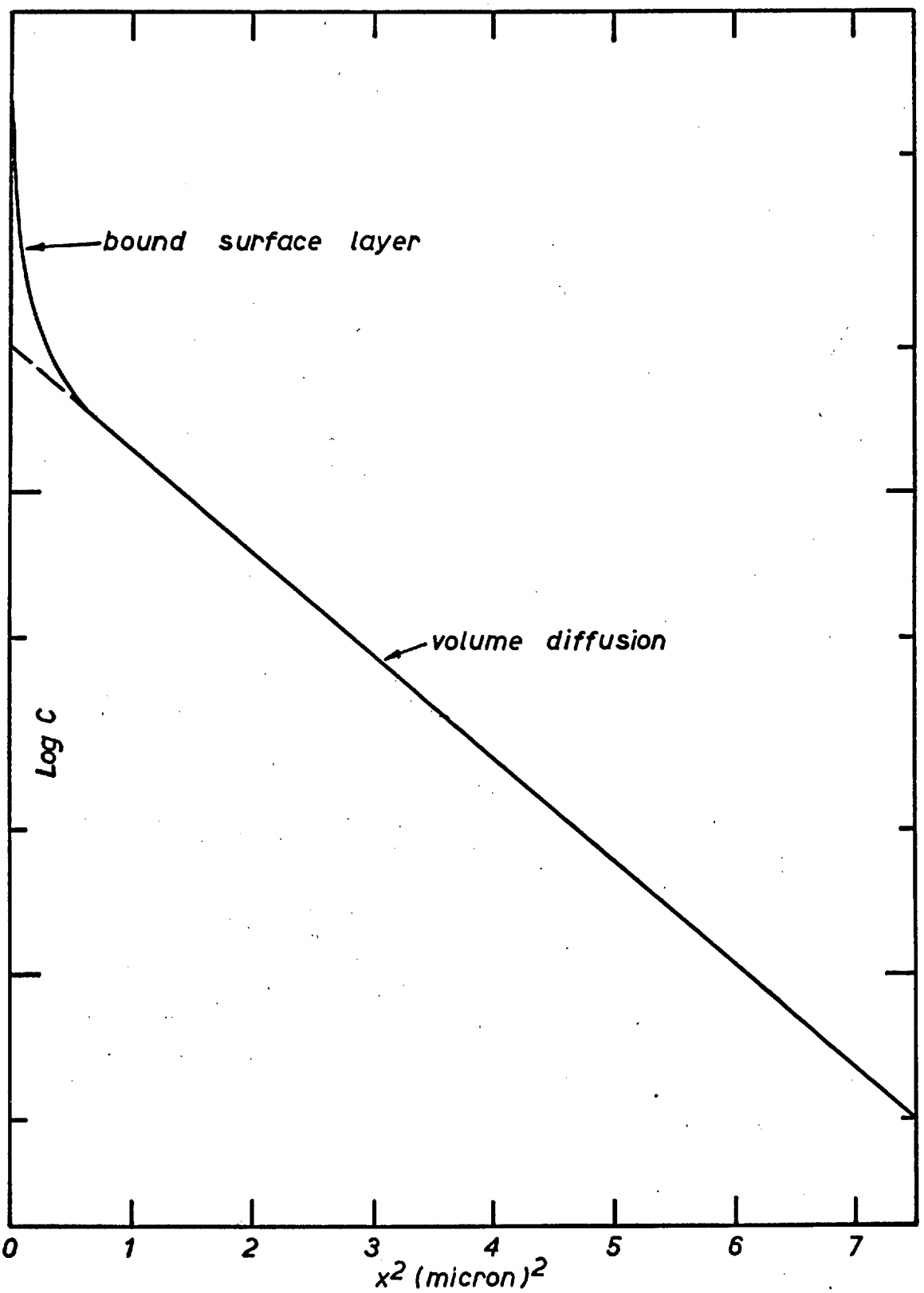


FIG. 18 THEORETICAL PROFILE FOR DIFFUSION IN SINGLE CRYSTALS

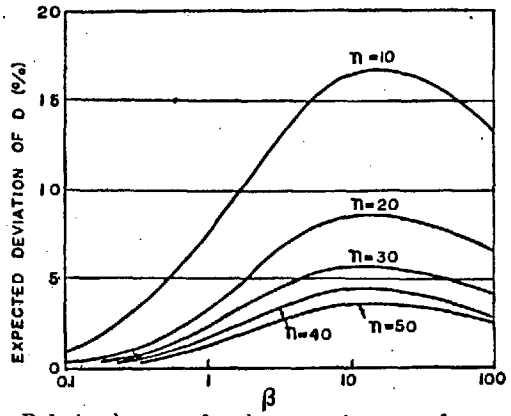


Fig. 9 Relation between β and systematic error of apparent D due to grain boundary diffusion for various grain sizes, when D is determined from the penetration depth of $\eta=0$ to 3.

$$n = b / (Dt)^{1/2}$$
$$\beta = 2a(\Delta - 1) / (Dt)^{1/2}$$
$$\eta = x / (Dt)^{1/2}$$

Fig. 19. Error in D from first part of log C vs. x^2 plot.(52)

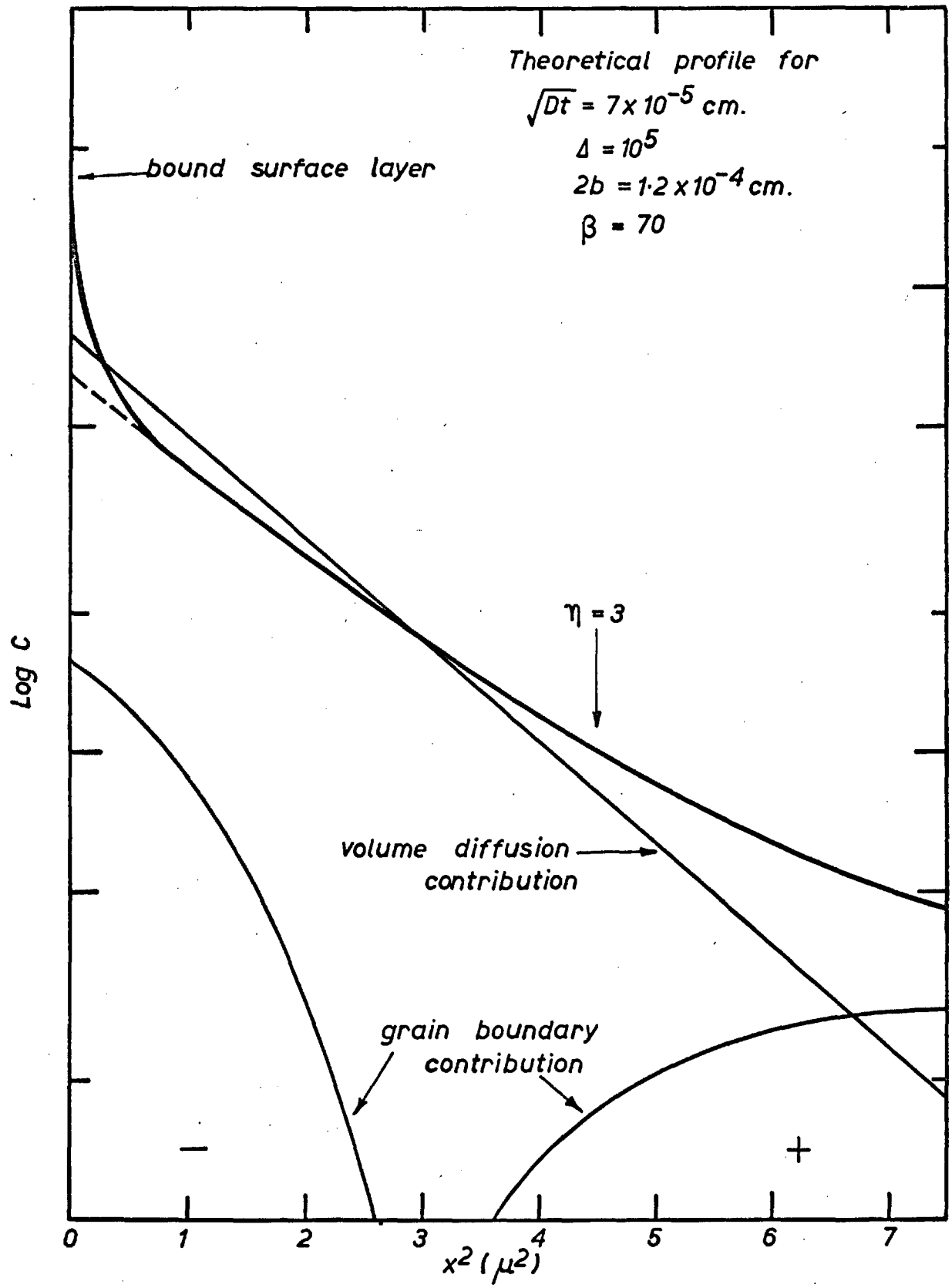


FIG. 20 THEORETICAL PROFILE FOR DIFFUSION IN POLYCRYSTAL

Thus it can be seen that for small errors in D, n should be large, i.e. b should be large or $\sqrt{Dt}$ small; and β should be large, i.e. Δ should be large or $\sqrt{Dt}$ small.

For stoichiometric UO_2 the grain size was 12μ and the largest expected value of Dt was $5 \times 10^{-9} cm^2$, giving $n = 9$ with $\beta = 71$. Later runs in non-stoichiometric UO_{2+x}, where the grains had grown to 30μ gave a maximum value of Dt of about 10^{-8} giving $n = 30$, so the average error in determining D from the slope of "log (activity)" versus "x^2" in the range 0 to 3 $\sqrt{Dt}$ was about 5%. Thus, the full 'self-consistent' treatment (52) for finding D was not essential; but it was applied in all cases in an attempt to minimise errors.

A theoretical concentration profile (plotted as "log (concentration)" versus "x^2") is shown in Figure 20 for $Dt = 5.0 \times 10^{-9} cm^2$; grain size 12$\mu$ and $\Delta = 10^5$. The effect of a bound surface layer is also shown.

4.4.2 The self-consistent method for determining D

Suzuoka's self-consistent method requires graphical manipulation of the results. A modification of this method has been made so that most of the manipulation is arithmetic. The procedure is as follows:

1. The concentration profile is plotted as "log (concentration)" versus "x^2" and as "log (concentration)" versus "$x^{6/5}$" An estimate of D can be obtained from equation 1 and also from,

a) "log C" versus "x^2" should be a straight line to 2 or $3x\sqrt{Dt}$, and,

b) "log C" versus "$x^{6/5}$" should be a straight line beyond 5 or $6x\sqrt{Dt}$. These three estimates should be compatible.

2. The gradient of "log C" versus "$x^{6/5}$" gives γ $(= -\partial \log C/\partial (x^{6/5}))$ and using the estimated value of D the parameter β can be found from,

$$0.973 \log (\Delta - 1) = 6.567 - 1.644 \log \gamma - \log \sqrt{Dt} \quad (5)$$

$$\beta = 5 \times 10^{-8} (\Delta - 1)/\sqrt{Dt} \quad (17)$$

$(\Delta = D_b/D)$

3. Since the grain-boundary acts as a sink near the surface its contribution to the concentration profile is negative; so there is a depth where the contribution is zero (Figure 20). This point on the concentration profile c_{η_o}, is due to volume diffusion alone. Figure 21 is a plot of η_o versus β, ($\eta_o = \frac{x_o}{\sqrt{Dt}}$, is the position where $\overline{c_2} = 0$) Values of $\overline{c_2}$ (the grain-boundary contribution) for various β and η are available up to $\beta = 30$ (52) and these tables have been extended to $\beta = 200$ using the Imperial College computer (appendix 1).

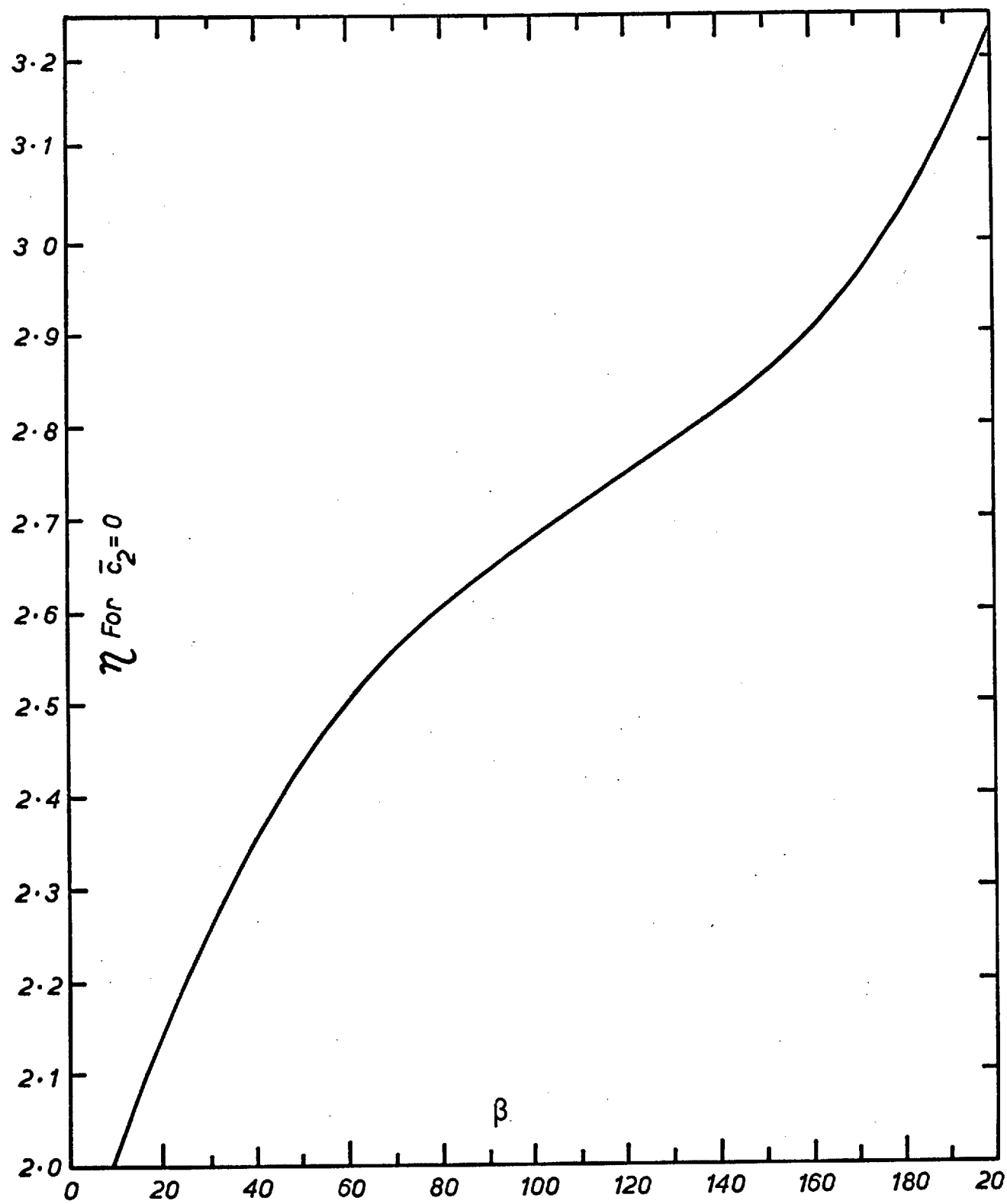


FIG.21 VALUES OF η AND β FOR ZERO GRAIN-BOUNDARY CONTRIBUTION

4. At a depth of $6\sqrt{Dt}$ the presence of the tracer is due to grain-boundary diffusion alone. For various values of β the count at this depth, $\overline{c_6}$, can be related to the grain-boundary contribution at a depth of 0.707μ ($0.5\mu^2$) This contribution is usually negative and Figure 22 shows $\overline{c}_{0.5\mu^2}/\overline{c}_{\eta=6}$ versus β for various values of $\sqrt{Dt}$. Intermediate values can be obtained with sufficient accuracy by interpolation. So $\overline{c}_{0.5\mu^2}$ is found, and if this is added to the experimental count at $0.5\mu^2$, c_{exp}, another point on the volume diffusion profile is obtained.

5. D is obtained from,

$$D = \frac{(\eta_o \times \sqrt{Dt})^2 - 0.5 \times 10^{-8}}{\log (c_{exp} + \overline{c}_{0.5}) - \log (c_{\eta_o})} \times \frac{1}{9.212t} \qquad (18)$$

(t = time of diffusion anneal)

This value of D should agree with the starting value of D if the correct value was chosen in 1; if not, then another starting value must be chosen and the procedure repeated. If a plot of "D initial" versus "D final" is made, then a good estimate of D can usually be made after two trials from the intercept on the line $D_{initial} = D_{final}$.

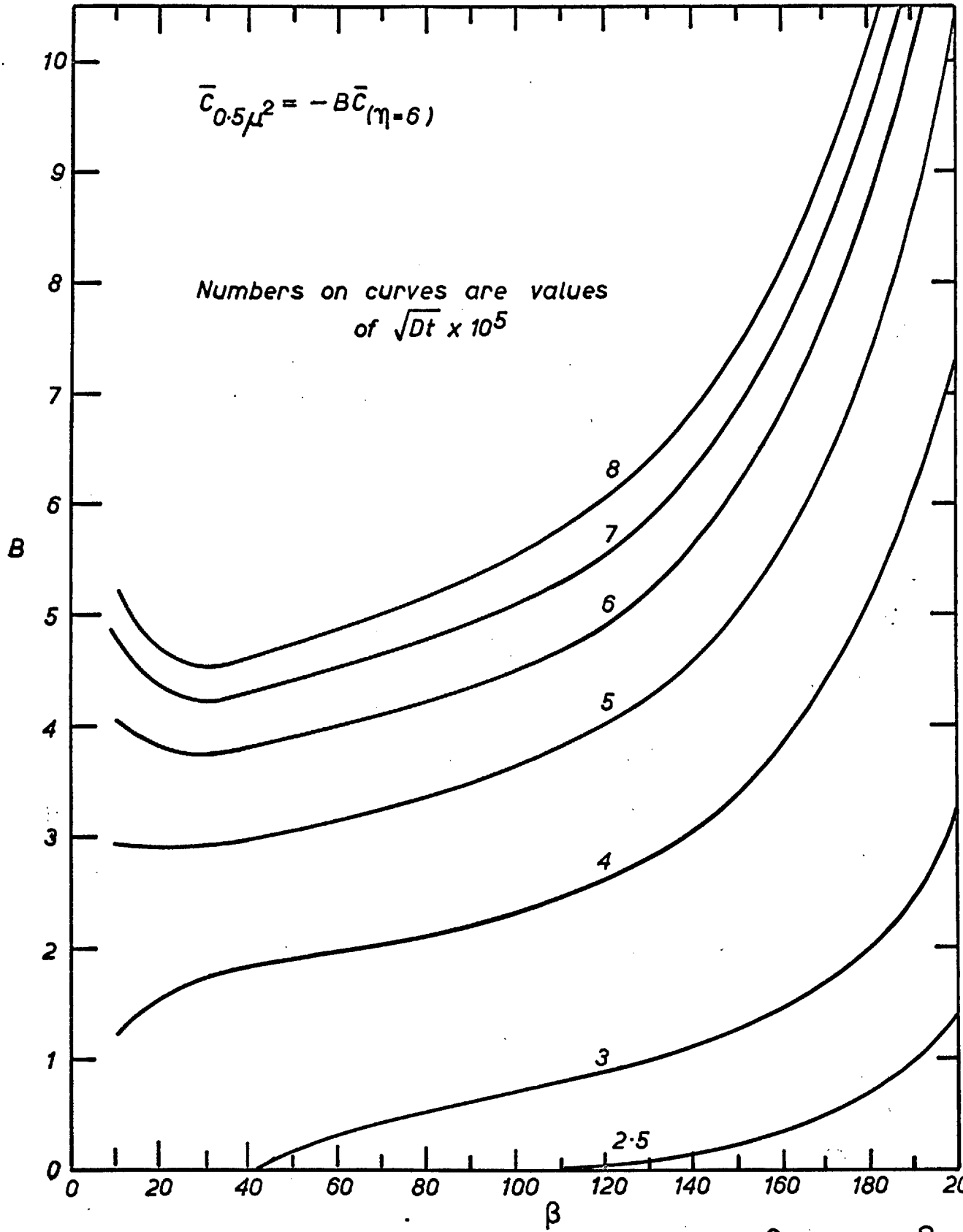


FIG. 22 GRAIN BOUNDARY CONTRIBUTION AT $x^2 = 0.5 \times 10^{-8}$ cm.^{2}

RESULTS

5. RESULTS

In this section typical results will be analysed in terms of the models referred to in section 4. Full figures for each diffusion run in UO_2, UO_{2+x} and ThO_2 are given in the appendix.

5.1 Stoichiometric UO_2 (Table 2). Figure 23 shows the concentration profile of the U-233 tracer after an anneal for 3 days at 1720°C.

There appears to be a bound surface layer when the profile is drawn as "log (concentration)" versus "x^2" (Figure 24). The gradient must be drawn away from the effects of this surface layer, i.e. beyond $0.5\mu^2$ (section 4.2).

A slight 'tail' is also apparent in Figure 24 although the sample is a single crystal. The activity was very low in this part of the profile and the effect could be a spurious one due to poor counting statistics; or it could be penetration down cracks in the single crystal which, although few in number, were visible on the surface of the sample. These probably resulted from mechanical and thermal shock.

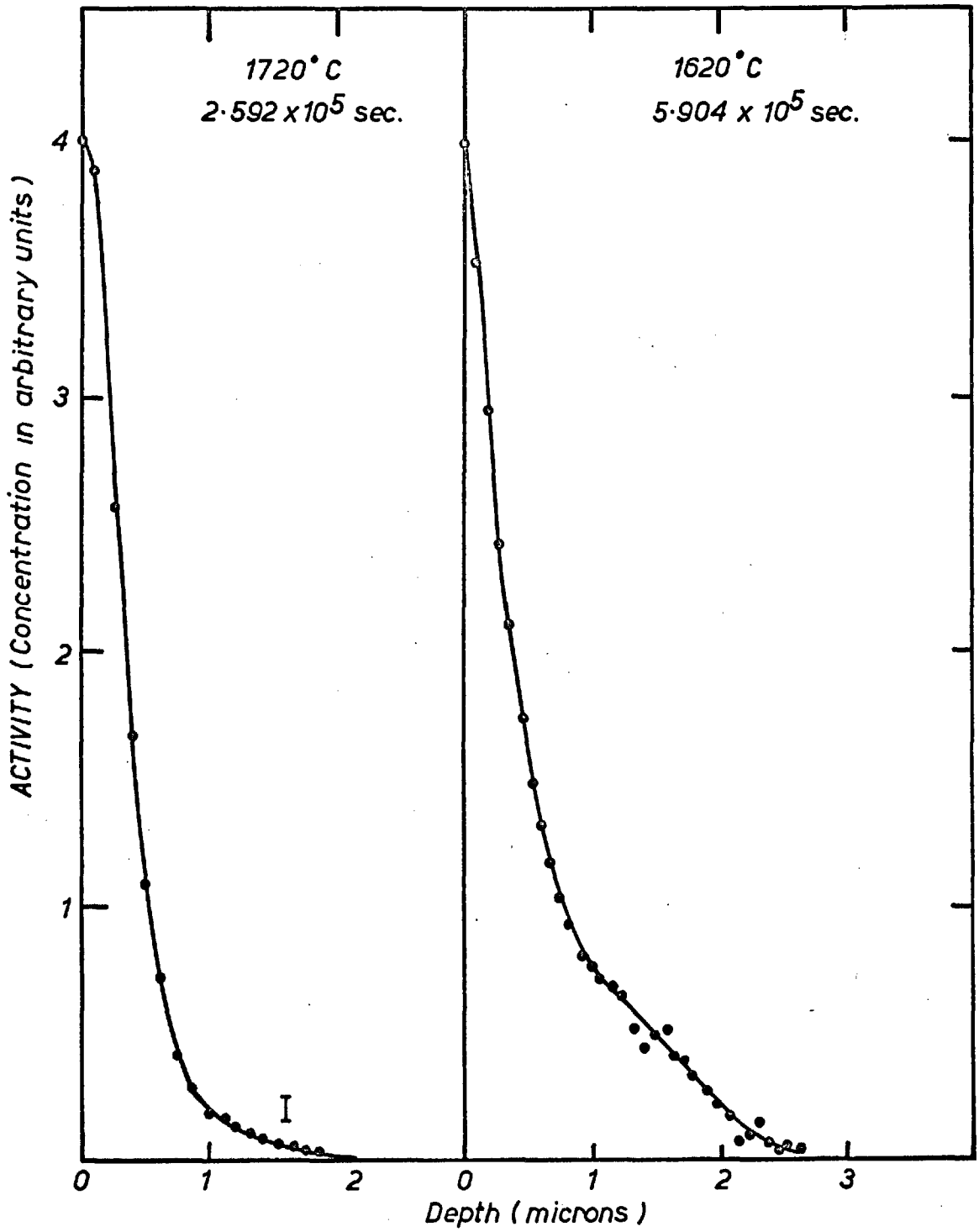


FIG. 23 CONCENTRATION PROFILES FOR TWO STOICHIOMETRIC SINGLE CRYSTALS

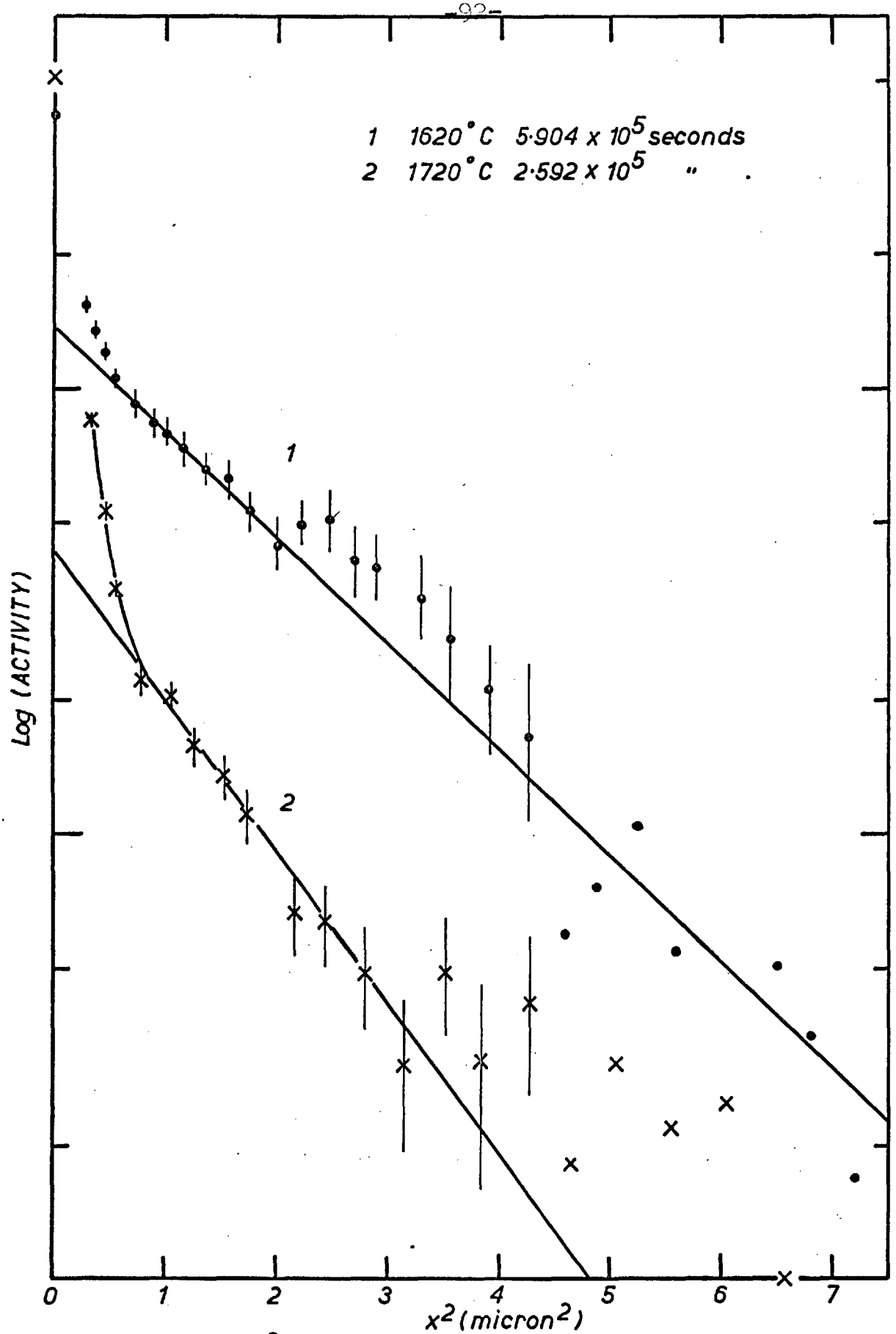


FIG. 24 Log C vs. x^2 FOR STOICHIOMETRIC UO_2 SINGLE CRYSTALS

The line beyond $x^2 = 0.5\mu^2$ was taken to represent the volume diffusion process.

As a check on the bound surface layer the volume diffusion part of the curve was subtracted from the experimental profile to give a spread which was slightly broader than a weightless source (Figure 25). This could be due to the finite thickness of the bound layer (about 0.1μ).

5.1.2 UO_{2+x} single crystal results (Table 3) Good straight lines were obtained for most specimens on a "log C" versus "x^2" plot. Figure 26 shows several typical results. The bound surface layer was much less in evidence in the non-stoichiometric work. This is to be expected because of the higher diffusion coefficients and the higher vapour pressure over UO_{2+x} allowing easier transfer of the tracer across voids.

5.2 Polycrystal Results Before the concentration profiles can be plotted the counts in the lower channels must be corrected to a constant channel width (section 2.3.3). To reduce calculations the concentration profile was averaged on an 'activity' versus 'channel number' plot (appendix 4) and the count every five channels was corrected and reduced by the background

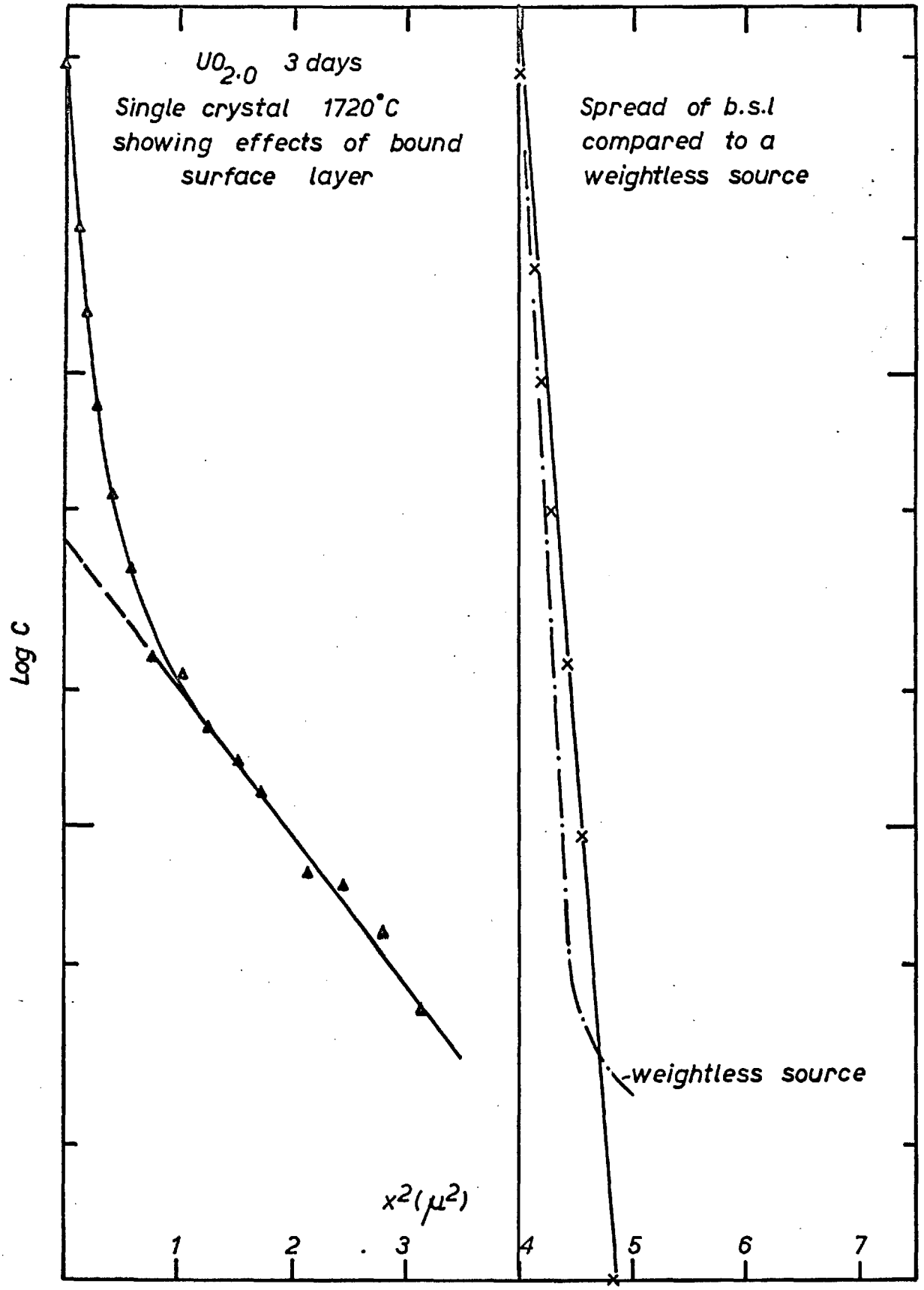


FIG. 25 EXPERIMENTALLY DETERMINED SURFACE LAYER BY SUBTRACTION OF VOLUME DIFFUSION PART

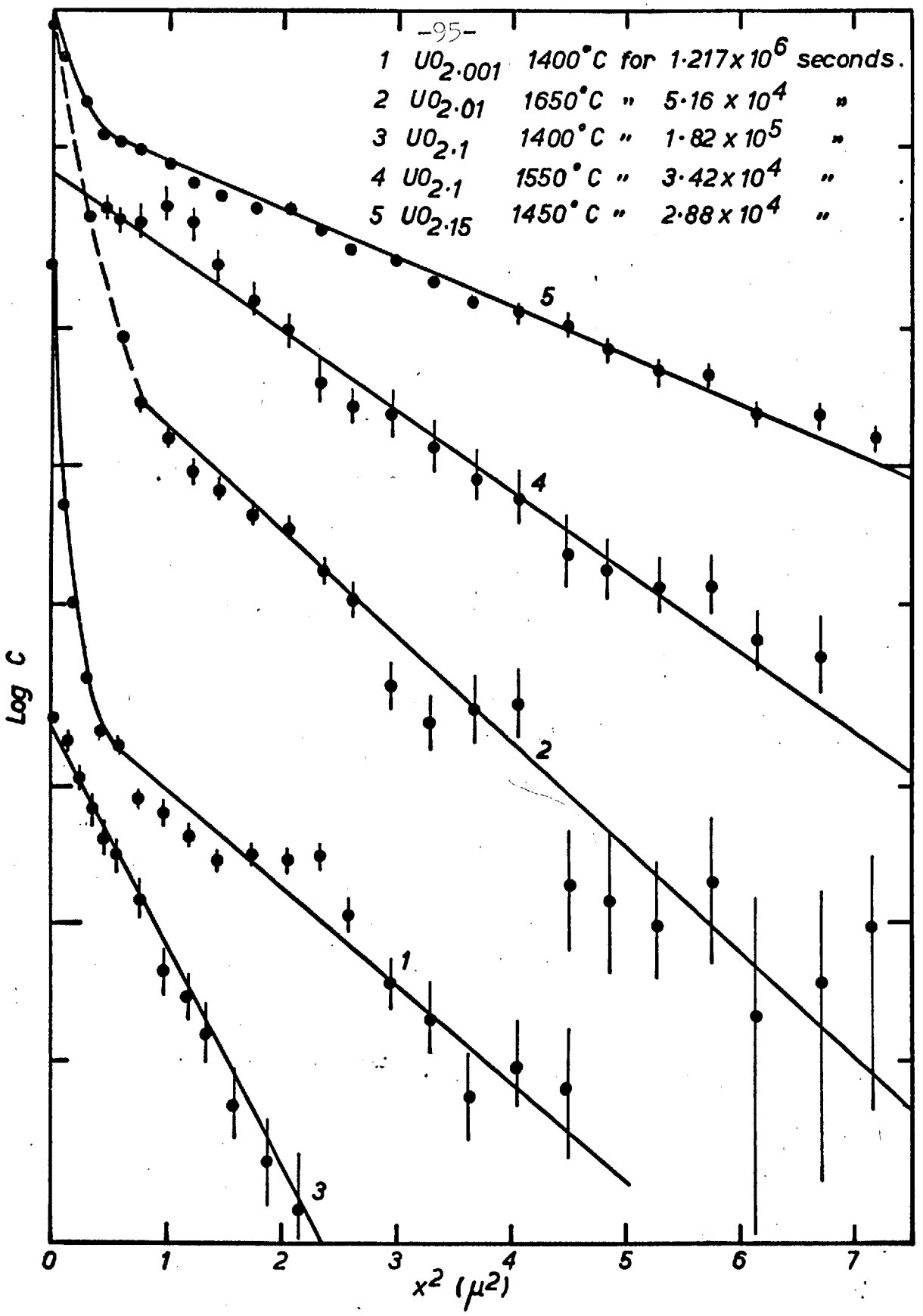


FIG. 26 DIFFUSION IN NON-STOICHOIMETRIC SINGLE CRYSTALS OF URANIA

count to give the tracer concentration. These values were used for the 'log C' versus '$x^{6/5}$' plot.

No smoothing of the profile was performed before the 'log C' versus 'x^2' plots were made and individual counts were corrected as necessary.

5.2.1 Polycrystalline stoichiometric UO_2 results (Table 2) The smallest value of Dt was obtained in the run at 1477°C for 6.912×10^5 sec. Using the method outlined in section 4.4.2 a value of $D = 9 \times 10^{-16}$ was assumed. A second trial with $D = 1.3 \times 10^{-15} cm^2 sec^{-1}$ gave $D_{final} = 1.48 \times 10^{-15}$ The intercept on the line $D_{initial} = D_{final}$ was at $D = 1.15 \times 10^{-15} cm^2 sec^{-1}$ Using this value D_{final} was calculated to be $1.16 \times 10^{-15} cm^2 sec^{-1}$ So $D_{1477°C}$ was found. Figure 27 shows the concentration profile plotted as "log C" versus "x^2", with the volume and grain-boundary contributions shown.

The biggest value of Dt was for the run 1600°C for 2.25×10^6 secs. Here the 'self-consistent' analysis agreed very well with the value of D calculated from the first part (but beyond $0.5\mu^2$) of the "log C" versus "x^2" plot (section 4.4.1) (Figure 28).

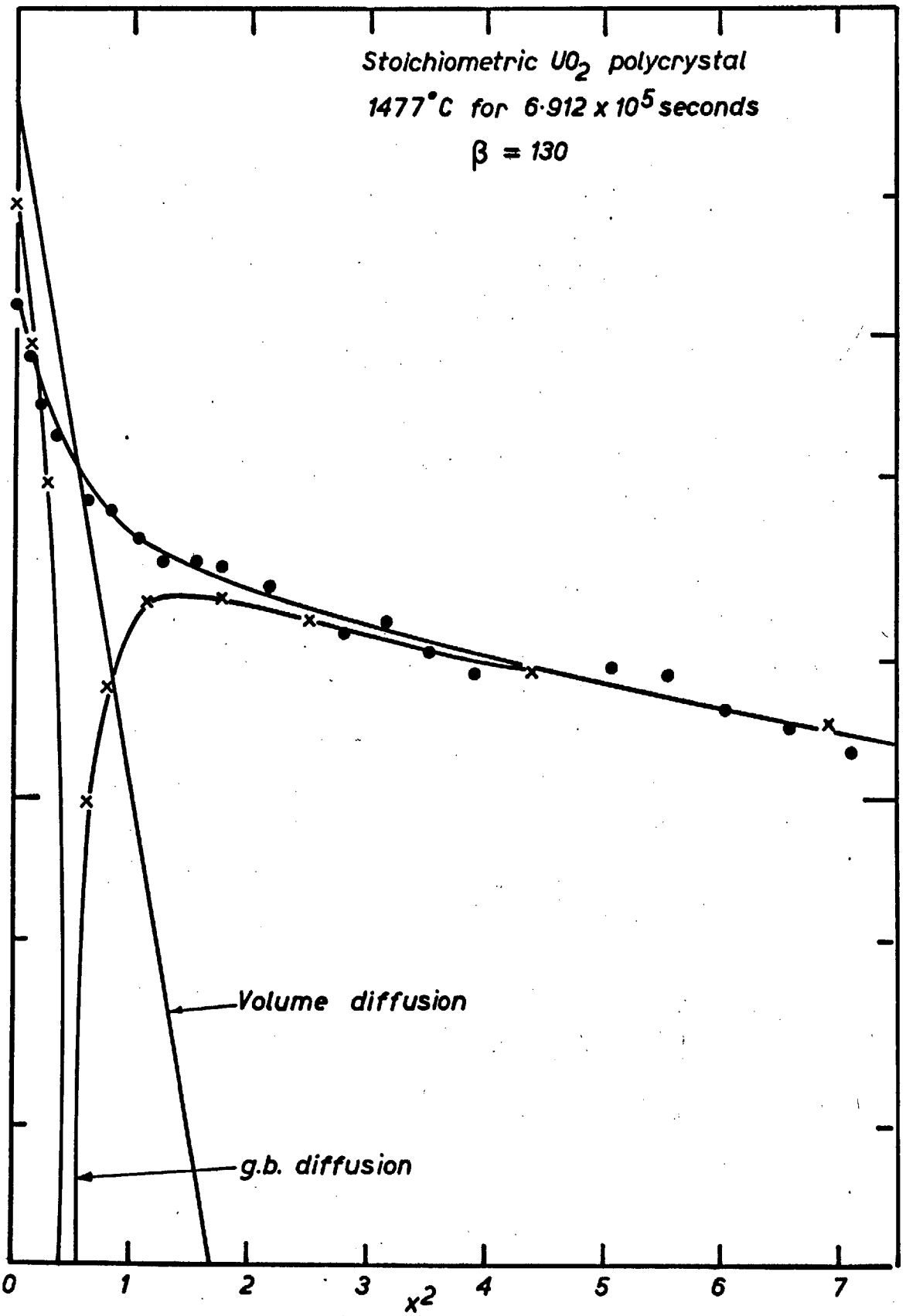


FIG. 27 SUZUOKA ANALYSIS OF POLYCRYSTAL PROFILE

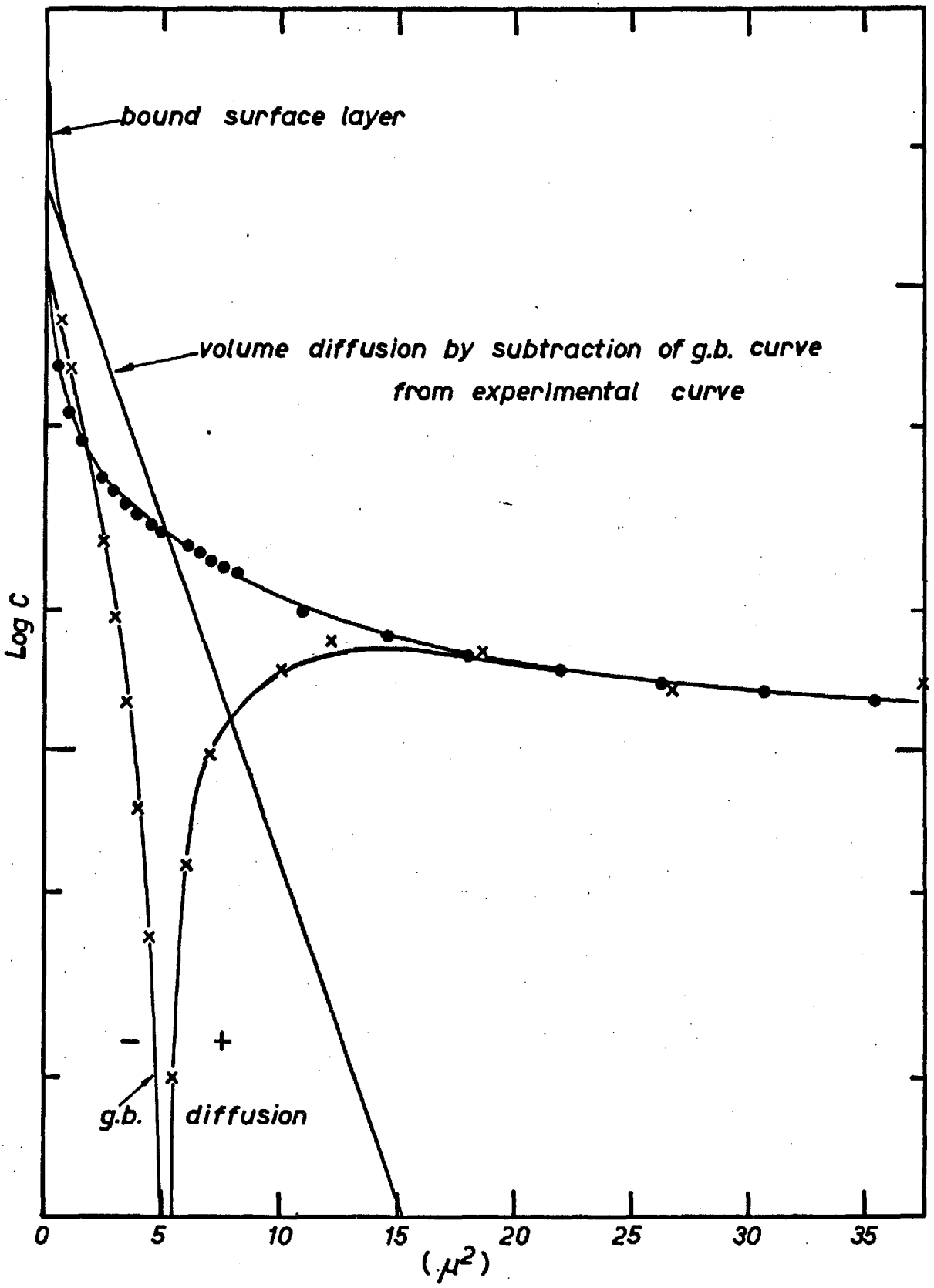


FIG. 28 SUZUOKA ANALYSIS OF U DIFFUSION IN STOICHIOMETRIC UO_2 AT 1600°C FOR $2{\cdot}25 \times 10^6$ SECONDS

For most of the "log C" versus "x^2" plots a straight line section was not apparent near the surface. The best line that could be drawn was a tangent at $0.5\mu^2$ but this could only give the upper limit for D. Using a higher amplification, a channel width of about 0.03μ was employed to determine the concentration profile more precisely near the surface. This helped in some cases, but it was decided that the 'self-consistent' method would give more reliable results.

5.2.2 Polycrystalline UO_{2+x} results (Table 3). The 'self-consistent' analysis was applied in the determination of the diffusion coefficients. In most cases the results agreed with the value of D from the first straight line section of "log C" versus "x^2." Differences were observed with low and high values of Dt. The latter can be accounted for by a large grain-boundary contribution strongly depleting the surface regions and markedly affecting a shallow volume diffusion gradient. In several samples the concentration normally increasing towards the surface, actually started to decrease before reaching the surface, showing large depletion of the surface layers by the grain boundaries. Several profiles are shown in Figure 29.

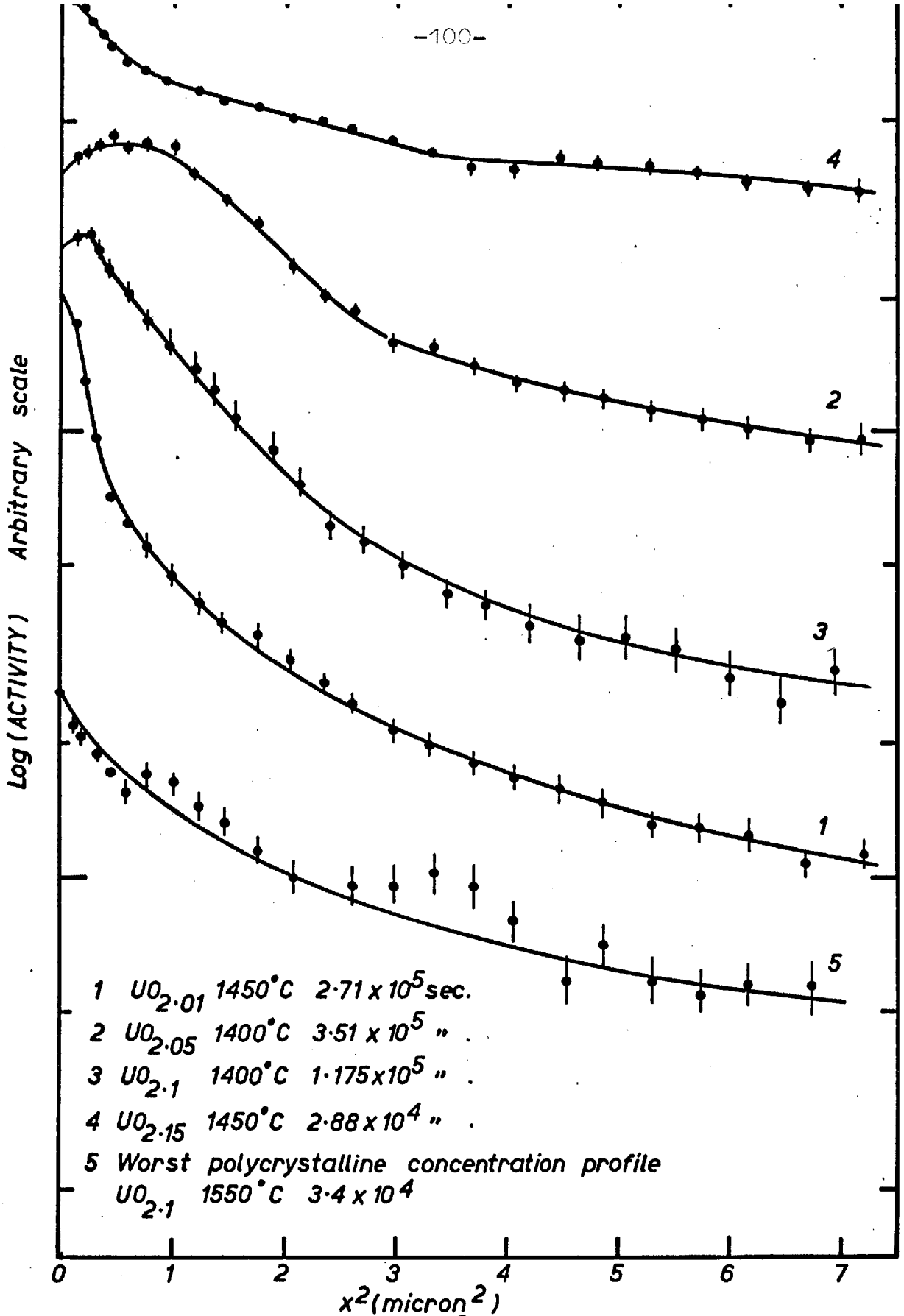


FIG.29 Log(Concentration) vs. x^2 FOR SEVERAL POLYCRYSTALLINE NON-STOICHIOMETRIC UO_2 DIFFUSION SAMPLES

5.2.3 Th in UO_2 results (Table 4). The analysis of the concentration profiles of Th^{230} diffused into $UO_{2.0}$, $UO_{2.01}$ and $UO_{2.1}$ followed exactly the same lines as U^{233} in urania. (Sections 5.2.1 and 5.2.2).

5.2.4 Polycrystalline ThO_2 results (Table 5) All graphs of "log C" versus "x^2" for Th diffusion in ThO_2 were straight lines except for the effect of a bound surface layer. The profiles could be explained satisfactorily in terms of volume diffusion alone. The grain size was much larger than in UO_2 so grain-boundary effects were expected to be much smaller. Some results are shown in Figure 30.

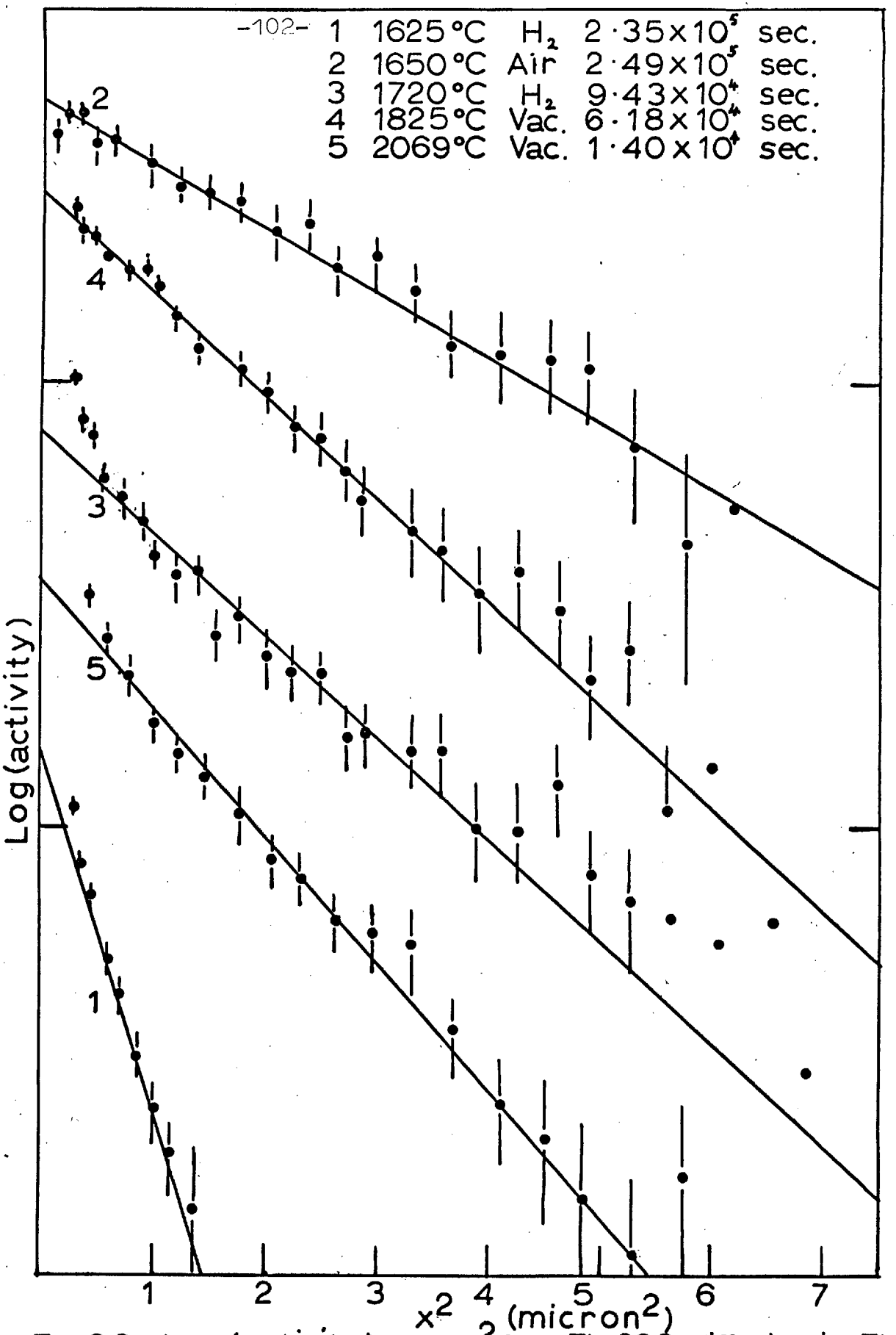


Fig.30. Log(activity) vs. x^2 for Th-230 diffusion in ThO_2

TABLE 2 U^{233} diffusion in stoichiometric UO_2

Material	Plating Method	Temperature °C	Time sec.	$D_v \times 10^{15}$ $cm^2 sec^{-1}$	$Log_{10}\Delta$
P(M)	a	1477	6.912×10^5	1.2 (0.2)	4.9
P	b	1490	2.25×10^6	1.4 (0.1)	5.02
				1.38(0.07)	5.1
P(M)	a	1547	6.912×10^5	2.45(0.2)	4.76
S	c	1584	8.691×10^5	2.86(0.3)	-
P(M)	a	1600	4.32×10^5	4.2 (0.5)	4.8
P	c	1600	2.25×10^6	3.30(0.1)	5.21
				2.15(0.15)	5.23
S	d	1620	5.904×10^5	7.5 (1.0)	-
P(M)	a	1650	5.184×10^5	4.825(0.3)	4.96
S	b	1720	2.592×10^5	13.0 (3)	
				18.2 (4)	-

P Polycrystal

S Single crystal

(M) Results marked (M) were diffusion anneals performed by McNamara,[1] but analysed here using the self-consistent method.

a Vacuum sublimation from a tungsten filament

b " " " " tantalum filament

c Tetraethyleneglycol method

d Perchlorate method

Numbers in brackets are errors estimated from the slope of "log C" vs. "x^2" or from self-consistent method.

Table 3

U^{233} diffusion in UO_{2+x}

Composition O/U ratio	Material	Temp. °C	Time sec.	$D_v \times 10^{15}$ $cm^2 sec^{-1}$	$\log_{10}\Delta$
2.001	S	1400	4.248×10^5	4.9(3)	-
	S	1400	1.217×10^6	4.2(0.7)	-
	P	"	"	3.0(0.15)	4.87
2.01	S	"	3.465×10^5	6.0(1.1)	-
(2.1 to 2.01)	S	"	"	6.1(1.5)	-
	P	"	4.295×10^5	1) 5 (3)	5.32
				2) 7 (3)	-
	P	"	7.931×10^5	1) 5 (3)	5.36
				2) 4 (1.5)	-
	P	"	1.1396×10^6	4.3(1)	4.82
	S	1450	2.709×10^5	14.5(3)	-
	P(d)	"	"	13.5(1.1)	5.41
	S	1550	1.626×10^5	32 (6)	-
	P	"	"	43 (7)	5.27
	S	1650	1.89×10^4	180(50)	-
	P	"	"	265(10)	5.27
	S	"	5.16×10^4	91.5(5)	-
	P	"	"	260(15)	4.65
2.03	P	1500	1.048×10^5	1)55(2)	4.61
				2)56(5)	4.64
	P	1600	1.74×10^4	1)200(10)	4.20
				2)250(50)	4.80
2.05	P	1400	1.98×10^5	1)24(5)	4.80
				2)25(5)	-
	P	"	3.51×10^5	1)10(2)	4.97
				2)10(2)	-
2.1	S	"	1.80×10^5	15(2)	-
	S	"	1.817×10^5	13(2)	-
	P	"	2.012×10^5	1)22(1)	5.13
		"		2)20(1)	-

Composition O/U ratio	Material	Temp °C	Time sec.	$D_v \times 10^{15}$ $cm^2 sec^{-1}$	$\log_{10} A$
2.1	S	1400	3.617×10^5	14.5(2)	-
	P	"	3.812×10^5	22.5(2)	5.63
	P	"	3.829×10^5	25(2)	-
	S	1477	2.79×10^4	160(40)	-
	S	"	9.18×10^4	170(50)	-
	P	"	"	110(10)	4.14
	P	"	1.026×10^5	1)110(10)	4.5
				2)110(10)	-
	S	1550	1.80×10^4	190(20)	-
	P	"	"	190(20)	4.77
	S	"	3.42×10^4	181(20)	-
	P	"	"	190(40)	4.75
	S	1650	4.74×10^3	1640(150)	-
	P	"	"	1400(200)	4.69
2.12	S	1400	9.33×10^4	55(2)	-
	P	"	"	35(5)	4.74
2.15	S(d)	1350	9.84×10^4	70(7)	-
	S	1400	3.45×10^4	240(30)	-
	P	"	"	180(20)	5.15
	S	"	5.28×10^4	85(20)	-
	P	"	"	170(40)	-
	P	"	9.12×10^4	210(35)	4.38
	S	1450	2.88×10^4	354(23)	-
	P	"	"	300(30)	5.26

Symbols. See footnote to table 2.

Table 4

Th^{230} diffusion in Urania

Comp.O/U ratio	Material	Temp. °C	Time sec.	$D_v x10^{15}$ $cm^2 sec^{-1}$	$\log_{10}\Delta$
stoic	P	1620	$5.904x10^5$	4.7(0.1)	5.1
2.01	S	1600	$5.574x10^3$	118(5)	-
2.1	P	1620	$5.7x10^3$	1)40(1)	4.69
				2)40(6)	4.78

Table 5

Th^{230} diffusion in ThO_2

Atmosphere	Temperature °C	Time sec.	$D_v x10^{15}$ $cm^2 sec^{-1}$
air	1584	$4.071x10^5$	16.4(5)
H_2	1625	$2.349x10^5$	22.6(2)
H_2	1640	$2.214x10^5$	20.2(2)
CO/CO_2	1640	$4.383x10^5$	15.2(2)
air	1650	$2.49x10^5$	1) 29(5)
			2)40.7(5)
H_2	1660	$8.94x10^4$	20.8(3)
H_2	1670	$1.548x10^5$	1)31.4(1)
			2) 30(5)
H_2	1720	$9.432x10^4$	59(5)
vac	1825	$6.18x10^4$	98(8)
vac	2069	$1.398x10^4$	1)400(40)
			2)380(40)
vac	1890	$3.282x10^4$	134(35)

Table 6

Decrease in Surface Activity Results in UO_{2+x}

Composition	Material	Temp. °C	Time sec.	$D_{D.S.A.} \times 10^{4}$ $cm^2 sec^{-1}$
2.001	S	1400	4.248×10^5	6.15
	P	"	"	7.30
2.01	S	"	3.465×10^5	20
(2.1to2.01)	S	"	"	40
	S	1550	1.626×10^5	36.7
	P	"	"	27.5
	S	1650	5.16×10^4	260
	S	"	1.89×10^4	223
	P	"	"	468
2.05	P	1400	1.98×10^5	1)142
				2) 59
	P	"	3.15×10^5	1) 46
				2)500
ditto different range				1) 65
				2)700
	P	1400	6.932×10^5	51
2.1	S	"	1.80×10^5	120
	P	"	2.838×10^4	1)812
				2)524
	P	"	1.1748×10^5	1)245
				2)227
	S	1477	9.18×10^4	300
	S	"	2.79×10^4	630
	P	"	1.026×10^5	1)135
				2)155
	S	1550	3.42×10^4	545
	S	"	1.80×10^4	713
	P	"	"	4860
	S	1650	7.2×10^3	47000
	S	"	4.74×10^3	18 0

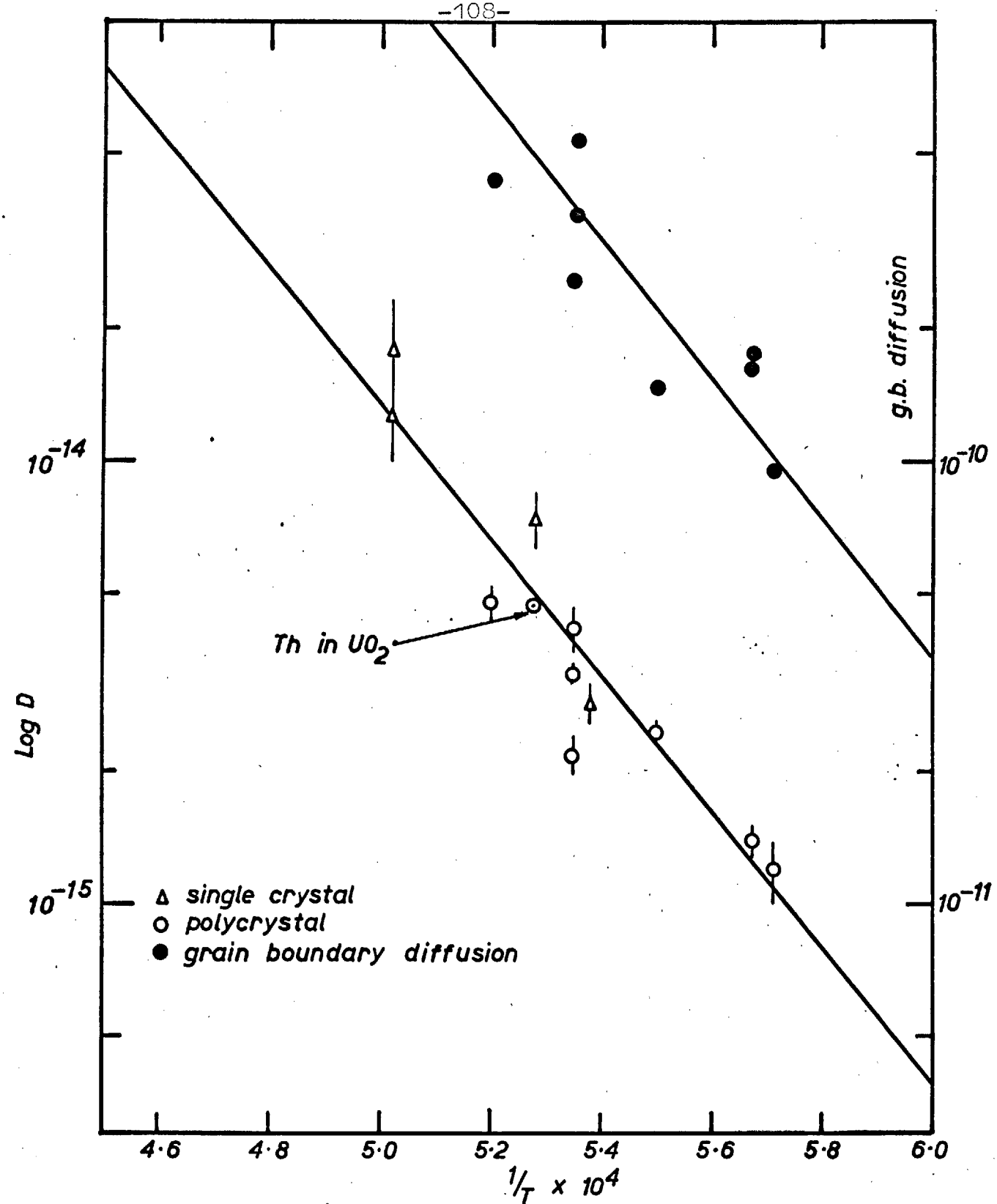


FIG. 31 Log D vs. $^1/_T$°K FOR U DIFFUSION IN STOICHOIMETRIC UO_2

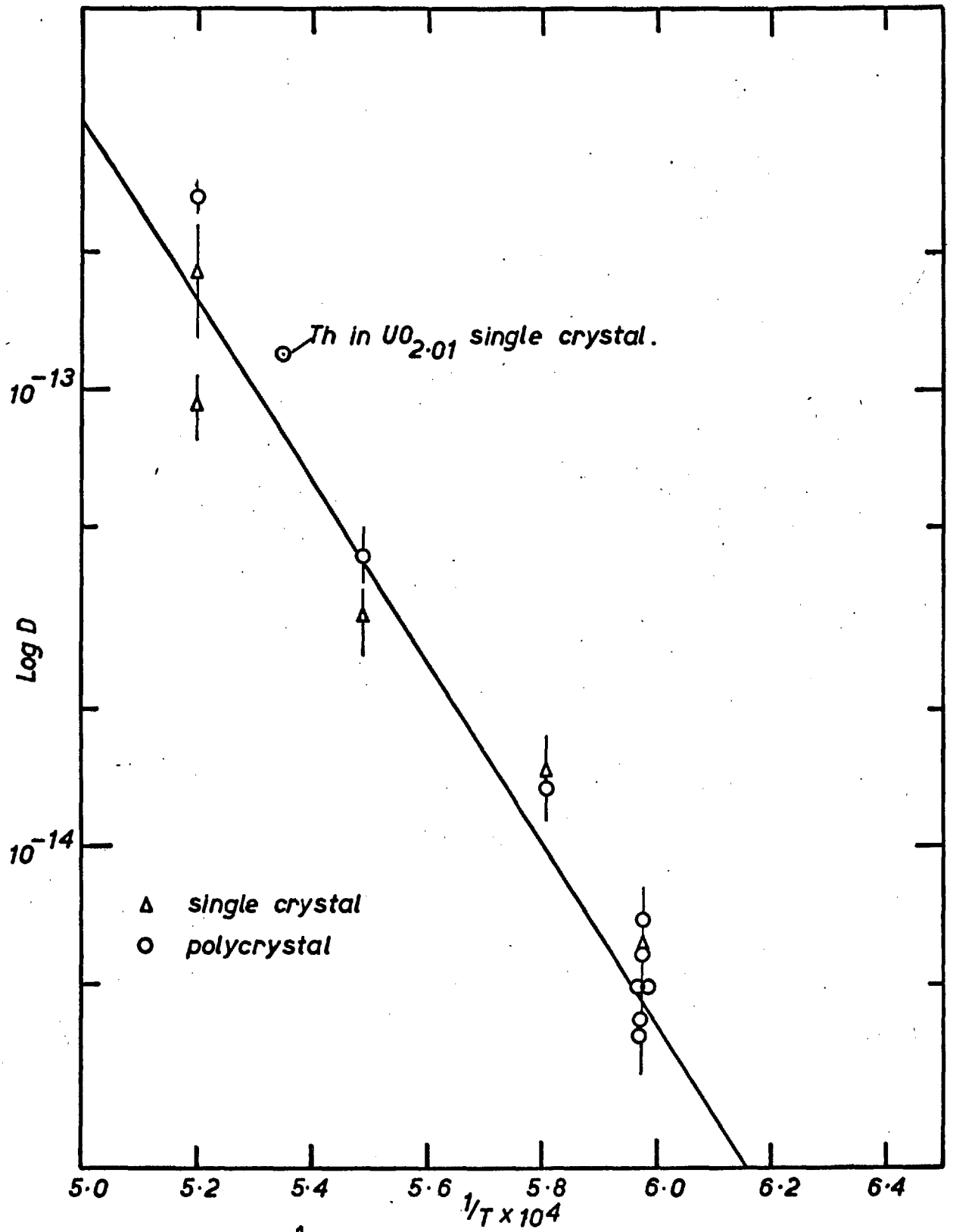


FIG.32 Log D vs $^{1}/_{T}$°K FOR U DIFFUSION IN $UO_{2\cdot01}$.

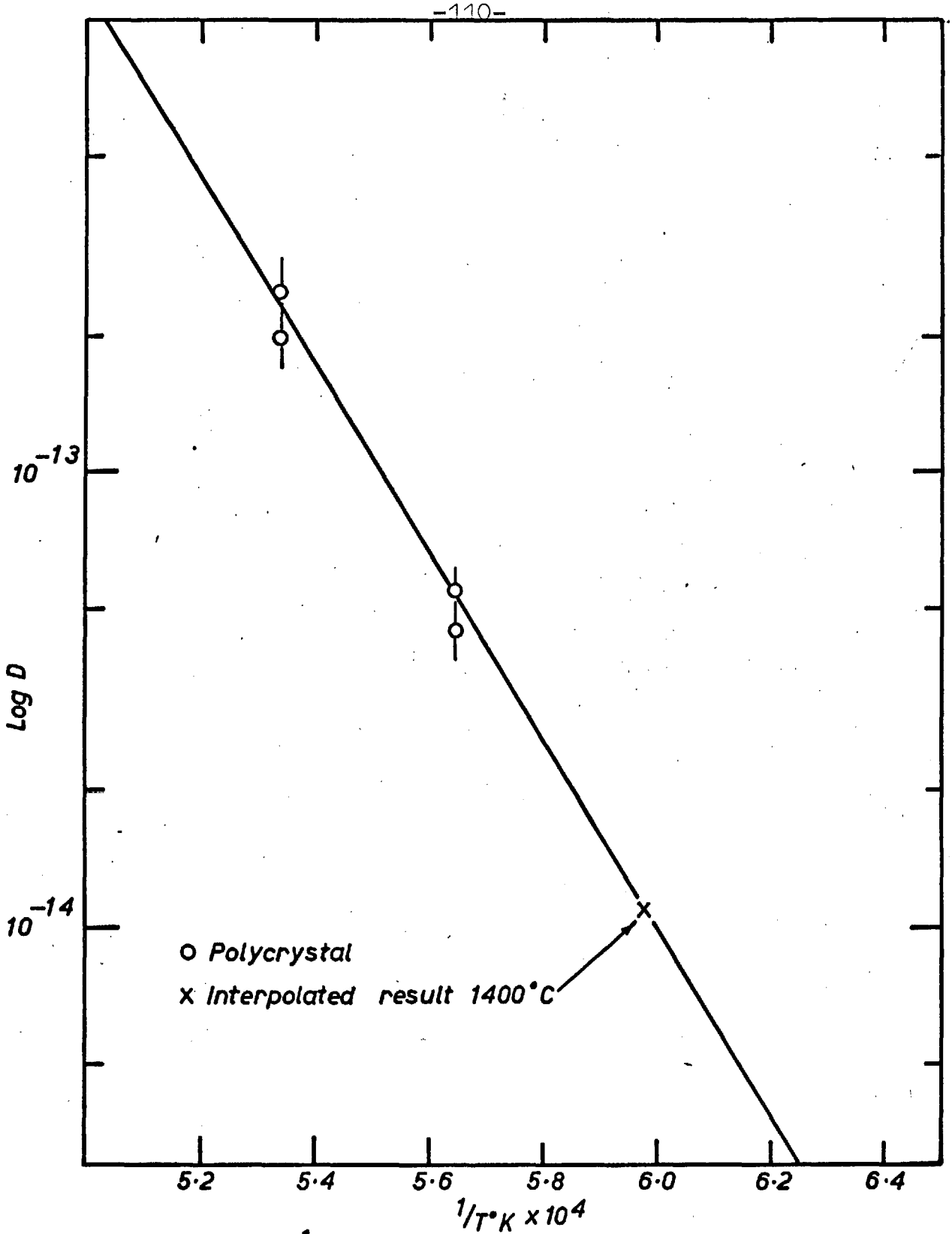


FIG. 33 Log D vs $^1/_{T°K}$ FOR U DIFFUSION IN $UO_{2\cdot03}$

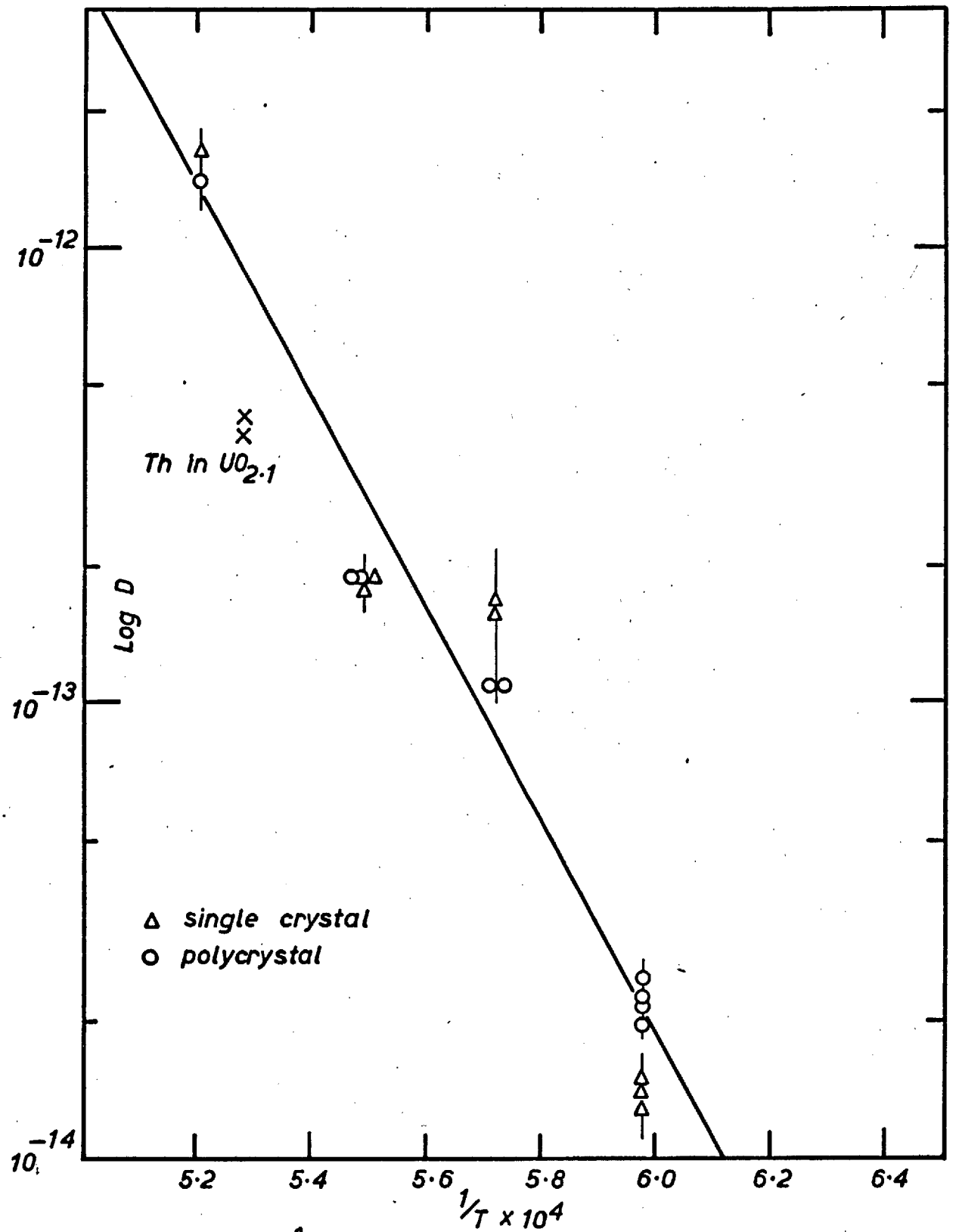


FIG. 34 Log D vs. $1/T$ FOR U DIFFUSION IN $UO_{2\cdot1}$

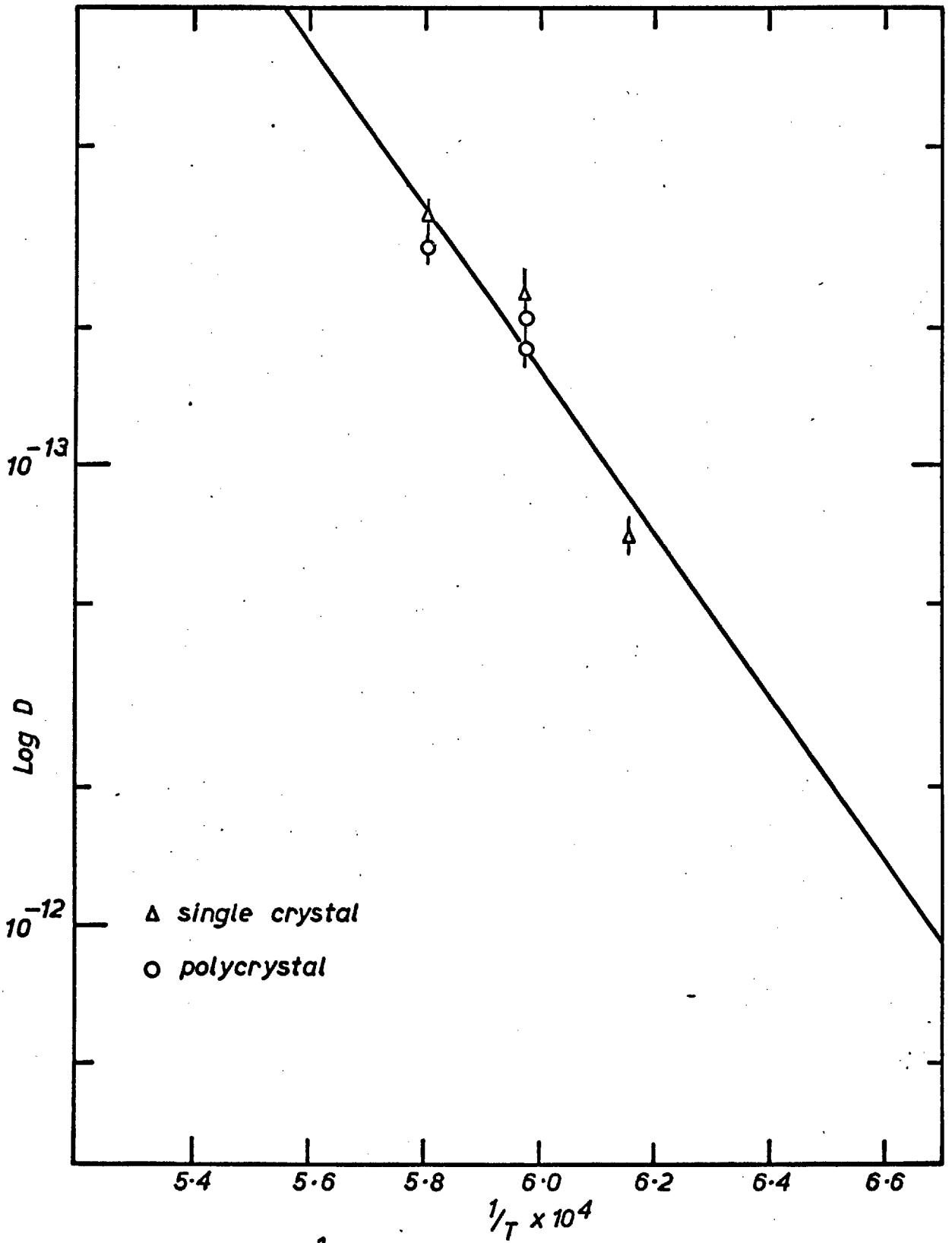


FIG. 35 Log D vs. $1/T°K$ FOR U DIFFUSION IN $UO_{2\cdot15}$

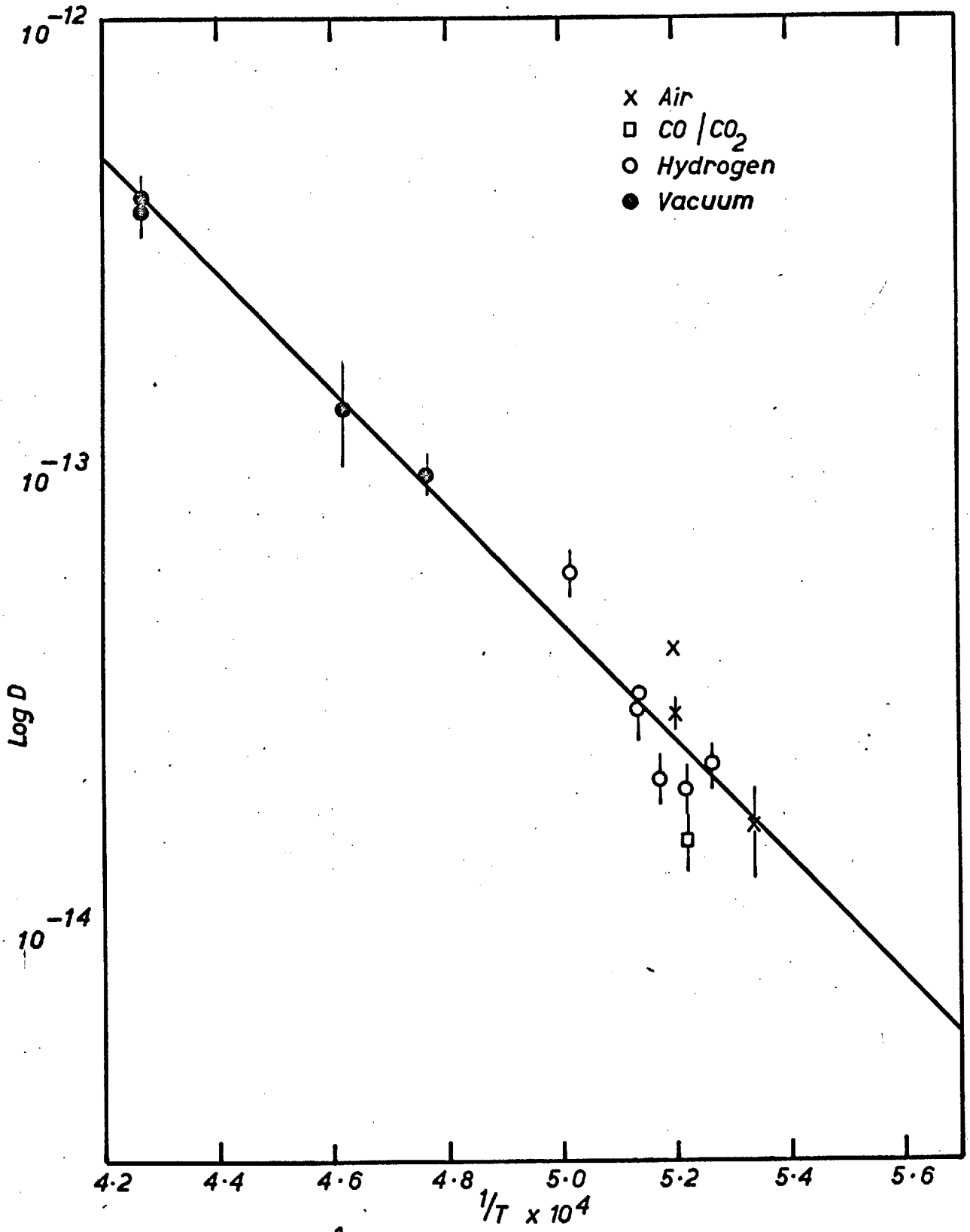


FIG.36 Log D vs. $1/T°K$ FOR THORIUM DIFFUSION IN ThO_2

5.3.1 D_o and the activation energy Least mean squares analyses of the results give the following equations for volume diffusion. (Figs.31-36).

U in UO_2 1477 - 1720°C

$$D_{2.0} = 6.06 \times 10^{-7} \exp(-70,000/RT) \quad (19)$$
$$\log D_o = -6.22 \pm 0.9. \quad Q = 70 \pm 8 \text{ kcal}$$

U in $UO_{2.01}$ 1400 - 1650°C

$$D_{2.01} = 2.04 \times 10^{-3} \exp(-88,900/RT) \quad (20)$$
$$\log D_o = -2.69 \pm 0.66. \quad Q = 89 \pm 2 \text{ kcal}$$

U in $UO_{2.03}$

$$D_{2.03} = 2.79 \times 10^{-2} \exp(-94,900/RT) \quad (21)$$
$$\log D_o = -1.55 \pm 0.1 \quad Q = 95 \pm 3.5 \text{ kcal}$$

U in $UO_{2.1}$ 1400 - 1650°C

$$D_{2.1} = 1.09 \exp(-105,000/RT) \quad (22)$$
$$\log D_o = 0.036 \pm 0.9 \quad Q = 105 \pm 7 \text{ kcal}$$

U in $UO_{2.15}$ 1350 - 1450°C

$$D_{2.15} = 6.79 \times 10^{-3} \exp(-80,900/RT) \quad (23)$$
$$\log D_o = -2.17 \pm 1.7 \quad Q = 81 \pm 13 \text{ kcal}$$

Th in ThO_2 1600 - 2100°C

$$D_{ThO_2} = 1.25 \times 10^{-7} \exp(-58{,}800/RT) \quad -24$$

$$\log D_o = -6.90 \pm 0.3 \quad Q = 59 \pm 3 \text{ kcal}$$

5.3.2 Grain-boundary diffusion Figure 31 shows "log D_b" versus "1/T" for stoichiometric UO_2. The activation energy is about the same as that for volume diffusion.

The ratio $\triangle = D_b/D$ is shown in tables 4 and 5. Generally $\triangle = 10^5$ for UO_2 and UO_{2+x}. No good estimate of the activation energy for grain-boundary diffusion could be made for UO_{2+x} as the results were not very reproducible.

5.4 Dependence of D on p_O and x Figure 37 shows "log D" versus "x" (in UO_{2+x}) at 1400°C. A very small departure from the stoichiometric composition produces a large change in the cation diffusion coefficient. When plotted as "log D" versus "log x" the relationship was found to be, (Figure 38) (O/U = 2.001 to 2.1),

$$\log D_{1400^\circ C} = 0.434 \log x - 13.31 \quad -25$$

$$(0.434 \pm 0.056; \quad 13.31 \pm 0.1)$$

When plotted as "log D" versus "log p_{O_2}" (Figure 39)

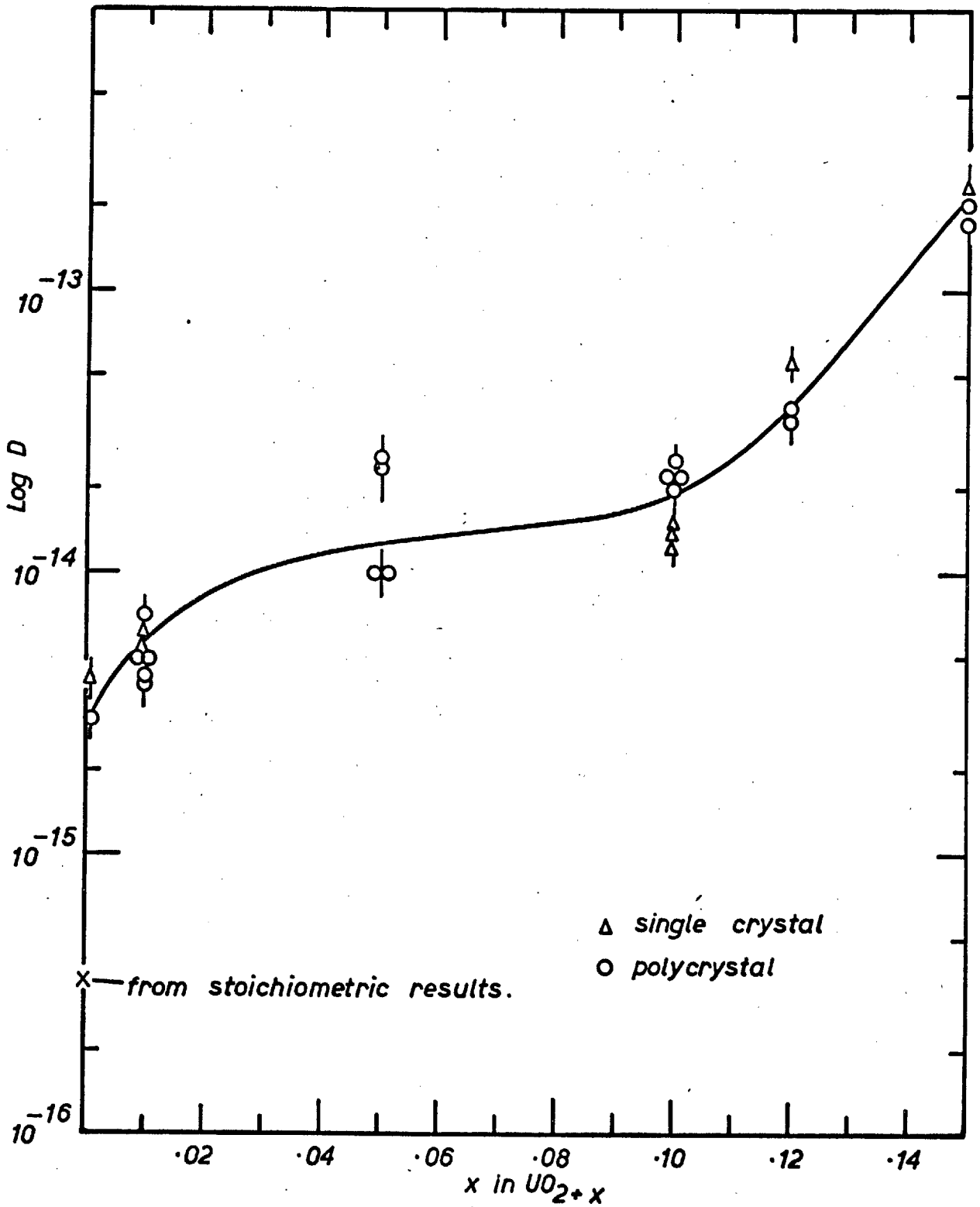


FIG. 37 Log D vs. x AT 1400°C

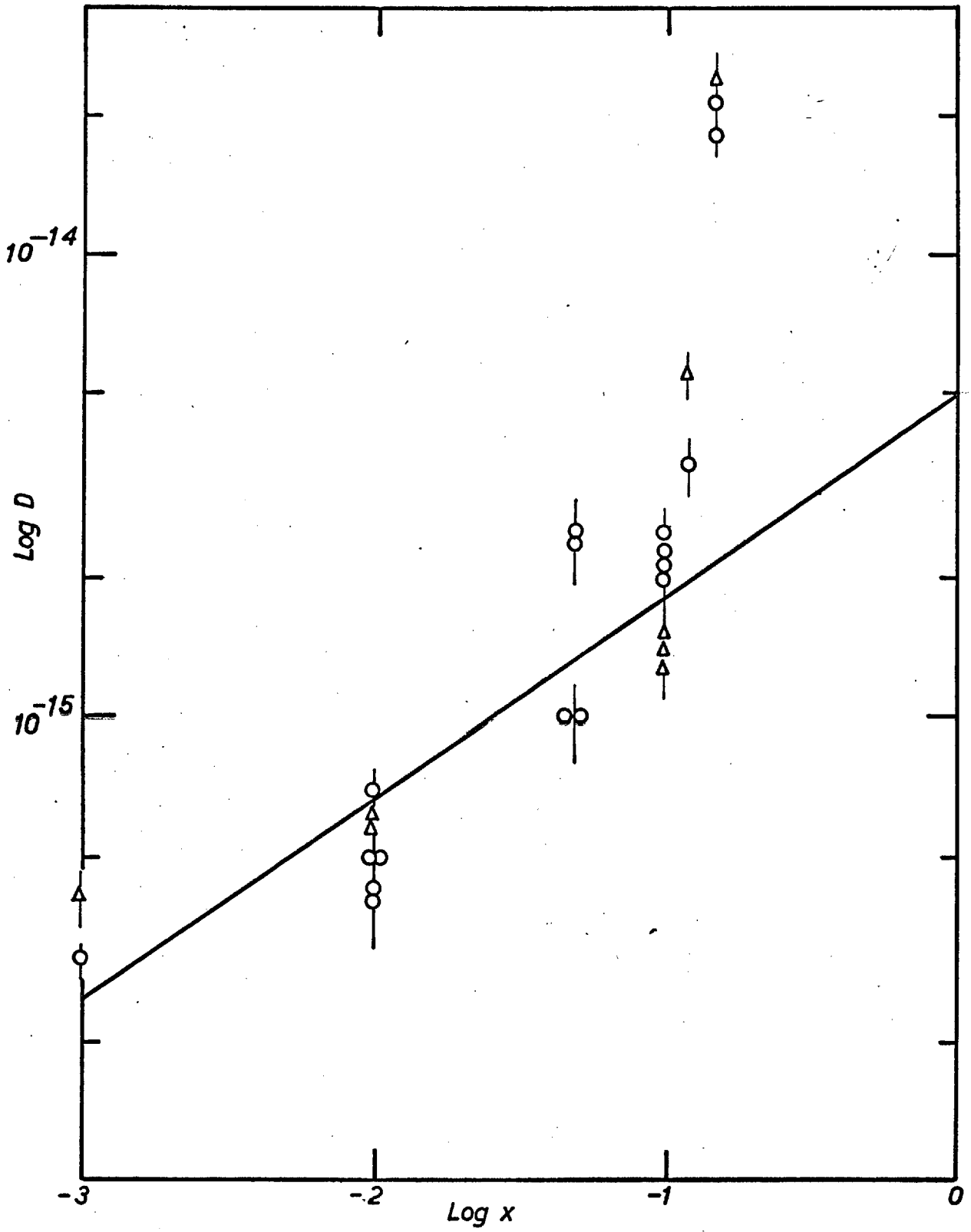


FIG. 38 Log D vs. Log x AT 1400°C.

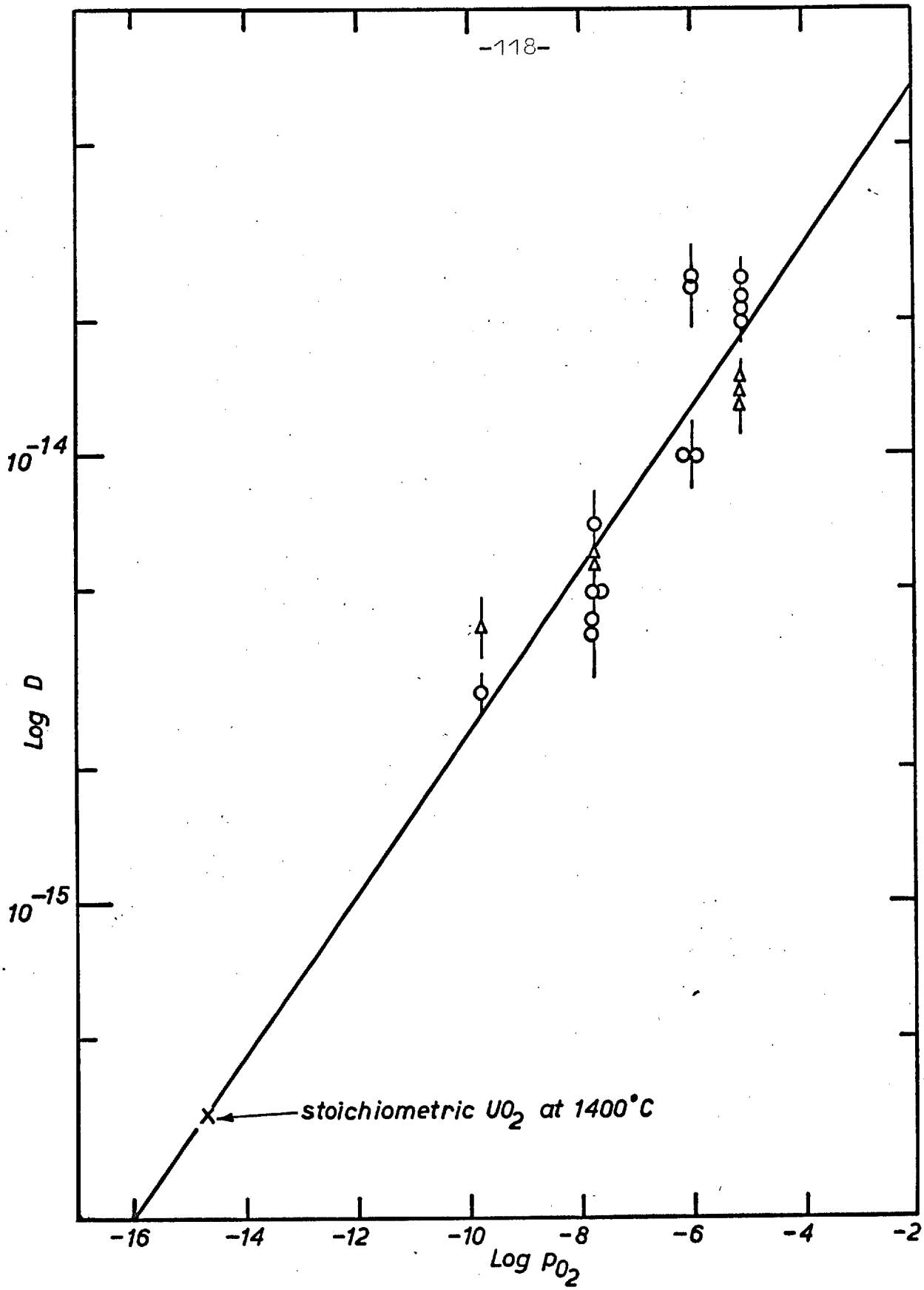


FIG. 39 Log D vs. Log p_{O_2} AT 1400°C

(O/U = 2.001 to 2.1)

$$\log D_{1400^{\circ}C} = 0.184 \log p_{O_2} - 12.78 \quad (26)$$

$$(0.184 \pm 0.021;\ 12.78 \pm 0.14)$$

5.5 D.S.A. Results Decrease in surface activity measurements were made for a range of compositions, temperatures and times in UO_{2+x}. The results are shown in Table 6. A large scatter was observed in these measurements and a discussion of the value of these results will be found in section 5.8.

5.6 Discussion of results and errors In the following sections the value of the results will be discussed. All three materials, UO_2, UO_{2+x} and ThO_2 will be discussed together, and special cases will be referred to as necessary.

5.6.1 Composition of UO_2 and UO_{2+x} (Section 3.5.2) Even under an atmosphere of pure, dried H_2 "x" will have a finite value, but only the upper limit is known. (section 3.5.1). This value of x will probably change with temperature since the equilibrium partial pressures over UO_{2+x} for very small values of x are not known and no attempt could be made to keep the composition constant.

Assuming that the alumina reaction tube does not admit more oxygen at the higher temperatures (it is jacketed with forming gas) then the H_2/H_2O ratio measured with the oxygen meter at 1250°K can be used to estimate p_{O_2} at the temperatures of the diffusion anneals,

Table 7

Estimated p_{O_2} in H_2 atmosphere

Temperature	-log p_{O_2}
977°C	-19.95
1400°C	-14.64
1500°C	-13.77
1600°C	-12.96
1650°C	-12.58
1700°C	-12.24

If it assumed that the relationship between "log p_{O_2}" and "log x" is the same up to 1700°C as it is from 1100°C to 1400°C (as given by Aukrust et al) then the approximate value of x can be found over the range of p_{O_2} and temperatures used for the stoichiometric runs.

Table 8

Estimate of x in UO_{2+x} in H_2 atmosphere

Temperature	log x	x
1400°C	-5.21	6.2×10^{-6}
1500°C	-4.95	1.1×10^{-5}
1600°C	-4.79	1.6×10^{-5}
1700°C	-4.62	3.0×10^{-5}

The values of x in Table 8 are only approximate and indicate that the value of x could change by a factor of about 3 in the stoichiometric experiments. Roughly, using equation 25, a change of 0.3 in log x (1500°C to 1700°C) would correspond to an error of 0.12 in log D at 1700°C compared to log $D_{1500°C}$. This would lower the activation energy calculated by about 7%. This would mean that both U and O have the same activation energies for diffusion in stoichiometric UO_2.

The composition is fixed for the non-stoichiometric experiments and the error in log x from 1400°C to 1650°C is not more than 0.15 for $UO_{2.01}$ and about 0.02 for $UO_{2.1}$ (section 3.5.2). These give changes in activation energies which are within the experimental error.

Thoria diffusion anneals were carried out under a wide range of oxygen potentials at 1600 and 1650°C. No significant change in the cation diffusion coefficient was observed when annealed in H_2, CO/CO_2 or air.

5.6.2 Vaporization of the tracer The experimental assembly for the UO_{2+x} diffusion anneals was such that the active faces were quite well protected. It was found that the results were just as reproducible as those for the diffusion couples used for stoichiometric UO_2. In one experiment with two single crystals one pellet was well protected and the other not at all. Both gave the same value for D from a "log C" versus "x^2" plot (the D.S.A. measurement gave two D's differing by a factor of 2).

The evaporation will be from the surface layer alone. In the first few seconds of the diffusion anneal a concentration profile is established beyond the surface and this portion of the tracer can continue to diffuse in with, it is assumed, little influence from evaporation except that the amount of tracer coming from the surface will be slightly less.

5.6.3 The calculation of D The agreement between single crystal measurements and the volume diffusion coefficient calculated from the polycrystalline concentration profiles was, in general, very good. The single crystal profiles and the large grain ThO_2 polycrystals were expected to follow equation 1 and the fit was very good except for cases in which there was a bound surface layer.

According to the Suzuoka model the first part of the profile for polycrystalline samples should be mainly volume diffusion. As stated above, these results accorded well with single crystal results and the first part of the profile on a "log C" versus "x^2" plot showed an extending straight line section near the surface as the time of the anneal increased (Figure 40).

Thus it is reasonable to suppose that these results do indeed represent the volume diffusion process in urania.

5.6.4 Compatibility of the diffusion measurements Since it was possible that diffusion in nominally stoichiometric UO_2 was governed by the prevailing oxygen partial pressure it was thought expedient to see how the results fitted on "log D" versus "log p_{O_2}" plots.

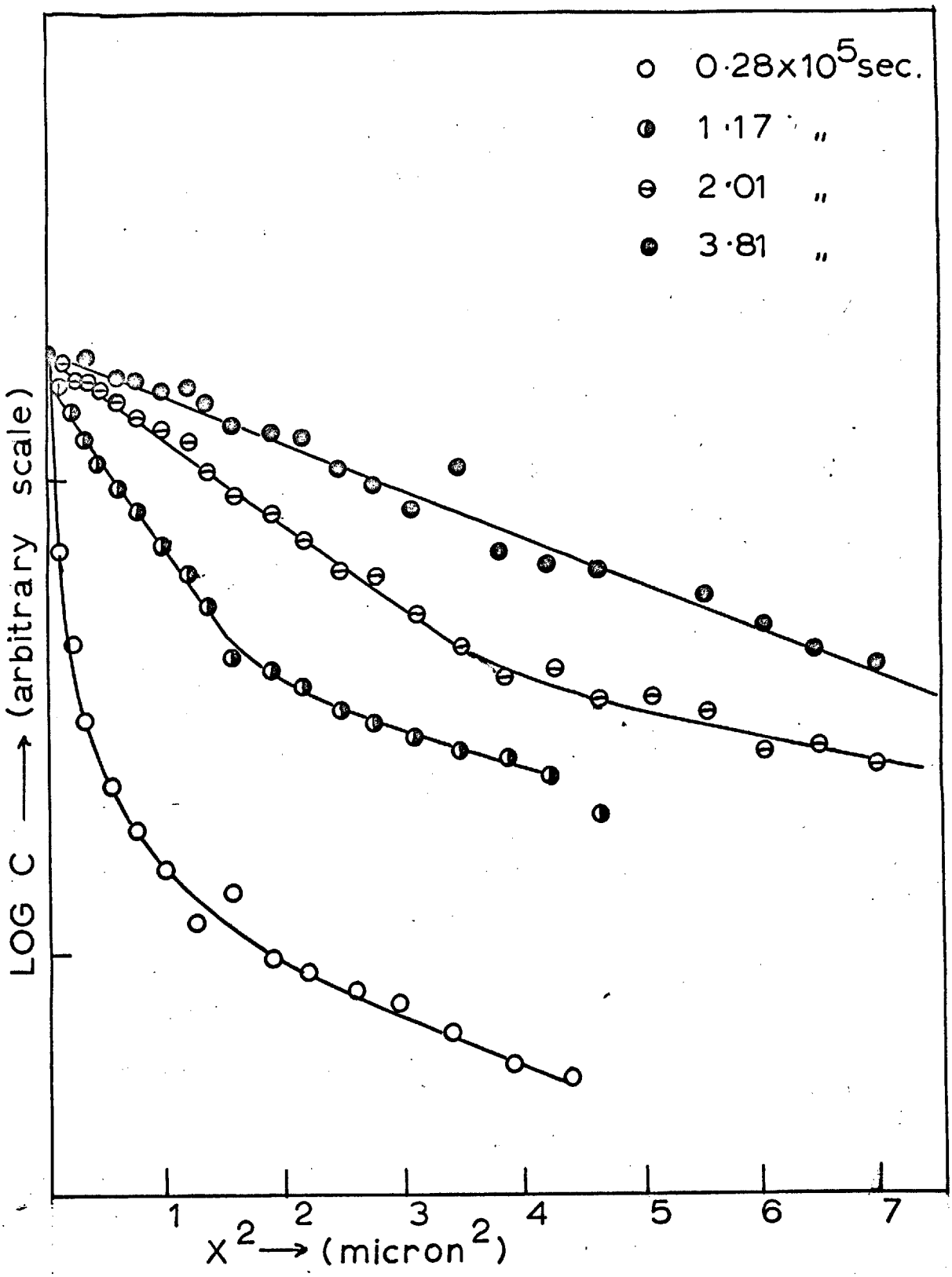


Fig. 40. U-diffusion in $UO_{2.1}$ at 1400°C.

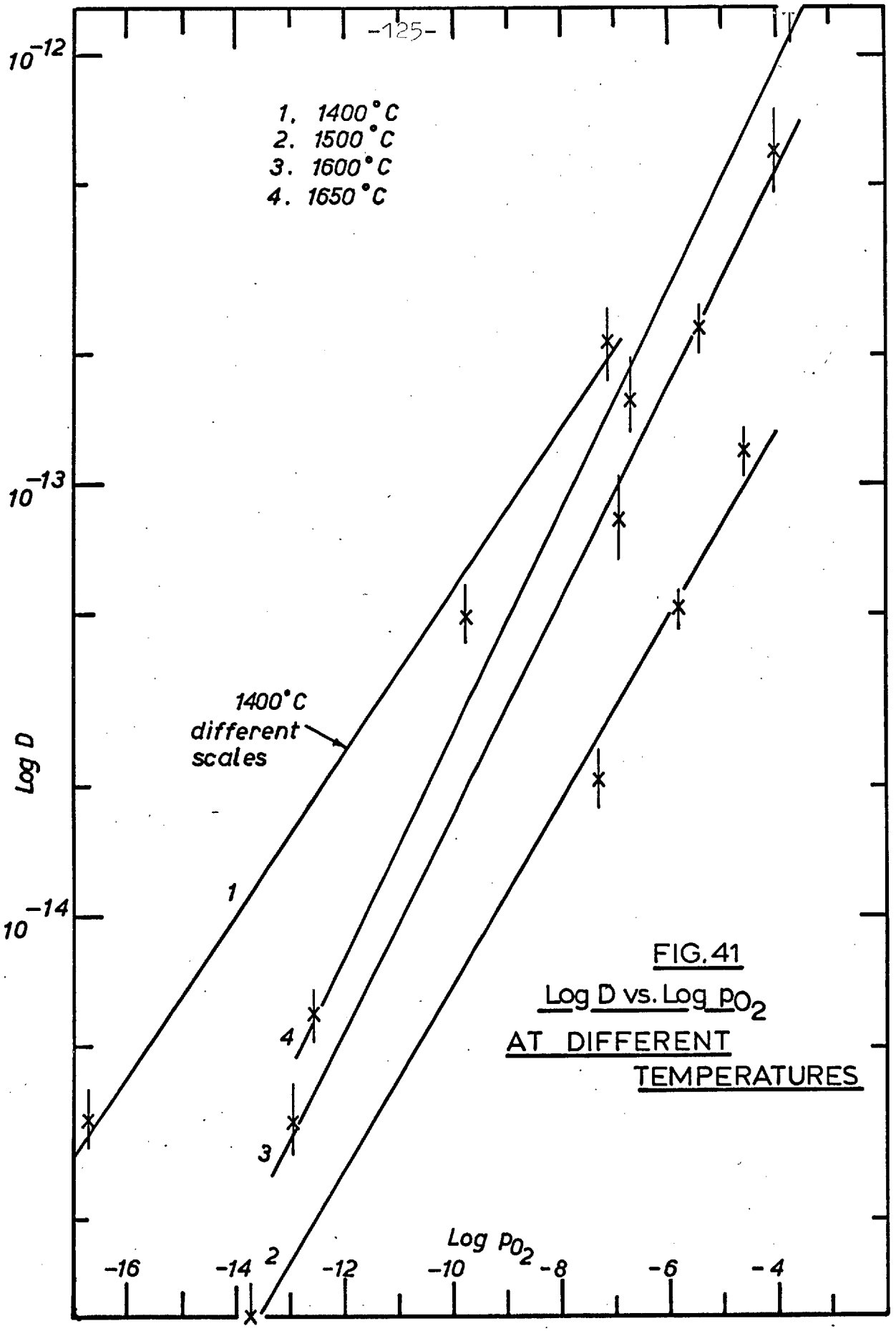


FIG. 41

Log D vs. Log P_{O_2} AT DIFFERENT TEMPERATURES

The value of D for stoichiometric UO_2 was not used in deriving equation 26. However, using values from table 7 for p_{O_2} in the stoichiometric runs indicated that, at 1400°C, the stoichiometric result fell exactly on the extrapolation of the "log D" versus "log p_{O_2}" line (point A figure 39) Similarly, within the experimental error, the plot of "log D" versus "log p_{O_2}" was a straight line up to 1650°C for $x = 0.00003$ to $x = 0.1$ (Figure 41). The values for $D_{2.0}$, $D_{2.03}$, $D_{2.01}$ and $D_{2.1}$ were taken from equations 19 to 22 giving a fit of the straight line equally good from 1400°C to 1650°C. The fit of the line at 1400°C was not as good as when the full results at this temperature were used.

$D_{2.15}$ does not fit on any straight line through the results for $x < 0.1$. It should be noted that "log p_{O_2}" versus "log x" turns up quite sharply after $UO_{2.1}$ probably arising from changes in the UO_{2+x} lattice which may, in turn, affect D.

5.7 Grain-boundary diffusion Grain-boundary diffusion was investigated using Suzoaka's model. An analysis using Fisher's model to obtain D_b for stoichiometric UO_2 has been published for this work,[57] but in view of the limitations of the model these results

may have large errors; but they give order of magnitude measurements.

5.7.1 Stoichiometric UO_2 In section 5.3.2 values of D_b were given which were obtained from Δ and D found by the self-consistent method. The results show a considerable scatter and the reasons for this will be discussed in section 5.7.4.

5.7.2 UO_{2+x} grain-boundary diffusion Δ showed considerable variation and the calculated D_b's were too scattered to obtain a useful equation for grain-boundary diffusion.

5.7.3 Grain-boundary diffusion in ThO_2 The grain size in thoria polycrystals was ten times that of the UO_2 samples consequently the grain-boundary contribution to the diffusion profile would be ten times less if Δ were the same as in UO_2. This would explain why no grain-boundary diffusion was detected in ThO_2.

5.7.4 Variation of Δ Suzuoka's model makes several assumptions;

1. The grain-boundaries are slabs perpendicular to the free surface. (This is probably true very close to the surface, but farther in this condition will not

hold and diffusion away from the grain-boundaries will not be parallel to the surface. The overall effect, as shown by Suzuoka using Fisher's model, will be small provided the angle between the grain-boundaries and the surface does not become too large).

2. Diffusion takes place only within the monolayer of grains at the surface (For the values of $\sqrt{Dt}$ used in this work this condition holds).

3. Every grain boundary has an equivalent and isotropic diffusivity. (This is probably incorrect[52] and is the most likely cause for the variation in Δ determined from diffusion anneals at the same temperature The materials used were sintered pellets and the porosity and impurities in the grain boundaries could vary. The tracer could easily be transported across the grain-boundary void by an evaporation-condensation process in UO_2, but it is difficult to assess whether or not this process would be faster than ordinary grain-boundary diffusion).

From consideration of condition 3 it is likely that Δ will vary. For an activation energy of half of that for volume diffusion Δ should change from 10^5 at 1400°C to about $10^{4.2}$ at 1700°C for $UO_{2.1}$. This is well within the experimental scatter for Δ. The sets of values for

2.0, 2.01 and 2.1 do show a tendency to decrease towards higher temperatures indicating that the activation energy for grain-boundaries diffusion may be less than that for volume diffusion.

However, no firm conclusions can be formed, except that cation grain-boundary diffusion is about 10^5 x D in $UO_{2.0}$ and UO_{2+x}.

Impurities were sought in the grain-boundaries with an electron-probe microanalyser. No impurities were detected indicating that the concentration of impurities in the grain boundaries was less than 100 - 200 ppm.

5.8 Decrease in Surface Activity results in UO_{2+x}

These were expected to be high even in single crystals because of the high evaporation losses in UO_{2+x}. When the surface layer has a high concentration of tracer i.e. in the first few seconds of the experiment evaporation losses will have a large effect.

No use can be made of the D.S.A. results because of the large inherent errors in applying this method to UO_2. Although results in polycrystalline samples can be obtained that appear to be self-consistent, different workers have produced results which differ by more than the experimental error in any set.

GENERAL DISCUSSION

6. GENERAL DISCUSSION

Having established (section 5) that the measurements of U self-diffusion in UO_2, UO_{2+x} and Th in ThO_2 were meaningful, other workers results were examined in the light of the present work.

A model for U self-diffusion in UO_{2+x} [43] was tested together with other possible models and it was found that a composite mechanism could explain experimental observations quite well.

Other work on cation diffusion in UO_2 solid-solutions, and other fluorite-type lattices was investigated in an attempt to obtain information on the diffusion process. Some results were available for cation diffusion in oxides showing a range of stoichiometry but none of these cases was close to the conditions obtaining in UO_{2+x}. Finally, a survey of oxides exhibiting enhanced cation grain-boundary diffusion showed that this phenomenon was not rare and has been observed in urania by four different workers.

6.1 Other work on U self-diffusion in UO_2

6.1.1 Decrease in Surface Activity results This work has been discussed in section 1.4.1. All three sets of measurements were made in material close to stoichiometry and provided that impurity effects were negligible, the difference in the results could be ascribed to grain-boundary diffusion. When grain-boundary diffusion is present the range chosen for the D.S.A. measurements is important. This is shown in a paper by Schmitz and Lindner[58] where the value of D changes by a factor of 2 by considering the integral activity at different depths. There is no reason why the value obtained for D should not vary from very close to the true value, D_v, to perhaps 100 times D_v, depending on the profile in the polycrystal.

It is interesting to note that if the activation energy for grain-boundary diffusion is less than that for volume diffusion then the D.S.A. values of D should lead to a lower activation energy for the process than would be obtained with correct values of D_v. However, the vapour pressure of UO_2 rises rapidly with temperature and evaporation losses will consequently be higher at higher temperatures, leading to high values of D. This would increase the apparent activation energy. So it seems likely that the

evaporation of the tracer is playing an important part in producing a higher activation energy, whereas the grain boundary contribution just gives a general increase in D. An estimate of the activation energy for grain-boundary diffusion has been made using Fisher's and Suzuoka's models; both indicate that $Q_{g.b} = Q_v$ so that the proportion of grain boundary diffusion should not be very much different at different temperatures.

In the paper by Auskern and Belle[2] a diagrammatic representation of the annealing furnace shows that the H_2 used to maintain stoichiometry was first passed through the alumina insulation of themolybdenum furnace. Furthermore, the preparation of the UO_2 pellets involves the use of tank hydrogen at 1750°C but mentions no purification process. Thus, the UO_2 is almost certain to be non-stoichiometric - probably becoming more so at higher temperatures (when more water is released from the alumina) when the H_2/H_2O ratio should really be increased to maintain a given stoichiometry.

Many samples, both stoichiometric and non-stoichiometric, were analysed by D.S.A. and α-ray spectrometry and produced different results for the two methods. Thus, the difference in measured D's by the two methods is not in compositional variation. In section 6.1.1 the main reason for the higher activation energy was

presumed to be loss of tracer by evaporation. In the present work the presence of a bound surface layer was observed for most of the stoichiometric specimens. Assuming that the tracer which takes part in the diffusion process does so from $t = 0$ onwards, and that which is bound at $t = 0$ does not subsequently become released into the specimen, then the actual concentration profile is not expected to be affected very much by evaporation at the surface (provided $x = 0$ does not change much) whereas the total activity will be strongly affected by vaporisation of the high activity bound layer.

6.1.2 D by sectioning Nagels et al.[5] used material which was described as 'nearly stoichiometric' single crystals. The as-grown composition was reported to be $UO_{2.003}$ to $UO_{2.007}$ but it was then reduced and the diffusion anneals were performed in a UO_2 crucible in a vacuum furnace at 10^{-5} mm.Hg. The results of three experiments at 1300, 1450 and 1465°C were close to the line of Auskern and Belle ($D = 4.3 \times 10^{-4} \exp(-88000/RT)$ Their value for D at 1400°C would be $1.3 \times 10^{-15} cm^2 sec^{-1}$ and using the graph of "log D" versus "log x" (Figure 38) this would correspond to a composition of $UO_{2.00015}$ i.e. nearly stoichiometric). Moreover, since their

results were slightly below those of Auskern and Belle the activation energy would be less than 88 kcal. In the present work for UO_{2+x} the activation energy rises from 70 kcal at x = 0 to 88.9 kcal at x = 0.01. Thus, these results could be explained if the material is assumed to be slightly non-stoichiometric.

Yajima et al.[59] have also used a sectioning method. Part of the preparation of the pellets was a 2 hr. sinter at 2,300°C in 7 to 8 atm. of argon. They state that very few uranium metal inclusions were visible and almost all were concentrated near the surface. These were removed prior to the diffusion treatment by grinding. This means that the pellets were probably sub-stoichiometric since the rate of oxygen diffusion is very high at 2,300°C and the evidence of a gross depletion near the surface means that there would certainly be a depletion of oxygen from very much farther in although not detectable by microscopic examination or X-ray diffraction (which they used to check stoichiometry). So these results are of doubtful value since the stoichiometry is not known. Enhanced diffusion in sub-stoichiometric urania is indicated. As in the present work, the very small pre-exponential factor may indicate an extrinsic control of the diffusion process.

6.1.3 Alpha-ray Spectrometry The diffusion anneal performed by Marin and Michaud[63] was at 1700°C with an argon atmosphere purified by Mg in the presence of C and Ta. The results of $D = 5 \times 10^{-16} cm^2 sec^{-1}$, would fit with the present work if p_{O_2} was about 10^{-18} at 1700°C. This does seem unlikely unless the apparatus were completely leak free or the gettering action were very efficient.

Schmitz[58] claims that his α-ray spectrometry results agree with the D.S.A. measurements. McNamara[1] showed that the concentration profile probably consisted of a volume diffusion region and a grain boundary diffusion region. (See section 1.5.3); although agreement with D.S.A. results could be obtained if the first steep part of the concentration profile were ignored. Concentration profiles determined by Schmitz all show a very pronounced steepening near to the surface, which is attributed to the finite resolution of the spectrometer. Using data published in ref.58 the spread from the top of the peak of a plated Pu^{239} source to the end of the low energy tail was about 0.34 microns ($0.115\mu^2$) and $\sqrt{2}\sigma$ is about 0.15μ (see section on instrumental error). Thus, the spread from a bound surface layer finishes at about $0.12\mu^2$ and large effects from the Gaussian spread extend only to 0.6μ ($0.36\mu^2$)

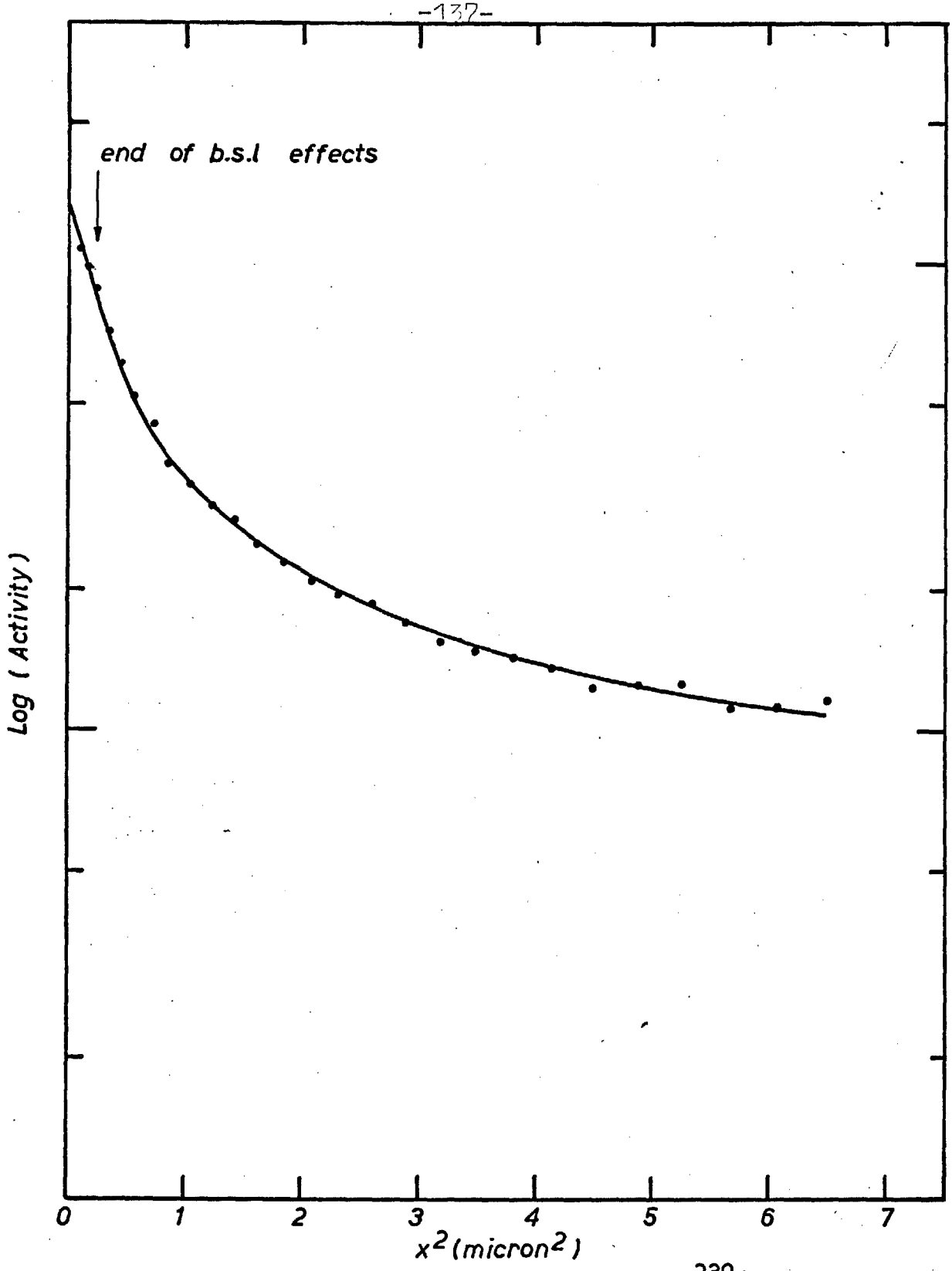


FIG. 42 CONCENTRATION PROFILE OF Pu^{239} IN UO_2 AT 1500°C FOR $5{\cdot}76 \times 10^4$ seconds

(Appendix 3). Clearly in Figure 42, for Pu^{239} diffusion in UO_2 at 1500°C for 5.76×10^4 sec., the section between $x^2 = 0.4^2$ and $x^2 = 2.5^2$ must be accounted for in terms of some diffusion process since the spread from the surface and instrumental effects cannot extend as far as this.

Schmitz's analysis of samples using the α-ray spectrometer was such that it amounted to a series of D.S.A. measurements. In ref.58 figures are given for the integral activity and an integrated form of equation 1 is used,

$$Q_x = Q_o \operatorname{erfc} \left(\tfrac{1}{2}x/(\pi Dt)^{\frac{1}{2}}\right) \qquad (27)$$

Q_x = activity beyond depth x

This equation is probably wrong since integrating 1 gives

$$\int_o^x c_x d_x = c_o \operatorname{erf}\left(\tfrac{1}{2}x/(Dt)^{\frac{1}{2}}\right)$$

and $$Q_x = c_o \operatorname{erfc}\left(\tfrac{1}{2}\, x/Dt\right)^{\frac{1}{2}}) \qquad (28)$$

i.e. there is no 'π' in 28.

Equation 28 would only be valid for volume diffusion from an instantaneous source. This means that "log C" versus "x^2" should be a straight line. The concentration profile was plotted from their results by taking the difference in the integral activity every five channels.

Figure 42 shows that "log C" versus "x^2" is not a straight line so equation 27 cannot hold. A further examination of Figure 42 shows that the plot is of the same general form as those for polycrystalline material in the present work, and in that of McNamara. The shape of the curve can be satisfactorily explained in terms of a volume diffusion part and a grain boundary diffusion part.

6.2 Theories for cation diffusion in UO_{2+x} and ThO_2

6.2.1 Lidiard's Model By relating the defect concentrations on the anion and cation sub-lattices via Frenkel and Schottky products, Lidiard[43] has produced equations describing U self -diffusion in UO_2. The assumptions in the theory are: that the Frenkel and Schottky products, F_o F_u and S are independent of composition; and that the mechanism of diffusion in UO_{2+x} is via vacancies on the f.c.c. U sub-lattice.

Denoting the mole fractions of interstitials and vacancies as o_i, u_i, o_v, u_v the Frenkel and Schottky products were,

$$u_i u_v = F_u(T); \quad o_i o_v = F_o(T); \quad u_v o_v^2 = S(T).$$

and the equation of electroneutrality was given as

$$2u_v + o_i = o_v + y + 2u_i \qquad (29)$$

y = defects introduced by non-stoichiometry or impurities
Assuming u_v and u_i to be small compared to o_i and o_v equation 29 becomes,

$$o_i = o_v + y \qquad (30)$$

Now y = defects introduced by impurities or excess oxygen (other than o_i, o_v). In non-stoichiometric urania these defects will be electron holes probably present as U^{5+}

so $o_i = o_v + \frac{1}{2} \times$ (number of holes)

Since the number of holes is 2x the equation becomes,

$$o_i = o_v + x$$

If z were the mole fraction of a trivalent cation impurity then $y = -\frac{1}{2}z$; divalent, $y = -z$; monovalent $y = -1\frac{1}{2}z$. Lidiard's final equations would be slightly modified by some numerical factor whenever x appears. The final equations are,

$$\begin{aligned} o_i &= x \\ u_v &= Sx^2/F_o^2 \\ o_v &= F_o/x \\ u_i &= F_u F_o^2/Sx^2 \end{aligned} \qquad (31)$$

(for $T < 1700^{o}C$ and $x > 10^{-4}$)

and in pure, stoichiometric UO_2,

$$o_i^{o} = o_v^{o} = F_o^{\frac{1}{2}}$$
$$u_v^{o} = S/F_o \qquad (32)$$
$$u_i^{o} = F_u F_o / S$$

The random walk treatment of the atomistics of the diffusion process gives,

$$D = \frac{1}{6} \Gamma \alpha^2 \qquad (33)$$

α = the jump distance;

Γ = number of jumps per second of the defect

For the movement of an atom by a vacancy mechanism in the f.c.c. lattice,

$$\alpha = a_o/\sqrt{2}$$

and, $\Gamma = 12 \omega_v N_v$

(12 = number of nearest neighbours; N_v = the probability that a near neighbour site is empty; and ω_v = the probability that the atom will jump into that particular site).

Giving $D = a_o^2 \omega_v N_v$

This diffusion coefficient is not exactly right since for a tracer atom the most likely move after a jump is right back into the vacant site it has just formed, and

so cancelling out the previous jump. Thus a correlation factor[43,93] must be introduced giving,

$$D_t = f a_o^2 \omega_v N_v \qquad (34)$$

For the f.c.c. lattice,

$$f = 0.7815$$

$$\omega_v = \nu \exp(-\Delta G_m/RT)$$

$$N_v = \frac{S}{F_o^2} x^2 = x^2 . \exp(\Delta G_s - 2\Delta G_{F_o}).$$

ν is normally taken as the Debye frequency;

ΔG_m = free energy of movement of the vacancy.

So equation 34 becomes, for $x > 0$,

$$D = f a_o^2 \nu x^2 \exp\left(\frac{\Delta S_m + \Delta S_s - 2\Delta S_{F_o}}{R}\right). \exp\left(\frac{-\Delta H_m - \Delta H_s + 2\Delta H_{F_o}}{RT}\right) \qquad (35)$$

(Lidiard's equation had a factor 1/12 in it. This would apply to a tracer (impurity) with associated vacancy).

For interstitial diffusion the number of sites into which an interstitial can move is constant and independent of the number of interstitial atoms, here

$$\alpha = a_o/\sqrt{2}$$

$$\Gamma = 8\nu_i.1.$$

(The number of nearest neighbour sites = 8 in the f.c.c. lattice; the probability that it is empty = 1 in dilute solution; and ω_i = probability that the

intersitial will jump).

In this case the correlation factor is unity since all sites are equivalent after the move.
Substituting for α and Γ in 33 gives, for the tracer,

$$D = \tfrac{2}{3} a_o^2 \omega_i N_i \qquad (36)$$

(N_i, since the average occupancy of an interstitial site by a tracer is N_i).
For an interstitialcy mechanism the jumps are correlated. The numerical factos in this equation for D will depend on the exact mechanism. For UO_{2+x} comparing equation 35 with the empirical equation $D = D_o \exp(\frac{-Q}{RT})$ shows that "log D_o" versus "log x" should have a slope of 2. Figure 43 shows that the slope is close to this, being 2.20 ± 0.3.

A further test of the theory would be to estimate D_o[43] since the very small experimental value is significant in indicating that the cation diffusion may be extrinsic.

Taking $f = 0.7815 \times 10^{-8}$cm,

$\nu = 5 \times 10^{13}$sec^{-1},

$x = 0.01$,

and $\exp(\Sigma \Delta S/R) = 1$, gives $D_o = 10^{-5}$cm^{2}sec^{-1} (experimentally, $D_o = 2 \times 10^{-3}$). The discrepancy

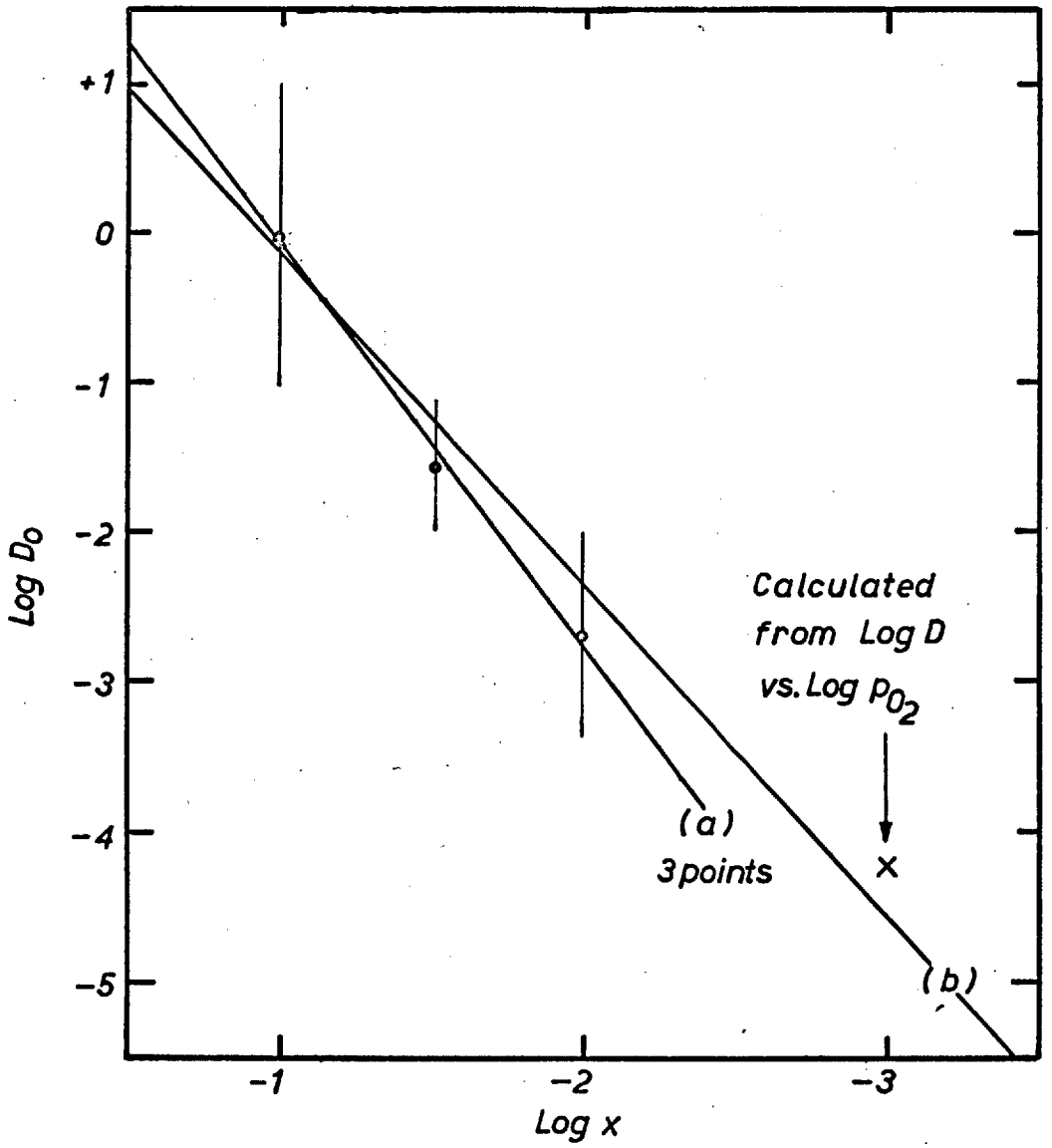


FIG. 43 Log D_o vs. Log x FOR U DIFFUSION IN UO_{2+x}

can be allowed for in the error of ν and exp ($\Sigma\Delta S/R$). Agreement would be given if $\Delta S_m + \Delta S_s - 2\Delta S_{F_o} = 5R$. This value is not unreasonable.

As far as the pre-exponential term is concerned the agreement with theory is quite good. Equation 35 shows that the activation heat is a composite quantity being equal to $\Delta H_m + \Delta H_s - 2\Delta H_{F_o}$. Now ΔH_s and ΔH_{F_o} have not been calculated for UO_2 although an estimate of the magnitude of these heats can be obtained from work by Franklin[92] on CaF_2, SrF_2 and BaF_2. His values for CaF_2 were, ΔH_{F_o} = 62.25 kcal. (which is in very good agreement with the experimental value, 65 kcal.[8]), and ΔH_s = 117.5 kcal. An estimate of ΔH_{F_o} in urania can be obtained from oxygen self-diffusion measurements[43,72] Here, ΔH_{F_o} = 71 kcal. This value is only approximate since the stoichiometric UO_2 was in fact $UO_{2.002}$. No estimate of ΔH_s is available although it is expected to be of the same order as ΔH_s for CaF_2. Since, ΔH_s in CaF_2 is approximately 2 x ΔH_{F_o} this might be expected in UO_2. Thus the activation heat in equation 35 is about ΔH_m. An estimate of the maximum value of ΔH_m in $UO_{2.12}$ at 800°C can be made from the results given by Willis[34] The occupation number for uranium on normal lattice sites is given as 1 $\pm$ 0.01 (standard deviation). At the most 0.01

sites are empty. Using equation 34,

$$D_{800^\circ C} = 0.718 \times 2.99 \times 10^{-15} \times 0.01 \times 3 \times 10^{12} \exp(\Delta H_m)$$

For $UO_{2.1}$, $D_{800} = 10^{-23}$ cm.^{2}sec.$^{-1}$

Giving $\Delta H_m = 85$ kcal.

If ν were 10^2 different ΔH_m could be 76 to 95 kcal. ΔH_m is quite insensitive to a large change in one of D, N_v or ν, but all three are reasonable estimates and the value of ΔH_m calculated here lends support to $Q \doteqdot \Delta H_m$. No good estimate of the number of defects was possible from thermal expansion and lattice parameter data since there is good agreement between the actual expansion and that calculated from change in lattice parameter with temperature.(10) However, if the whole expansion is attributed to the formation of cation vacancies, although this will be a gross over-estimation of the number of defects, the upper limit for ΔH_m can be found. At 1500°C, the volume expansion is about 5% in stoichiometric UO_2 so, assuming this to be due to a 5 mole % uranium vacancies and knowing D_{1500} for $UO_{2.0}$, gives ΔH_m as 85 kcal at the most. Q from diffusion measurements is 70 kcal in stoichiometric urania. Thus Lidiard's theory seems to be reasonable although an exact fit with experiment cannot be obtained because most of the parameters in equation 35 are not known with sufficient

accuracy. However, the theory only seems to apply for $x < 0.1$ since results for $UO_{2.12}$ and $UO_{2.15}$ do not fit with those for lower values of x. Log D_o increases steadily with increasing log x up to $x = 0.1$ but for $UO_{2.15}$ it decreases again and Q decreases too. Also "log D" versus "log p_{O_2}" (or "log x") is a reasonable straight line up to $x = 0.1$ but above this value D rises very rapidly.

6.2.2 Other factors in U self-diffusion in UO_{2+x}

Prior to the publication of Lidiard's theory and before activation energies were established, it was observed that a plot of "log D" versus "log x" could be correlated quite well with the formation of U^{5+}:

The relationship between x and p_{O_2} requires the formation of associated defects,(84)

$$\tfrac{1}{2}O_2 + 2U_L = O_iU_2^{5+} \qquad (37)$$

(log p_{O_2} is proportional to log x. This is found experimentally up to $x = 0.1$)

Two electron holes are associated with O_i and these could exist as U^{5+}. As the O_i moves rapidly through the lattice different U^{4+} ions would become U^{5+}. If a U^{4+} adjacent to a U vacancy becomes U^{5+} it will move easier

into the vacancy because of its smaller size although it may cease to be U^{5+} after it has jumped.

For U^{5+} to take part in a diffusion process it must be virtually dissociated from the defect complex,

$$\underset{x-a}{O_i U_2^{5+}} = \underset{a}{O_i U^{5+}} + \underset{a}{U^{5+}} \qquad (38)$$

For small a, $(< \frac{x}{10})$

$$a \propto x^{\frac{1}{2}}$$

In equation 33,

$$\Gamma = 12 N_v \, k x^{\frac{1}{2}} \, \nu \, \exp\left(\frac{-\Delta G_m^{5+}}{RT}\right)$$

($12 N_v$ is the probability of a vacancy as a nearest neighbour; $u^{5+} = kx^{\frac{1}{2}}$; ΔG_m^{5+} for movement of U^{5+})

Substituting for Γ and α $(= a_o/\sqrt{2})$ in equation 33 gives,

$$D = f k a_o^2 \, \nu \, N_v \, x^{\frac{1}{2}} \exp\frac{\Delta Sm}{R} \cdot \exp\left(\frac{-\Delta Hm}{RT}\right) \qquad (39)$$

If ΔG_m and N_v are assumed to be constant with x (see later) then "log D" versus "log x" at constant temperature will have a slope of $\frac{1}{2}$ as found by experiment.

Since equation 39 appears to fit the experimental data under the special conditions of constant N_v and ΔG_m, it seems expedient to examine these two terms more closely. The assumption of constant ΔG_m requires experimental verification, but the assumption of constant N_v, the number of cation vacancies, does not appear to be sound theoretically. Lidiard's determination of N_v shows that it is not independent of x, as is required here. The relationship between the number of defects on the two sublattices is via the Schottky product. Both stoichiometry and electroneutrality must be considered when establishing the Schottky product, for example, the charge imbalance due to the formation of a uranium vacancy could be allowed for by four electron holes (as U^{5+}), but the composition would be changed and two oxygen vacancies must be formed instead to maintain stoichiometry. It is assumed that the equation,

$$u_v o_v^{\,2} = S(T) \qquad -(40)$$

applies to all compositions of UO_{2+x}, although, of course, it will not be correct for large deviations from the stoichiometric composition.

It was found experimentally that $\Sigma\Delta H$ (equation 35) was not constant with composition implying that any, or all, of ΔH_m, ΔH_{F_o}, ΔH_S may change. Thus the fact that 'log D' versus 'log x' has a slope of $\frac{1}{2}$ is fortuitous. However, the concept of U^{5+} being responsible for the diffusion process was pursued and a combination model (U_v/U^{5+}), will be examined in section 6.2.5., where a more critical test of the diffusion model is found in the value of the slope of 'log D_o' versus 'log x'.

The requirement of a virtual dissociation of U^{5+} and O_i for the diffusion jump does not necessarily mean a chemical dissociation. Equation 38 implies that only a few U^{5+} are capable of taking part in the diffusion process- although in a wider sense they are still associated with the O_i. This might be interpreted as the diffusion jump requiring a specific coordinated jump of the oxygen interstitial and the U^{5+}.

If U^{5+} dominate the diffusion process, then the sudden increase for $x>0.1$ can be explained. A graph of 'log p_{O_2}' versus 'log x' begins to deviate from a straight line of slope 2 for $x>0.1$.[84] This implies a dissociation of the defects, which will eventually give,

$$O_i U^{5+} = O_i + 2U^{5+} \qquad -(41)$$
$$\qquad\quad x \qquad 2x$$

giving, $u^{5+} \propto x$.

So, "log D" versus "log x" should have a slope of 1 beyond x = 0.1. The gradient is close to this (Fig.38) The reason for the complete dissociation is that at x = 0.12 there is on average one U^{5+} per cell. Thus, it is possible that a particular electron-hole is not associated with a particular interstitial when the concentration is so high and the holes may act rather like electrons in metals.

6.2.3 Condition for U^{5+} to dominate in diffusion

Movement from a normal U lattice site into a vacancy would result in a jump in a <110> direction. Consideration of the projection along <110>, Figure 44, shows that if the jump were directly into the adjacent vacancy then two oxygens would have to move apart a distance equal to the diameter of the moving ion. A more likely mechanism is for the ion to move through the interstice between four oxygen ions in a <100> type direction into a $(\frac{1}{2},0,0)$ position and then move between another four oxygens to the vacancy. When in the $(\frac{1}{2},0,0)$ position the U ion is closer than normal to 4 U ions (the other two positions being vacancies), but the distance of approach, $a_o/2$, is 2.73Å so the ions are far from touching (r_u = 0.97Å). The jump could also proceed via $(\frac{1}{2},\frac{1}{2},\frac{1}{2})$. Here, charge effects are neglected.

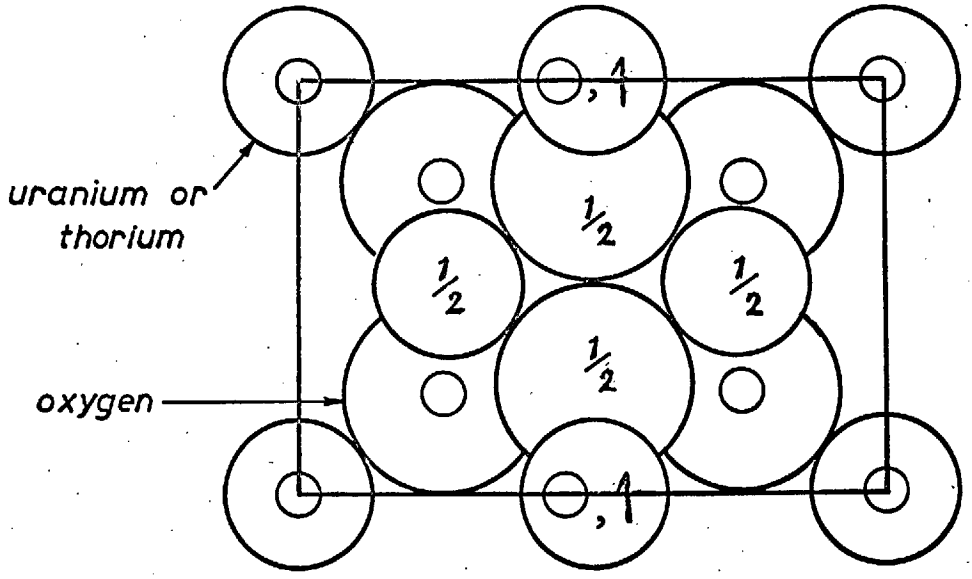


FIG. 44 <110> PROJECTION OF FLUORITE STRUCTURE

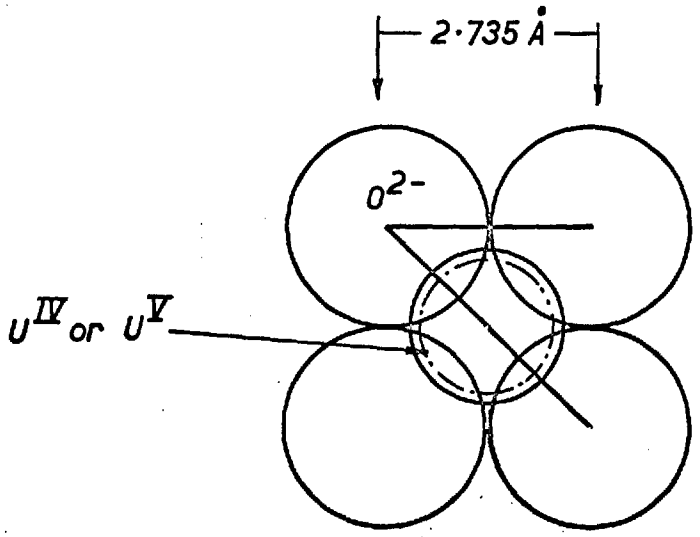


FIG. 45 OXYGEN CONFIGURATION ALONG <100>

The difference in energies for the movement of a U^{5+} and a U^{4+} can be estimated roughly be considering the elastic work done in moving. Figure 45 shows the four oxygen ions. The distance between their centres is 2.735Å so the hole has a radius of about 0.56Å. When an ion moves through the interstice each of the four oxygens must move r - 0.56 Å. The work done in moving is given by,[96,97]

$$\Delta G_m = \int_{x=o}^{0.56} f\,dx = \left[\mu x^2\right]_o^{0.56}$$

f = force; taken to be proportional to the displacement

μ = an elastic modulus for the region.

Since the radius of U^{4+} is 0.93 Å and that of U^{5+} is ·87 this treatment shows that the movement of U^{5+} requires only about 57% of the work required to move a U^{4+}. A reasonable estimate for the work to move a U^{4+} would be 100 kcal (giving U^{5+} 60 kcal, c.f. experimental results). The difference of 40 kcal means that the U^{5+} is 12,000 times more likely to jump than U^{4+} at 1400°C. So when x = 0.00008 half of the diffusion is accounted for by U^{5+} and half by U^{4+} (N.B. As x becomes less than 0.0001, U^{4+} jumps will dominate giving a higher diffusion coefficient than for U^{5+} jumps alone. This agrees with

experiment where D for the stoichiometric composition does tend to be above the "log D" versus "log p_{O_2}" straight line).

6.2.4 Thorium diffusion in UO_{2+x} In order to obtain information concerning the nature of the diffusing species (U^{5+}, vacancy, or interstitial mecahnism) Th^{4+} was diffused into $UO_{2.0}$, $UO_{2.01}$ and $UO_{2.1}$. Although a chemcial gradient was present this was considered to be about the same in all three cases and any increase in the diffusion coefficient was attributed to the defect chemistry.

In stoichiometric UO_2. U^{233} and Th^{230} have the same diffusion coefficient at 1620°C. This agrees with the findings of Lindner and Schmitz, but their results show a possible difference in the activation energies for U and Th diffusion, so the agreement at 1620°C may be fortuitous. In $UO_{2.01}$ at 1600°C D_U and D_{Th} are very close, but in $UO_{2.1}$ D_u is about 2 x D_{Th}. So, the diffusion coefficient for Th^{4+} in UO_{2+x} increases with x in the same way as D_u for low x at about 1600°C, but the increase is less when x is about 0.1.

If the diffusion is related to U^{5+} then as the number of U^{5+} increases, the vacancies (number fixed for this model) would move around faster and would return

quicker to the vicinity of the Th^{4+}. Thus diffusion of Th^{4+} would be enhanced. There would be some strain in the lattice around the Th^{4+} (0.99Å) and this might help it to jump preferentially into the vacant site (rather than U^{4+}). The difference in D_u and D_{Th} in $UO_{2.1}$ could be explained in that the rate of movement of Th^{4+} depends on the probability of there being an adjacent vacancy whereas the rate of movement of a U^{233} tracer depends on the same probability of there being an adjacent vacancy and that the tracer should be a U^{5+} which can dissociate from an O_i. This second probability increases suddenly around x = 0.1 and so accounts for the bigger increase in D_u than in D_{Th} at this composition

An interstitial mechanism for diffusion might be postulated by assuming that U^{5+}form interstitials more easily than U^{4+} and that the defects on the cation lattice are independent of those on the anion lattice, but the closeness of U and Th diffusion in UO_{2+x} implies a similar mechanism for the two ions. Since it is unlikely that more interstitial thorium will be formed with increasing x it might be concluded that the mechanism must involve vacancies. However, it is possible that the formation of Frenkel defects by U^{5+} could produce vacancies for U and Th diffusion - provided that the defects on the two sub-lattices are independent.

Some other work on actinide diffusion in UO_2 has been performed, but in view of the doubtful validity of the analysis of their results the figures given by Schmitz and Lindner[58] must be treated with caution (section 6.1.4). On the assumption that Th, Pa, U, Np, Pu and Am all move via the defects already present in UO_2, the difference in activation energy can be loosely correlated with the charge or different radii of the diffusing tracer. But the nature of the defects was not established.

6.2.5 Models for Diffusion in UO_{2+x} and experimental results

i) U_V/U^{5+} model. For the U^{5+} mechanism "log D" versus "log x" should have a gradient of 0.5 if ΔH_m is constant. It is not. So the slope of 0.43 $\pm$ 0.6 does not indicate U^{5+} control. However, a diffusion model combining Lidiard's model and the U^{5+} model can account for experimental observation.

Combining equations 31 and 39,

$$D = \text{const.}\ x^{2.5} \exp\left(\frac{\Delta S}{R}\right) \exp\left(\frac{\Delta H}{RT}\right) \qquad (42)$$

$N_V \propto x^2$; $U^{5+} \propto x^{\frac{1}{2}}$.

Thus, "log D_o" versus "log x" should have a slope of 2.5 (to x = 0.1).

The limit of U^{5+} control is at about x = 0.001, and although D_o can be calculated for different compositions from the "log D" versus "log p_{O_2}" (or log x) lines, these may not be true straight lines. Using the three experimental values for D_o at $UO_{2.1}$, $UO_{2.03}$, $UO_{2.01}$ gives a slope of 2.67 $\pm$ 0.2, showing that this composite model is reasonable.

In order to explain conductivity measurements Hoch[42] and Roberts and Markin[41] postulated that half the electron holes were free and half bound to oxygen interstitials. It is possible that one U^{5+} is strongly associated and one loosely associated so that the latter can take part in the conduction process. This could mean that the free holes can take part in a reaction as implied in equation 40. The number of U^{5+} (loosely associated) capable of taking part in a diffusion process would be proportional to x, so that "log D_o" versus "log x" would have a slope of 3. This does not fit the experimental results as well as equation 42 where only very few of the U^{5+} are free. However, the conductivity and diffusion processes are different in

that the former requires the movement of holes and the latter the movement of a U ion. The evidence here is that only a few of the 'free' U^{5+} can take part in the diffusion process, which is compatible with a correlated movement of oxygen and uranium.

ii) U_v model. Thorn and Winslow[73] explain the shape of the "$\overline{\Delta H}_{O_2}$" versus "x" curve by the filling of 'new' interstitial sites at about x = 0.1. These defects, since they are formed last, would require a larger positive free energy of formation. So an increase in F_o ($= \exp(-\frac{\Delta G_o}{RT})$) is expected leading to a sudden increase in D. Results for $UO_{2.1}$ and $UO_{2.15}$ show that $\Delta H_m + \Delta H_s - 2\Delta H_{Fo}$ becomes larger - since this term contains the main effects of adding interstitial oxygen. D_o decreases which means that ΔS_o probably increases. It is of course possible that the changes in Q and D_o are in the free energies of movement and of formation of Schottky defects.

This model would give a sudden change in "log D_o" versus "log x" at about x = 0.1 and then continue with a slope of 2. No equations were established for diffusion for x greater than 0.15 so this cannot be checked.

This model could not explain Th^{230} diffusion in UO_{2+x}. Vacancies are the only defects assumed to take part in the diffusion of the cation and the change in D_{Th}/D_u at x = 0.1 requires a difference in mechanism for U and Th diffusion. The experiments for Th diffusion in UO_{2+x} were poorly defined in that there was a chemiical gradient, so this model cannot be ruled out completely on the basis of these results.

iii) Interstitial model. An interstitial mechanism can be ruled out if the defects on the uranium and oxygen sub-lattices are related via Schottky and Frenkel products, since the number of U_i decreases with increasing x according to Lidiard's equations. Experimental evidence suggests that the defects are related - probably by equations such as equation 40.

Thus, two possible models for U diffusion in UO_{2+x} are, i) U_v/U^{5+} model. U^{5+} moving into a vacancy.

ii) U_v model. U^{4+} moving into a vacancy.

The first explains experimental results marginally better than the second. An extension of diffusion measurements for values of x greater than 0.15 could distinguish between the two, but because of excessive vaporization of urania these measurements would be difficult.

6.2.4 Diffusion in ThO_2 The non-stoichiometric range of thoria is extremely small or non-existent. This was confirmed by the diffusion experiments where no significant change in D was observed with change of atmosphere from H_2 (10^{-18} to 10^{-20}, p_{O_2}) to air ($p_{O_2}=10^{-0.7}$) Since the valency of Th^{4+} is fixed, (unless the energies of formation of Schottky and Frenkel products approach those for removal of an electron from O^{2-} or for the formation of Th^{3+}), then the defect concentrations should be given by Lidiard's equations for ideal stoichiometric UO_2, e.g.,

$$th_v = S/F_o$$

and $$th_i = F_u F_o/S$$

So, for a vacancy mechanism,

$$D = fa_o^2 \nu \exp\left(\frac{\Delta S_m + \Delta S_s - \Delta S_{F_o} - \Delta S_s}{R}\right) \cdot \exp\left(\frac{-\Delta H_m - \Delta H_u - \Delta H_{F_o} + \Delta H_s}{RT}\right)$$

Experimentally D_o is very small ($1.25 \times 10^{-7} cm^2 sec.^{-1}$) and if the diffusion is via vacancies, (as seems probable in UO_2), since $fa_o^2\nu$ is about 7×10^{-3},

then $\Delta S_m + \Delta S_s - \Delta S_{F_o} = -17.1$ e.u.

Now Zener's theory[43] maintains that ΔS_m must be positive but the theory only really works for close packed metals[94] Movements from a (0,0,0) position to a $(\frac{1}{2},\frac{1}{2},0)$ position

in a f.c.c. metal would produce disorder during the process and a positive entropy change. However, if a Th ion (or U) has to squeeze between oxygen ions then a large negative entropy might be expected. (The steric factor in old style kinetics, $e^{\Delta S/R}$ can be 10^{-6} for complex formation in gases i.e. $\Delta S = -27.5$ e.u.[33]). So the small value of D_o can be accounted for if the diffusion process involves a negative entropy change. It is interesting to note that a small value of D_o is often taken to imply extrinsic control of the diffusion process. But it is possible that the main factor in $\Sigma\Delta S$ is the intrinsic entropy of movement.

Lidiard's equation is more likely to apply to ThO_2 than to UO_{2+x} since there is no complication of hole formation.

So, unless the number of cation vacancies is fixed by an impurity ion of fixed valency the results for Th^{230} diffusion in ThO_2 are,

$$\Sigma\Delta H = \Delta H_m + \Delta H_s - \Delta H_{F_o} = 58.5 \text{ kcal.}$$
$$\Sigma\Delta S = \Delta S_m + \Delta S_s - \Delta S_{F_o} = -17.1 \text{ e.u.}$$

6.3 Cation diffusion in UO_2 solid solutions

A study of diffusion in UO_2 solid solutions could shed light on the diffusion process. Measurement of U self-diffusion in UO_2-MO_x solid solutions has been performed by two workers using the decrease in surface activity method.

McNamara used two solid solutions, UO_2/20 mole%ZrO_2 and UO_2/20 mole% Y_2O_3. The diffusion anneals were performed in an atomosphere of dry, high purity hydrogen. Diffusion was enhanced in the zirconia solid-solution by a factor of about 30, but no change was reported for the yttria solid solution. Since the D.S.A. method was used the factor 30 can only be used as an order of magnitude result.

Matzke investigated U self-diffusion in UO_2 with 0.1 mole % additions of Y_2O_3, La_2O_3 and Nb_2O_5 at 1400°C and 1550°C. He found that at 1550°C U-diffusion coefficients in UO_2 with Y_2O_3 and La_2O_3 additives were about 0.1 times those in stoichiometric UO_2 (Lindner's values) whereas Nb_2O_5 made no measurable difference; and at 1400°C, Y_2O_3 and La_2O_3 reduced D by a factor of 50 whilst Nb_2O_5 increased it by 225 times. No significance can be attached to the actual figures since the 1400°C results indicate that D_u (in UO_2/Y_2O_3 and UO_2/La_2O_3) is

about 4 x 10^{-16} $cm^2 sec^{-1}$. This is beyond the limits of the D.S.A. method (10^{-14} to 10^{-15} $cm^2 sec^{-1}$) since to obtain a 5% reduction in the total activity (down to a depth of 4 microns) would require a diffusion anneal of 5 x 10^7 sec. Most probably the active layer was bound on the surface and no diffusion took place at all in the case of these very low diffusion coefficients. Since the 1550°C results were within the range of applicability of the D.S.A. method these results can be taken as slight evidence of D decreasing on incorporating trivalent cations. The results for UO_2 with Nb_2O_5 require some comment too. The factor of 225 at 1400°C gives D_u (in UO_2/Nb_2O_5) equal to 5 x 10^{-12} $cm^2 sec^{-1}$ and the other reported value is 3 x 10^{-13} at 1550°C. It is not possible to have confidence in the results when a decrease in D by a factor of 0.06 is reported on increasing the temperature from 1400°C to 1550°C. Perhaps there is a misprint in the paper in which case Matzke's conclusions of increased diffusion in UO_2/1% Nb_2O_5 and decreased diffusion in UO_2 with 1% La_2O_3 and with 1%Y_2O_3 can be taken to give slight support for a vacancy mechanism for cation diffusion in UO_2.

6.4. Self-diffusion in fluorite lattices and other oxides

6.4.1. Fluorite-type lattices Both cation and anion diffusion coefficients are known in CaF_2, UO_{2+x}, ThO_2 and calcia-stabilised zirconia (CSZ). In the fluorite lattice most of the defects are accommodated on the anion sub-lattice.[96] This was substantiated in CaF_2 by conductivity measurements using NaF and Y_2F_3 dopants[8] and in UO_{2+x} by oxygen diffusion, X-ray and neutron-diffraction work.[10,11]

Unlike UO_{2+x} cation diffusion in CSZ is only affected in a small way by anionic defects. ThO_2 does not exhibit a large range of non-stoichiometry with changing oxygen partial pressure implying that the defects are few on both lattices. However, one thing is common to all fluorite lattices so far investigated:

The ratio of the anion to cation diffusion coefficients is very large at most temperatures (Figure 46 and Table 9) This might be expected with a relatively perfect cation lattice and an anion lattice containing the defects.

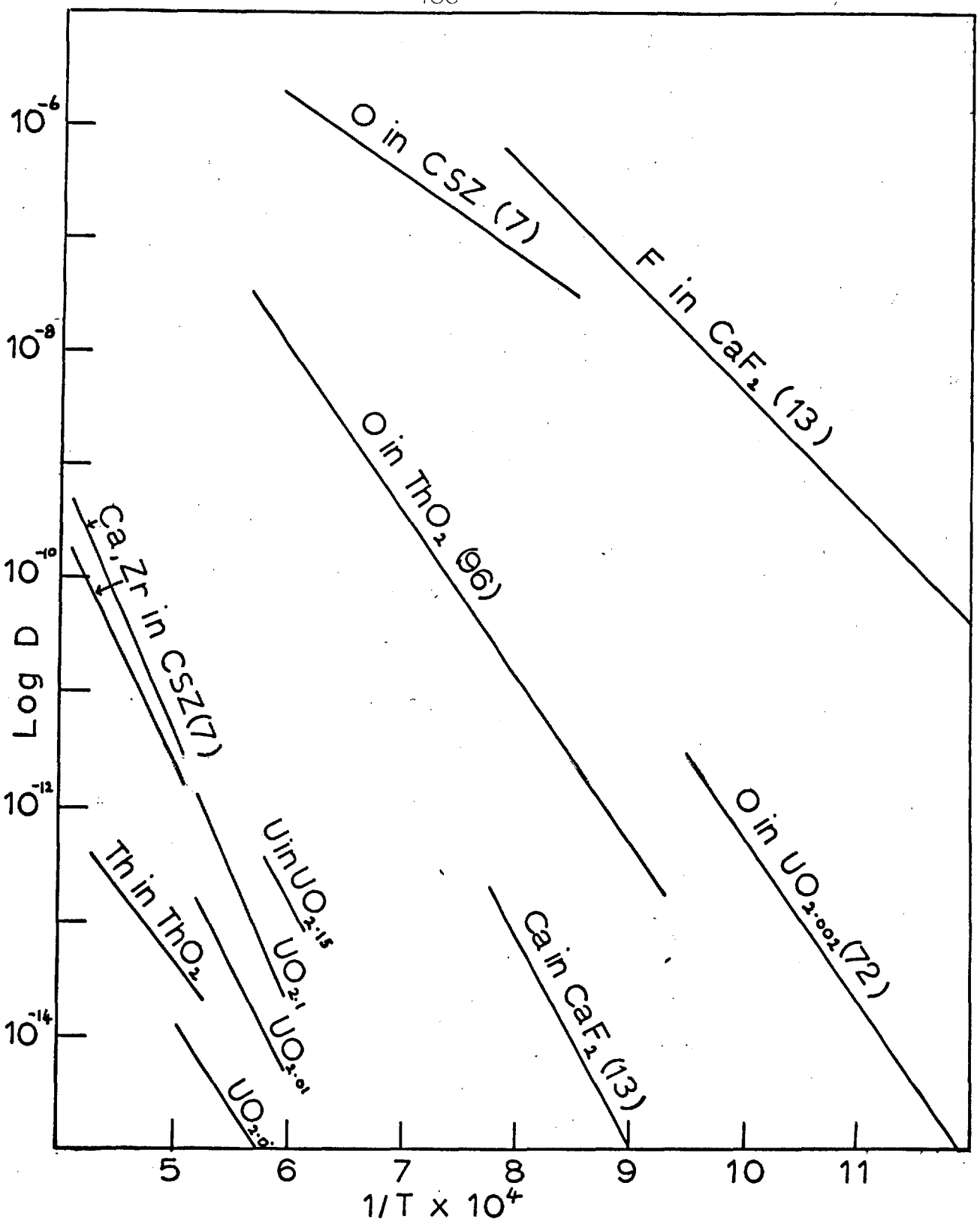


Fig. 46. Cation and anion self-diffusion in fluorite-type lattices

Table 9

Anion and cation self-diffusion in fluorite-type lattices

	Anion		Cation	
	Do $cm.sec.^{-1}$	Q kcal.	Do	Q
CaF_2	50	46(13)	10^2	86.5(13)
$UO_{2.0}$	1.2×10^2	65,000(72)	6.06×10^{-7}	70
ThO_2	4.4	65,800(96)	1.25×10^{-7}	59
CSZ	1.8×10^{-2}	31.2(7)	Ca 0.44	100.2(7)
16m/o			Zr 3.5×10^{-2}	92.5(7)

Auskern and Belle's value of $D_o = 1.2 \times 10^3$ for oxygen diffusion in $UO_{2.002}$ does not fit their data. Their graph of "log D" versus "1/T" requires that $D_o = 1.2 \times 10^2$ to obtain the experimental values of D.

6.4.2 ThO_2 and stoichiometric UO_2 Since ThO_2 does not show a range of non-stoichiometry like UO_{2+x} it is expected that the anion lattice will have fewer defects. This could explain the smaller oxygen diffusion and the pre-exponential terms for cation diffusion. D_o seems to be related to the disorder on the anion lattice in UO_{2+x}. The more nearly perfect anion lattice of ThO_2

could be responsible for a larger negative entropy for movement of Th in ThO_2 than for U movement in UO_2 making D_o for the ThO_2 case less than that for $UO_{2.0}$.

6.4.3 Diffusion in other oxides Since both D_o and Q increase with x in UO_{2+x} (up to x = 0.1) a survey of diffusion in other non-stoichiometric compounds was undertaken to establish whether or not this increase was usual.

D_{Co} increases in CoO as the partial pressure of oxygen increases.[97] This is attributed to an increase in the number of vacant cation sites.

There is no significant increase in the activation energy, but the value of D_o increases. Both D_o and Q increase with non-stoichiometry for Fe diffusion in wustite.[98] More Fe sites become vacant as the composition deviates more from FeO. Another example of an activation energy for movement increasing as the number of vacant sites increases is for Fe diffusion in $Fe_{1-\delta}S$[100]

and for anion diffusion in CaO/ZrO_2 ; but here, as in FeO, Frenkel pairs may be found on the anion lattice (an extension from CaF_2 shows that less energy is required to create a Frenkel pair than a single vacancy).

Although similar effects have been observed with changing stoichiometry in other systems no conclusions can be carried over to UO_{2+x} since nothing is established beyond doubt for the other oxides. The interstitialcy mechanism for oxygen diffusion and the U_v/U^{5+} model for U diffusion in UO_{2+x} describe conditions for diffusion which are much more complicated than in other oxides so far investigated.

6.4.4 Grain-boundary diffusion in oxides

Several workers have reported enhanced cation grain-boundary diffusion; in fluorite-type lattices, U in (UO_{2-x})[59], U in UO_{2+x} (this work), Nb in UO_2[102]; and in other oxides Zn in ZnO;[103] Ni in MgO[104] and O and possibly Al in Al_2O_3.[105] (In Paladino's paper an autoradiograph shows a concentration of Al in the grain-boundaries). However, the grain-boundary diffusion of Ni in MgO (NaCl structure) has been attributed to impurities in the grain-boundary[106] (as has grain-boundary diffusion in NaCl[107]). An electron probe microanalyser was used to examine the grains and grain boundaries of the urania samples but no concentration of impurities was observed.

RELATIONSHIP OF DIFFUSION TO OTHER PHYSICAL PROPERTIES IN UO_2

7. RELATIONSHIP OF DIFFUSION TO OTHER PHYSICAL PROPERTIES IN UO_2

Once diffusion coefficients have been established it is then possible to investigate the relationship between diffusion and creep, sintering, grain growth and fission gas release.

The diffusion coefficients measured in the present work, D_t, were for a tracer moving by a vacancy mechanism on an f.c.c. sub-lattice. The flux which is of importance in relation to physical properties would be the vacancy flux, which is 12/f times D_t (where f is the correlation factor - equation 34).

7.1.1 Sintering The process of sintering may be controlled by,

1) Diffusion (volume, g.b., or surface).
2) An evaporation - condensation process.
3) Plastic or viscous flow.

J.R.Johnson and H.G.Sowman[10] have reviewed the sintering data for urania in various atmospheres and with various additions. Their conclusions are that volume diffusion probably plays an important part in sintering during the final stages, but that all three mechanisms of densification play their part at one stage or another. Both

oxygen and hydroxyl ions can create lattice defects and their presence accelerates the operation of the mechanisms. Since diffusion coefficients have been measured in hydrogen it is expected that there may be some correlation with sintering in H_2; but the effect of hydroxyl ions in U diffusion is not known and although the partial pressure of oxygen can be calculated for a steam atmosphere it is not expected that the diffusion coefficient for the equilbrium composition of UO_{2+x} (measured under CO/CO_2) will apply.

An equation relating the fractional shrinkage to a diffusion coefficient is,

$$\left(\frac{\Delta L}{L_o}\right) = \left(\frac{KD\,\gamma\,\Omega\,t}{r^3\,kT}\right)^m \qquad (44)$$

$\frac{\Delta L}{L_o}$ = fractional shrinkage;

t = time;

γ = surface energy;

Ω = vacancy volume;

k = Boltzmann constant;

T = temperature;

r = radius;

K and m = $20/\sqrt{2}$ and 0.40 or $31/\pi^2$ and 0.46;[109]

D = diffusion coefficient of rate controlling ion.

This equation fits well for cation diffusion in CSZ.[7]

Equation 44 contains a diffusion coefficient for the rate-controlling species. As densification proceeds the pores shrink and there is a vacancy flux, away from the pores, on both sub-lattices. This would enhance diffusion, but perhaps not in a predictable manner since the local stoichiometry could change through the diffusion of oxygen vacancies, The number of vacancies on the cation lattice, which will be highest near the pore, will not be in equilbrium with the oxygen sub-lattice since that too will have the greatest number of vacancies near the pore. Thorn and Winslow[73] maintain that sintering may be controlled by the faster moving species since densification requires the movement of oxygen and uranium in parallel.[10] This means that although diffusion of U is very slow relative to the oxygen lattice (tracer D), diffusion of oxygen is relatively very fast and the densification could be controlled by the movement of the faster ion - the U being carried along with the flow of oxygen. This would however, amount to a macroscopic flow of UO_2. Further complications can arise in sintering due to non-uniform behaviour of the point-contacts between grains and the strain energy introduced on pressing the compact.[108]

7.1.2 Sintering of UO_2 in dry hydrogen

Activation energies for the sintering of stoichiometric UO_2 are 76,[24] 79[111] 102,[112] and 95 kcal.[116] The first two values could fit with a macroscopic flow process[10] which may be controlled by the slower diffusing species, or not.[73,117]

Although published data cannot be used for finding D from equation 44 it is generally remarked that sintering begins at temperatures where U-diffusion is too small to measure. This suggests that diffusion of U does not control the process directly.

In view of the complexities of sintering in UO_2 as outlined in Belle's book[10] and in the introduction to this section, a simple correlation of activation energies for diffusion and sintering is not expected.

Nabarro[16] and Herring[15] showed that deformation of a body by viscous flow may be controlled by diffusion. Herring's equation for the effective viscosity is,

$$\eta = \frac{kTL^2}{4D\Omega_0} \qquad (45)$$

where L is the grain size of the quasi-spherical grains of a single element with a cubic structure; and D is the diffusion coefficient for the rate controlling species.

If the diffusion coefficient can be described in the form,[73,110,115]

$$D = N_1 D_2 + N_2 D_1 \qquad -46$$

for dilute solutions where the activity coefficient does not change with composition, then since the diffusion coefficients calculated from equation 45 lie between D for O and for U diffusion and N_1 and N_2 are less than unity, the important term in evaluating D is $N_u D_o$. Since the diffusion is a function of stoichiometry, i.e. a function of the number of defects on the lattice, it is reasonable to suppose that N_u should be closely related to the number of uranium vacancies. However, equation 46 was developed for a binary alloy in which the total number of moles per unit volume was constant, $C = C_1 + C_2$. Here, $C_1 = o_i$ and $C_2 = u_v$, which means that $C_1 + C_2$ is constant for o_i very much greater than u_v. This is true for all x in UO_{2+x}. So the term N_u can be written as ku_v, where k is a constant. Hence sintering by viscous flow is expected to have an activation energy for oxygen diffusion in uranias. Using Auskern and Belle's value of 65 kcal for oxygen self-diffusion in $UO_{2.002}$ gives 11, 14, 37, and 30 kcal for the heat of formation of uranium vacancies (using the sintering activation energies above). All are reasonable values when compared with the calculated values for CaF_2.[92]

7.1.3 Sintering in steam and CO_2 There appears to be a large scatter in the reported activation energies for the sintering of UO_{2+x} in steam. In degassed steam x should not change much - but most papers quote different and final compositions. This could drastically affect the activation energy (if it depended on diffusion).

Thorn and Winslow point out that sintering activation energies in steam are compatible with oxygen diffusion controlling sintering. The decrease of about 37 kcals in the activation energy for sintering in UO_{2+x} agrees very well with the decrease of 36 kcal for diffusion of oxygen in UO_{2+x}. Since Q increases for U diffusion in UO_{2+x}, control by U movement can be ruled out.

In a CO_2 atmosphere no effect of hydroxyl ions should be present and some attempt to correlate the activation energy of 40.3 kcal (ref.24) (in $UO_{2.03}$) with composition and known oxygen diffusion coefficients is possible. In a pure CO_2 atmosphere UO_2 will become slightly more non-stoichiometric as the temperature rises leading to an effective higher activation energy for oxygen diffusion. But the increase would be very small and the activation energy would still be close to 30 kcal. Using equation 46, as for stoichiometric UO_2, gives a value of 10 kcal for the heat of formation of

uranium vacancies. This is about the same as in stoichiometric UO_2 and is a reasonable value.

7.2.1 Creep Steady state creep has been considered in terms of,

1) Vacancy migration
2) Dislocation climb
3) Quasi-viscous movement of dislocations
4) Peierls stress mechanism
5) Grain boundary sliding

Mechanisms 1), 2) and 3) could be controlled by U diffusion, although 2) and 3) could depend on the impurities near the dislocation (ref.120). Creep in a number of ionic solids has been considered, with some agreement on the mechanism. Some authors have reported Nabarro-Herring diffusional creep in polycrystalline Al_2O_3[114] and BeO, but Warshaw and Norton suggested dislocation movement to account for creep in Al_2O_3 at high temperature, high stresses and large grain size. For Al_2O_3 Chang[119] favours a dislocation climb mechanism in single crystals. With so many variables the agreement between different workers is only fair. It is possible that different mechanisms will be responsible for controlling the deformation as the conditions of the

experiment are changed.

7.2.2 Creep in urania Grain boundary sliding occurs in non-stoichiometric urania during deformation (but not in stoichiometric UO_2 where intercrystalline cracks are observed). Activation energies for creep are 91 kcal[120] and 95[113] for $UO_{2.0}$, and for $UO_{2.06}$ and $UO_{2.16}$ values of 55.7 and 63;[120] and 72 and 65 kcal,[113] have been reported. The results for UO_{2+x} cannot be obviously related with dislocation or vacancy movement in the bulk of the grains, and it is doubtful whether the activation energy for $UO_{2.0}$ is significant since the propagation of a crack would contribute to the strain rate. However, some work has been performed on single crystal material.[121] Here the activation energy is 117 kcal and the authors conclude that the deformation proceeds by a quasi-viscous movement of dislocations, the movement being impeded by impurities.[122]

7.3.1 Grain-growth in urania The growth of a grain requires the transfer of atoms from one grain to another. In a high angle boundary the environment is highly affected so the rate of transfer would be high, and the activation energy should be the same as that for grain boundary diffusion.

Results reported by Amato et al.,[123] show an activation energy of 75 kcal (1155 and 1655°C) in a hydrogen atmosphere and 87 kcal (1550 to 2440°C) in vacuo or argon.[124] Their own results give 115 kcal for stoichiometric UO_2 with other results in less well defined UO_2 of 65 and 87 or 58 kcal. The first value of 75 kcal is in nominally stoichiometric UO_2 and is in very good agreement with the results obtained for volume and grain boundary diffusion under a hydrogen atmosphere.

For non-stoichiometric urania activation energies of 49.5 ± 6.8 kcal (1160 to 1350°C) in steam and 46 ± 6 kcal (1207 to 1398°C) in CO_2 have been reported.[26] In this latter case the value of x in UO_{2+x} will increase with temperature and the apparent activation energy should be about 100 kcal for vacancy movement. The discrepancy here could be accounted for if grain boundary diffusion is controlling - the more logical case - but no good check can be made since grain boundary diffusion activation energies are not known in UO_{2+x}.

The general conclusion of Amato et al.,[123] is that the large scatter in activation energies and pre-exponential factors cannot be justified theoretically since there is no model for predicting either of the factors. Since it is not possible to choose between

the results already published, which may indeed be correct and apply only to the material under examination at the time, further work is needed in which the conditions, particularly in p_{O_2}, are carefully controlled.

7.4.1 Fission gas release in UO_2 A vast amount of work has been performed on fission gas and rare gas release from UO_2, but agreement between different workers is rare.[10,13,125,126,127] For example, Xe release from UO_2 has been fitted to a rate equation with the pre-exponential term ranging from 10^{-10} to 24, and Q ranging from 40 to 127 kcal. As in practically all other experiments on UO_2 insufficient data is available on the stoichiometry of the samples used in the experiment. Many experimenters crush the samples after irradiation probably introducing many dislocations into the structure and providing sites for weak trapping. MacEwan and Stevens[134] found that irradiation dose was important too; as were closed porosity and other defects.

Lustman[10] recommends for diffusion of fission gases in UO_2, the equation,

$$D = 6.6 \times 10^{-6} \exp(-71,700/RT) \text{cm}^2\text{sec}^{-1}$$

This result was obtained by Bostrom in dense UO_2 plate. An activation energy of about 70 kcal was obtained by several workers but Booth and Rymer, and Lindner and Matzke reported 46 and 49 kcal in crushed and powdered UO_2 respectively. Booth and Rymer used a He atmosphere and it is possible that the difference between their results and those of Bostrom is due to differences in stoichiometry since Auskern obtained 65 and 73:8 kcal for UO_2 powder reduced with H_2, and about 45 kcal for UO_{2+x}.

Auskern et al., pointed out that the absolute values for D for Xe^{133} diffusion were close to those for cation diffusion in UO_2. The activation energy is close too. This suggested that the movement was by a lattice diffusion mechanism and relatively insensitive to grain boundaries and voids (but see refs. 125, 128,129). The tentative conclusion was that fission gases diffuse via cation vacancies. However, this is probably wrong since it is unlikely that a very large atom like Xe (radius about 2.1 Å - and univalent Xe is about 1.83 Å - apart from a high ionisation potential) would have a similar activation energy to U for a vacancy mechanism. The closeness of D_{Xe} to D_U is probably fortuitous (see section 7.4.2).

7.4.2 Mechanism of fission gas diffusion in UO_2

In several places in Lustman's review[10] similarities of fission gas diffusion with oxygen ion diffusion in UO_{2+x} are mentioned,

1) D_o for Xe diffusion in UO_{2+x} is proportional to x
2) Q is independent of x
3) Q decreases by about 30 kcal from $UO_{2.0}$ to UO_{2+x}
4) D_{Xe} is enhanced in crushed in UO_2 as is D_{ox}.
5) $D_{I^{133}}$ is about the same as D_{Xe}

The first three observations do not fit with U self-diffusion in UO_2.

If an activation energy for movement of Xe^{133} of about 45 kcal is used (as in UO_{2+x}), (c.f.oxygen) then this would require a low D_o factor, and a negative activation entropy is indicated. This could be due to short circuiting paths or possibly to ordering during the diffusion jump. The second possibility is quite likely since the fission gas atom is a misfit in the lattice and would probably require the simultaneous movement of adjacent oxygen ions in specific directions to achieve a jump. The higher activation energy in stoichiometric UO_2 could be due to the energy of formation of oxygen defects.

It is not known whether the Xe occupies lattice or interstitial sites - or it may occupy both. Over the range of temperatures investigated (700 to 1100°C) for Xe diffusion in UO_{2+x} a close connection with oxygen ion diffusion is indicated. In this case the Xe would occupy both kinds of sites. However, results of Anderson et al.,[10] for Rn diffusion in UO_2 indicate a change in activation energy which becomes higher at higher temperatures. If the Xe exists in UO_2 as a neutral atom it would probably be distributed on both sub-lattices (a U lattice site is the same size as an oxygen interstitial site). This could account for a diffusion mechanism changing with temperature, the one with the higher activation energy dominating at high temperatures.

7.5 Physical properties of ThO_2 Little quantitative information is available on the properties of ThO_2. Temperatures of about 1500°C are required for sintering of ThO_2 with little difference in final density when sintered in H_2, air or O_2.[74] The addition of CaO to ThO_2 enhances the sintering rate.[14] There is no liquid phase at temperatures of less than 2300°C for the amounts of CaO used, so the effect is in a solid state reaction. The addition of Ca^{2+} could create anion

vacancies leading to enhanced oxygen diffusion. This suggests that sintering is dependent on the faster moving species.

No sintering is reported in ThO_2 for temperatures less than 1000°C,[130] c.f. 850°C for UO_2 in hydrogen[112] and 750°C for UO_2 in steam.[131] At 850°C D_u in UO_2 is 1/26 times D_{Th} in ThO_2, but $D_{Ox.}$ in UO_2 is about 270 times $D_{Ox.}$ in ThO_2. This is further evidence of oxygen diffusion controlling sintering. The oxygen diffusion coefficient is about $2 \times 10^{-11} cm^2 sec^{-1}$ in all three cases when sintering begins.

Creep in ThO_2 is accompanied by grain-boundary sliding and the formation of intergranular cracks[12] as in UO_2. The controlling mechanism is not clear since addition of Ca^{2+} enhances creep whereas a decrease in the strain rate is observed with Al^{3+} additions.

Data for diffusion of Kr, Xe and Rn in ThO_2 are as varied as those for UO_2[13] and no attempt can be made to correlate the results with diffusion measurements.

CONCLUSIONS

8. CONCLUSIONS

1. Volume diffusion coefficients for uranium self-diffusion in urania were shown to depend strongly on the stoichiometry. Equations were established for diffusion in stoichiometric UO_2, $UO_{2.01}$, $UO_{2.03}$, $UO_{2.1}$ and $UO_{2.15}$.

2. Uranium diffusion in urania probably occurs by movement of a U^{5+} ion into a vacancy.

3. Th self-diffusion in thoria was shown to be independent of oxygen pressure (10^{-20} to $10^{-0.7}$) in the small temperature range investigated.

4. Grain boundary diffusion of the cation was established in UO_2 and UO_{2+x}; but the results were not very reproducible. An estimate of the activation energy for grain boundary diffusion for $UO_{2.0}$ showed it to be about the same as that for volume diffusion.

5. Attempts to correlate relevant physical properties with diffusion produced tentative conclusions that sintering, creep and fission gas diffusion are closely related to oxygen diffusion.

APPENDIX

Appendix 1

Grain-boundary diffusion

The grain-boundary contribution, $\bar{c}_2$, was evaluated from the second term in equation 2 using Gaussian quadrature[140]. $\sqrt{(\Delta - 1)/(\Delta - \sigma)}$ was taken to be unity and the upper limit of the integral was replaced by ∞. For η in the experimental range the integrand is only appreciable for $\sigma \ll \Delta$.[52] The grain-boundary width, 2a, was taken to be 5×10^{-8} Å in keeping with Suzuoka's computations. The method of integration used by Suzuoka was not stated, but the results obtained by Gaussian quadrature for N = 16 deviate slightly from Suzuoka's values for large values of η. Since the important part of the profile is at low values of η the results obtained by Gaussian quadrature were considered to be satisfactory.

Values of $\bar{c}_2$ are tabulated as, e.g. -9.031(-1) which means, $\bar{c}_2 = -9.031 \times 10^{-1}$.

Values of $\bar{c}_2$

	Suzuoka 20	G.Q. 20	Suzuoka 30	G.Q. 30	G.Q 40
0	-1.342(0)	-1.342(0)	-1.470(0)	-1.469(0)	-1.554(0)
0.5		-1.221(0)		-1.344(0)	-1.426(0)
1	-9.033(-1)	-9.031(-1)	-1.014(0)	-1.014(0)	-1.089(0)
1.5		-4.978(-1)		-5.905(-1)	-6.560(-1)
2	-1.214(-1)	-1.213(-1)	-1.939(-1)	-1.931(-1)	-2.467(-1)
3	3.072(-1)	3.074(-1)	2.752(-1)	2.758(-1)	2.460(-1)
4	3.628(-1)	3.630(-1)	3.611(-1)	3.617(-1)	3.510(-1)
5	2.908(-1)	2.910(-1)	3.081(-1)	3.084(-1)	3.110(-1)
6	2.135(-1)	2.138(-1)	2.409(-1)	2.410(-1)	2.521(-1)
8	1.099(-1)	1.102(-1)	1.417(-1)	1.415(-1)	1.598(-1)
10	5.511(-2)	5.532(-2)	8.179(-2)	8.120(-2)	9.977(-2)
12	2.699(-2)	2.699(-2)	4.644(-2)	4.561(-2)	6.160(-2)
18	2.777(-3)	2.426(-3)	7.760(-3)	7.555(-3)	1.468(-2)

	50	60	70	80	90
0	-1.616(0)	-1.663(0)	-1.700(0)	-1.729(0)	-1.755(0)
0.5	-1.486(0)	-1.532(0)	-1.568(0)	-1.598(0)	-1.622(0)
1	-1.145(0)	-1.188(0)	-1.222(0)	-1.249(0)	-1.273(0)
1.5	-7.053(-1)	-7.436(-1)	-7.739(-1)	-7.987(-1)	-8.201(-1)
2	-2.883(-1)	-3.211(-1)	-3.474(-1)	-3.691(-1)	-3.879(-1)
3	2.203(-1)	1.989(-1)	1.811(-1)	1.661(-1)	1.526(-1)
4	3.386(-1)	3.270(-1)	3.168(-1)	3.077(-1)	2.991(-1)
5	3.085(-1)	3.045(-1)	3.002(-1)	2.959(-1)	2.912(-1)
6	2.565(-1)	2.580(-1)	2.582(-1)	2.576(-1)	2.559(-1)
8	1.715(-1)	1.795(-1)	1.853(-1)	1.895(-1)	1.920(-1)
10	1.136(-1)	1.241(-1)	1.323(-1)	1.387(-1)	1.434(-1)
12	7.482(-2)	8.558(-2)	9.434(-2)	1.014(-1)	1.068(-1)
18	2.185(-2)	2.826(-2)	3.377(-2)	3.844(-2)	4.233(-2)

	100	110	120	130	140
0	-1.778(0)	-1.800(0)	-1.822(0)	-1.845(0)	-1.869(0)
0.5	-1.645(0)	-1.667(0)	-1.689(0)	-1.711(0)	-1.735(0)
1	-1.294(0)	-1.315(0)	-1.336(0)	-1.358(0)	-1.381(0)
1.5	-8.398(-1)	-8.591(-1)	-8.790(-1)	-9.000(-1)	-9.223(-1)
2	-4.055(-1)	-4.231(-1)	-4.415(-1)	-4.612(-1)	-4.824(-1)
3	1.395(-1)	1.256(-1)	1.104(-1)	9.354(-2)	7.490(-2)
4	2.899(-1)	2.795(-1)	2.674(-1)	2.532(-1)	2.370(-1)
5	2.854(-1)	2.779(-1)	2.684(-1)	2.566(-1)	2.426(-1)
6	2.528(-1)	2.478(-1)	2.404(-1)	2.307(-1)	2.187(-1)
8	1.926(-1)	.910(-1)	1.870(-1)	1.805(-1)	1.719(-1)
10	1.461(-1)	1.466(-1)	1.449(-1)	1.409(-1)	1.349(-1)
12	1.104(-1)	1.122(-1)	1.120(-1)	1.099(-1)	1.060(-1)
18	4.551(-2)	4.802(-2)	4.989(-2)	5.120(-2)	5.199(-2)

	150	160	180	200
0	-1.894(0)	-1.920(0)	-1.975(0)	-2.030(0)
0.5	-1.760(0)	-1.786(0)	-1.840(0)	-1.896(0)
1	-1.406(0)	-1.431(0)	-1.484(0)	-1.539(0)
1.5	-9.460(-1)	-9.707(-1)	-1.022(0)	-1.076(0)
2	-5.050(-1)	-5.288(-1)	-5.790(-1)	-6.311(-1)
3	5.463(-2)	3.296(-2)	-1.350(-2)	-6.233(-2)
4	2.190(-1)	1.995(-1)	1.568(-1)	1.114(-1)
5	2.267(-1)	2.092(-1)	1.702(-1)	1.282(-1)
6	2.047(-1)	1.889(-1)	1.536(-1)	1.149(-1)
8	1.612(-1)	1.488(-1)	1.201(-1)	8.803(-2)
10	1.270(-1)	1.176(-1)	9.513(-2)	6.954(-2)
12	1.006(-1)	9.382(-2)	7.727(-2)	5.801(-2)
18	5.234(-2)	5.231(-2)	5.136(-2)	4.958(-2)

Appendix 2

Range-energy relationship for α-particles in UO_2

The α-ray spectrum for a homogeneous source shows a fall-off in count towards lower energies. This could be due to either a non-linear energy-channel number or non-linear range-energy relationship. Both relationships were investigated.

The range-energy relationship for α-particles in noble gases is linear[56]. Since the range is proportional to the energy the energy loss, which is ΔE, of an alpha-particle travelling a distance r through argon at a pressure p, in which it has a maximum range R, is given by,

$$E = \frac{r}{R}E_o = \frac{rp}{K}E_o = K' E_o p = kp$$

(E_o = initial energy of α-particle ; and the range is inversely proportional to the pressure[56]).
So, the residual energy of the α-particle at the detector is,

$$E = E_o - kp \qquad -(47)$$

The position of the peak on the spectrometer (channel number) from a monoenergetic U^{233} weightless source was measured as a function of argon pressure. At channel 0 the residual energy E, is zero, so

$$k = E_o/p^o \qquad -(48)$$

The spread of the source increased towards lower energies and it was not possible to measure the position of the peak for very low channel numbers. An extrapolation to zero energy was made (Figure 47). Having found k in equation 48, equation 47 can be used to give a plot of "energy" versus "channel number" (Figure 48). Two different "source to detector" distances were used and the results agreed within the experimental error introduced by the extrapolation.

Using the calibration curve for "depth in UO_2" versus "channel number of the spectrometer" a plot of "energy" versus "distance" could be made (Figure 49). This showed that the range-energy relationship was indeed linear from 1.3 MeV to 4.816 MeV. The slope of this line was 448 keV/ micron. This agreed reasonably well with 486 KeV/micron obtained by McNamara.[1]

The non-linearity of the depth-channel number calibration curve could be attributed to the non-linear performance of the spectrometer. Using values of $\Delta E/dc$ (energy change per channel) (Figure 48) the channel width could be reproduced exactly using the value of 448 keV/micron, but the theoretically derived value, 283 keV/micron, used by Schmitz[58] gave a channel width which was 1.58 times too large. However, this latter

value of dE/dx agreed with the calibration for high energies if the energy per channel were determined using a multi-standard source. The source used covered a range of energies from 4.816 to 6.11 MeV and it was possible that within this range of energies the non-linear behaviour of the "energy-channel number" curve gave a value of dE/dc which was not representative of the energy range just below 4.816 MeV and the agreement between the two methods of calibration was fortuitous.

If it is assumed that the range-energy relationship is linear down to zero energy, then the maximum range for 4.816 MeV α-particles in UO_2 is about 10.7 microns. (McNamara's value of R showed that the maximum range would be greater than 9.5 microns). The range will probably fall off more rapidly at low energies and the value of 10.7 microns could be regarded as an upper limit of the range.

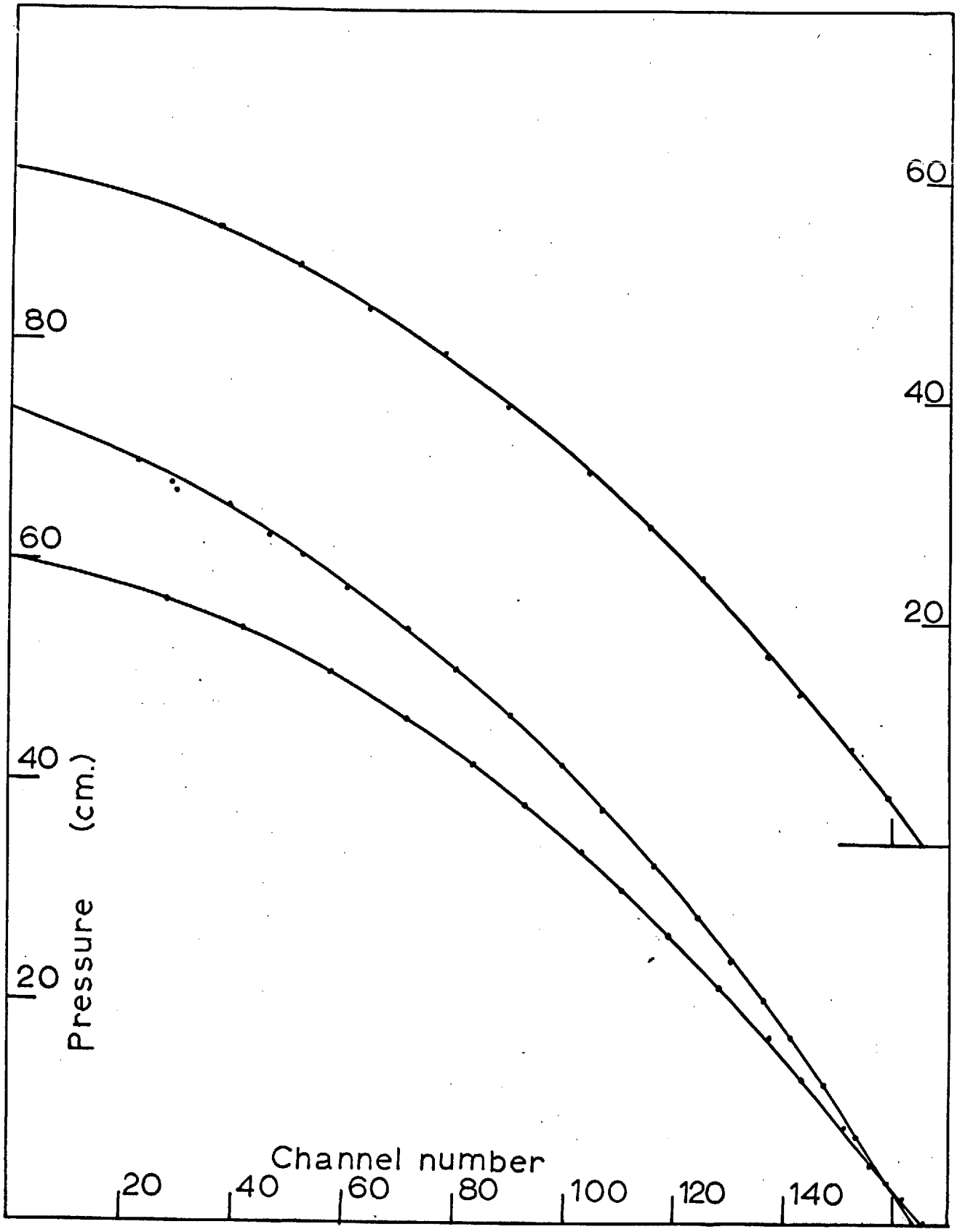
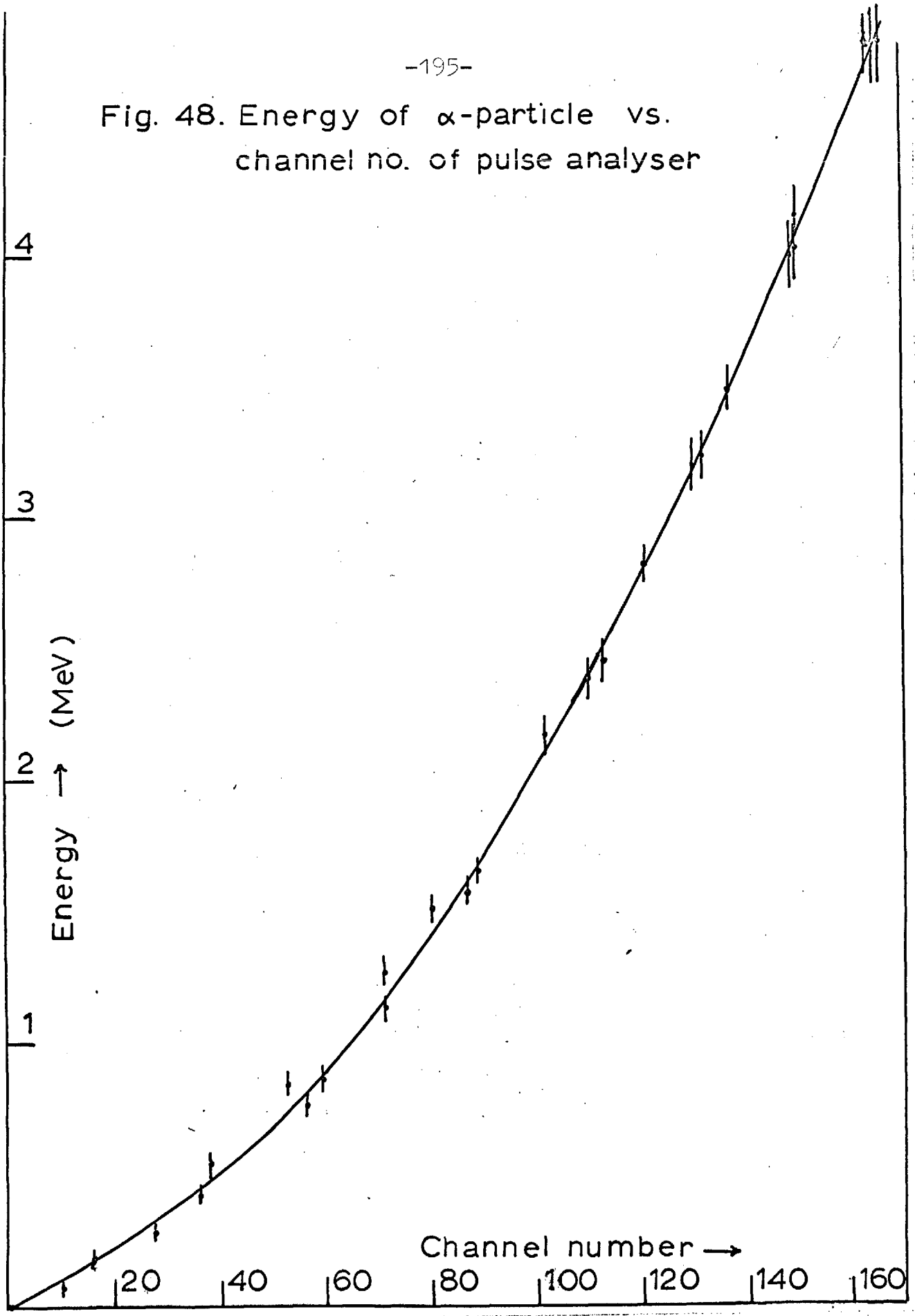


Fig. 47. Argon pressure vs. peak position.

Fig. 48. Energy of α-particle vs. channel no. of pulse analyser



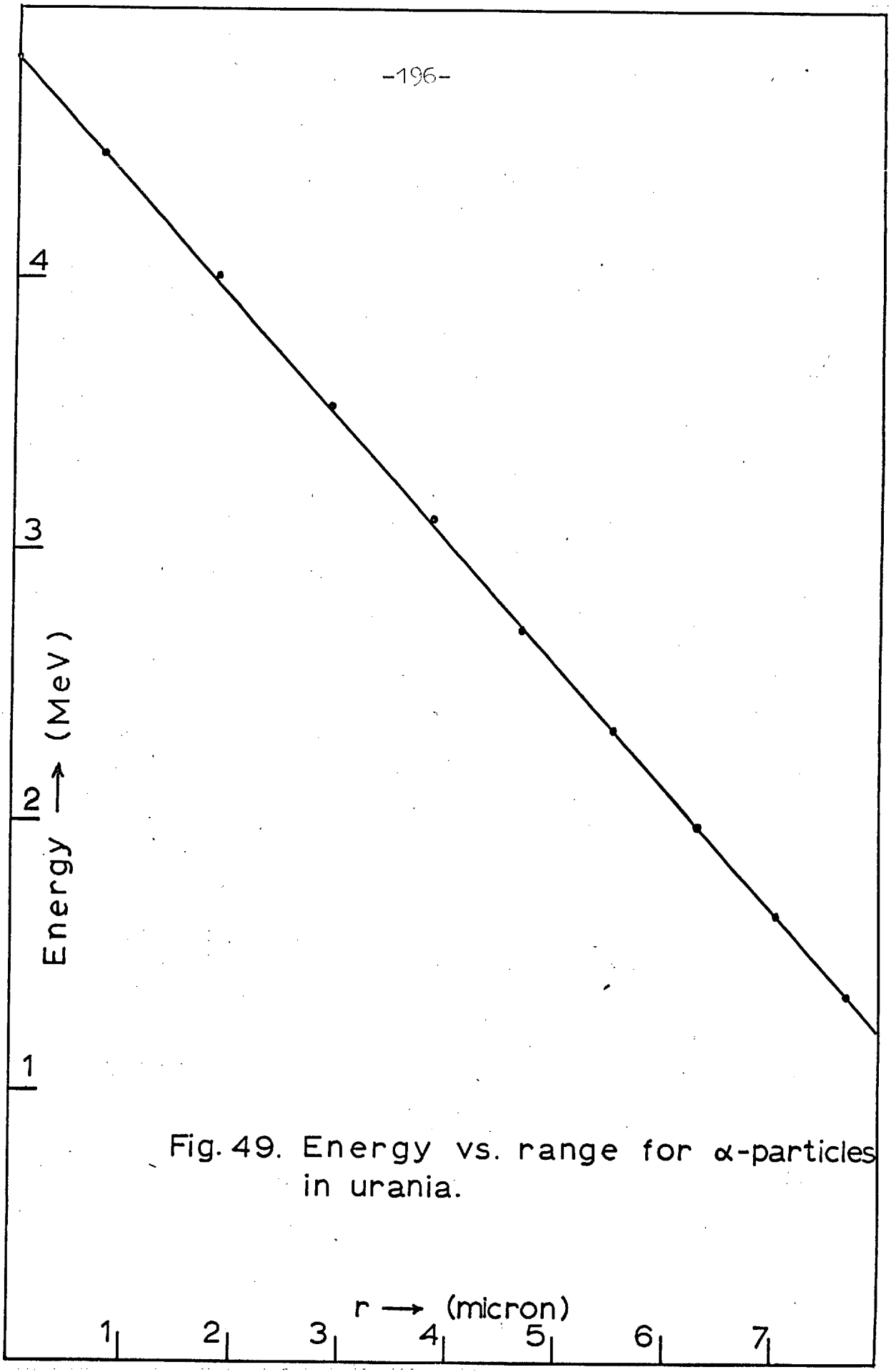


Fig. 49. Energy vs. range for α-particles in urania.

Appendix 3

Effect of Instrumental Error on the Diffusion Profile

Consider diffusion from an infinitesimally thin tracer layer into a semi-infinite solid.

Consider a collimated count and assume the spread of energies, due to instrumental error, to be normally distributed.(Figure 50).

The true concentration at depth ξ is given by the solution to Fick's equation for this geometry:-

$$C_{\xi} = \frac{C_o}{\sqrt{\pi Dt}} \exp \frac{-\xi^2}{4Dt}$$

Let Gaussian be $I = I_o \exp \frac{-(x-\xi)^2}{2\sigma^2}$; σ = standard deviation

$$\text{Now } I_{\xi} = I_o \int_{-\infty}^{+\infty} \exp \frac{-(x-\xi)^2}{2\sigma^2} \, d\xi$$

giving $$I_{\xi} = \sqrt{2\pi}\sigma \, I_o$$

Let the relationship between concentration and activity be:-

$$I_{\xi} = \beta' C_{\xi}$$

The activity at a point x due to spread at ξ is:-

$$I = \frac{\beta' C_{\xi}}{\sqrt{2\pi}\,\sigma} \exp \left(\frac{-(x-\xi)^2}{2\sigma^2}\right)$$

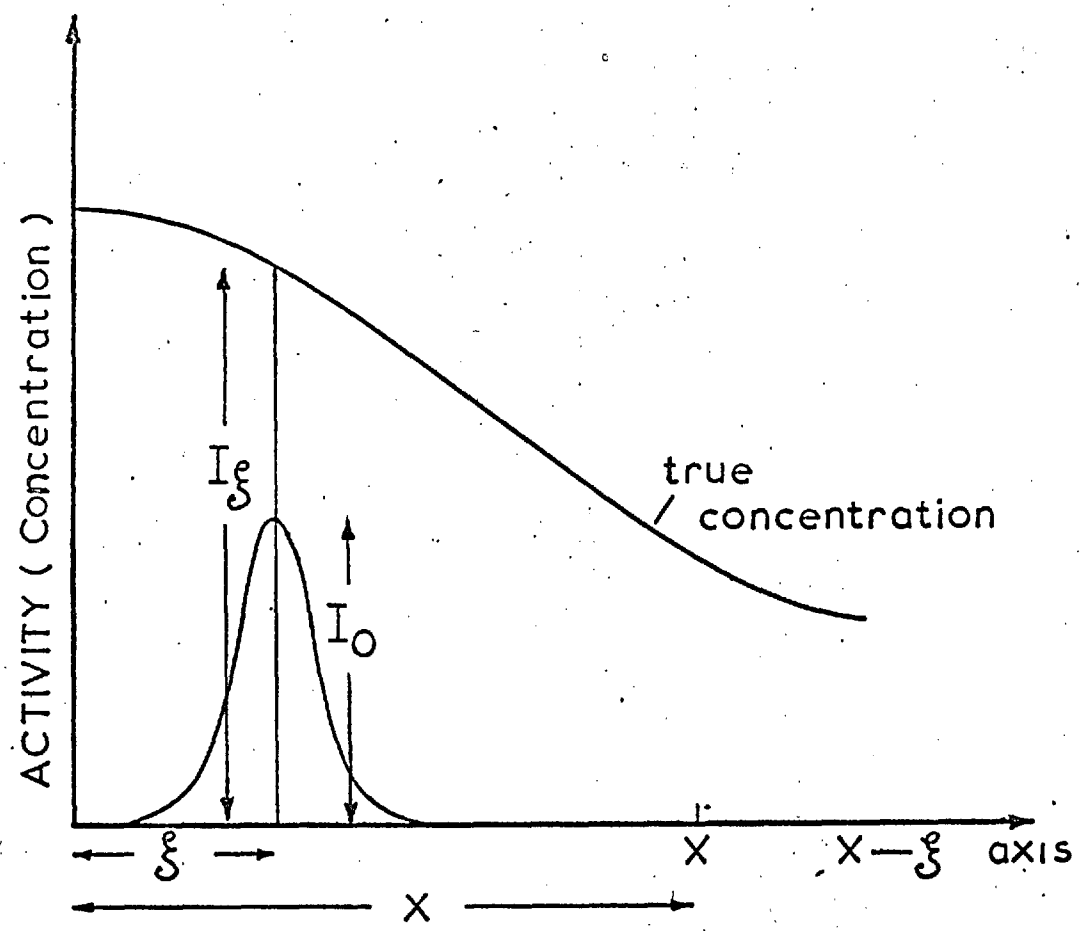


Figure 50. Effect of instrumental error on diffusion profile.

The total count at x, I_x is given by,

$$I_x = \int_0^\infty \frac{\beta'}{\sqrt{2\pi}\sigma} \frac{C_o}{\sqrt{\pi Dt}} \exp\left(\frac{-\xi^2}{4Dt}\right) \exp\left(\frac{-(x-\xi)^2}{2\sigma^2}\right) d\xi$$

$$I_x = C' \int_0^\infty \exp - (k_1 \xi^2 - k_2 \xi) d\xi$$

where $C' = \frac{\beta' C_o}{\pi \sigma \sqrt{2Dt}} \cdot \exp\left(\frac{-x^2}{2\sigma^2}\right) \neq f(\xi)$; $k_1 = \frac{1}{4Dt} + \frac{1}{2\sigma^2}$;

$k_2 = \frac{x}{\sigma^2}$

Completing the square:-

$$I_x = C' \exp \frac{k_2^2}{4k_1} \int_0^\infty \exp - (\sqrt{k_1}\xi - \frac{k_2}{2\sqrt{k_1}})^2 d\xi$$

$$= C'' \int_0^\infty \exp - (\sqrt{k_1}\xi - \frac{k_2}{2\sqrt{k_1}})^2 d\xi$$

Putting $\eta = \sqrt{k_1}\xi - \frac{k_2}{2\sqrt{k_1}}$

gives $d\xi = \frac{1}{\sqrt{k_1}} d\eta$.

$$\therefore I_x = \frac{C''}{\sqrt{k_1}} \int_{\frac{-k_2}{2\sqrt{k_1}}}^\infty \exp - \eta^2 d\eta$$

$$\therefore I_x = \frac{C''}{\sqrt{k_1}} \frac{\sqrt{\pi}}{2} \operatorname{erfc}\left(\frac{-k_2}{2\sqrt{k_1}}\right)$$

Substituting back for C", k_1 and k_2

gives $I_x = \frac{\beta' C_o}{2\sqrt{\pi}\sqrt{4Dt+2\sigma^2}} \exp\left(\frac{-x^2}{2\sqrt{2Dt + \sigma^2}}\right) \operatorname{erfc}\left(\frac{-x\sqrt{2Dt}}{\sqrt{2}\sigma\sqrt{2Dt + \sigma^2}}\right)$

Introducing the dimensionless parameters:

$$x^* = \frac{x}{\sqrt{2}\sigma} \quad \text{and} \quad D^* = \frac{\sqrt{2Dt}}{\sigma} \quad \left(= \frac{\sqrt{4Dt}}{\sqrt{2}\sigma}\right)$$

$$\text{Gives } I_x = \frac{\beta' C_o}{2\sqrt{2\pi\sigma^2(D^{*2}+1)}} \exp\frac{-x^{*2}}{D^{*2}+1} \operatorname{erfc}\frac{-x^* D^*}{D^{*2}+1}$$

For values of D^* for UO_2, "log I_x" versus "x^2" is a straight line beyond $x^* = 4$, of gradient,

$$G = \frac{1}{4Dt + 2\sigma^2}$$

$$D = \frac{1}{4Gt} - \frac{2\sigma^2}{4t}$$

For a given spread the correction term (c.f. equation 1) becomes more important for short diffusion runs and small diffusion coefficients.

For a "2π-count" for volume diffusion alone,

$$I_x = \frac{1}{\sqrt{2\pi}\sigma} \cdot \frac{NC_o R\sqrt{Dt}}{E_o\sqrt{\pi}} \int_o^\infty \frac{1-\exp(-\xi^2/4Dt)}{\xi^2} \exp(-(x-\xi)^2/2\sigma^2)\, d\xi$$

$$\text{or } I_x = \text{const. } D^* \int_o^\infty \left(1-\exp\left(\frac{-\xi^2}{D^{*2}}\right)\right) \frac{\exp(-(x^*-\xi^*)^2)}{\xi^{*2}}\, d\xi^*$$

It is possible to integrate this in terms of a series but serious difficulties arose when the limits are considered.

Putting $\xi^* = \frac{\eta - 1}{\eta + 1}$

gives $I_x = \text{const.} \times D^* \int_{-1}^{+1} \frac{1-\exp(-(\frac{\eta - 1}{(\eta+1)D^*})^2)}{(\eta - 1)^2} \times$

$$\exp(-(x^* - \frac{\eta - 1}{\eta + 1})^2)\, d\eta$$

From Weierstrass' Theorem:-

$$\int_{-1}^{+1} f(x)\, dx = \sum_{j=1}^{n} H_j f(a_j) \qquad (15)$$

Tables of H_j (weighting factors) and a_j are available[132] and here,

$$f(\eta) = \frac{1-\exp-(\frac{(\eta-1)}{(\eta+1)D^*})^2}{(\eta-1)^2} \cdot \exp -(x^* \frac{\eta - 1}{\eta + 1})^2$$

Values can be obtained for n = 2,3,4 etc. until the smallest acceptable error between successive determinations is reached.

Appendix 4

Results. Figures for concentration profiles

Figures for grain-boundary concentration profiles were "smoothed values" taken from curves such as those shown in Figure 51. Although individual counts showed considerable scatter the curve was usually quite well defined. Most curves were like the average cases, 2 and 3; but even curve 4, which showed the greatest scatter, was still fairly well defined. The tracer activities, corrected to constant channel width, are given every five channels in the following tables.

Figures in brackets in the tables are the standard errors in the count:

$$A - B = C$$

A = total count; B = background; C = tracer count. Error in A is $\sqrt{A}$; and in B is $\sqrt{B}$.

Error in C is $\sqrt{A + B}$. This is a slight over-estimate since B is the average background.

Calibrations A - G are for different settings on the spectrometer (D is for a different spectrometer). A typical setting is given in section 2.2.

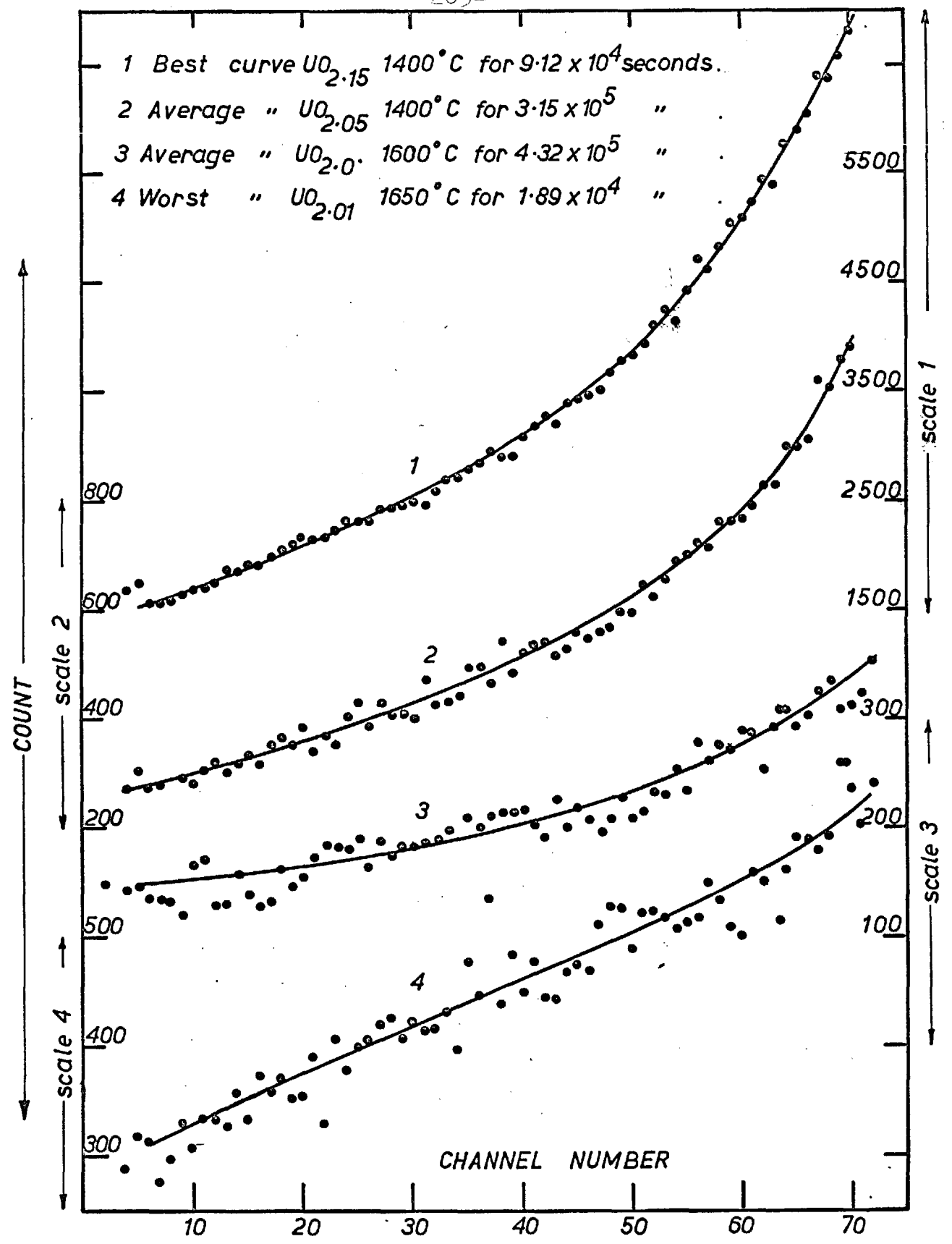


FIG.51 COUNT vs. CHANNEL NUMBER.- SMOOTHING CURVES. GRAIN-BOUNDARY PART OF DIFFUSION PROFILE

Calibration

Depth (microns) in UO_2.

Channel Number	A	B	C	D	E	F	G
5	7.88	2.871	7.73	7.95	7.51	6.91	6.20
10	7.70	2.739	7.38	7.59	7.21	6.58	5.90
15	7.37	2.585	6.99	7.22	6.91	6.24	5.58
20	7.04	2.418	6.57	6.84	6.57	5.88	5.22
25	6.70	2.258	6.13	6.42	6.22	5.49	4.88
30	6.32	2.093	5.68	6.02	5.85	5.10	4.52
35	5.93	1.930	5.19	5.60	5.46	4.39	4.15
40	5.52	1.762	4.71	5.15	5.05	4.26	3.76
45	5.10	1.624	4.19	4.71	4.63	3.81	3.39
50	4.68	1.462	3.67	4.25	4.20	3.37	2.98
55	4.28	1.292	3.14	3.78	3.77	2.92	2.56
60	3.84	1.121	2.57	3.31	3.32	2.44	2.15
65	3.38	0.954	1.97	2.84	2.86	1.95	1.73
70	2.88	0.784	1.37	2.36	2.39	1.45	1.32
75	2.37	0.619	0.76	1.86	1.92	0.94	0.95
80	1.85	0.412	80=0	1.37	1.43	0.41	0.54
85	1.32	0.240		0.87	0.87	84=0	86=0
90	0.77	0.066		0.37	0.33		
95	0.22	92=0		93=0	93=0		
	97=0						

ThO_2 calibration The energy loss per unit depth is smaller in ThO_2 than in UO_2. Thus the channel width (microns) is greater in thoria in urania. Results for ThO_2 were plotted as "log c" versus "x^2" using the UO_2 calibrations (D-G). The value of D obtained was multiplied by 1.28 (see section 2.3).

Stoichiometric UO_2 — 1477°C for 6.912×10^5 sec.
Polycrystal — Calibration: A
Counting time: 49000 sec. — Background: 61 above ch. 80

C	A	C	A	C	A	C	A
5	-	60	86(13)	80	197(18)	91	447(24)
10	16(16)	65	105(19)	81	209(18)	92	583(26)
15	21(16)	70	133(19)	82	240(19)	93	608(27)
20	26(16)	72	156(20)	83	230(19)	94	711(29)
25	31(17)	73	128(19)	84	244(19)	95	911(32)
30	36(17)	74	144(20)	85	287(20)	96	1152(35)
35	42(17)	75	159(20)	86	318(21)	97	1037(33)
40	46(17)	76	187(20)	87	327(21)	98	374(19)
45	51(17)	77	194(20)	88	327(21)	99	31(6)
50	61(17)	78	243(21)	89	368(28)	100	6(2)
55	70(18)	79	217(19)	90	418(23)		

Stoichiometric UO_2 — 1490°C for 2.25×10^6 sec.
Polycrystal 1 — Calibration: A
Counting time: 12100 sec. — Background: 14 above ch. 80

C	A	C	A	C	A	C	A
5	87(12)	60	211(16)	80	387(20)	91	1072(33)
10	94(12)	65	258(17)	81	391(20)	92	1416(38)
15	100(12)	70	263(16)	82	394(20)	93	1765(42)
20	106(13)	72	279(15)	83	435(22)	94	2250(47)
25	112(13)	73	255(16)	84	495(23)	95	3725(61)
30	120(13)	74	291(19)	85	539(24)	96	5530(74)
35	129(14)	75	271(16)	86	547(24)	97	6853(83)
40	136(14)	76	315(19)	87	604(25)	98	3598(60)
45	152(14)	77	298(18)	88	638(26)	99	797(28)
50	170(15)	78	340(19)	89	802(29)	100	240(15)
55	190(16)	79	378(20)	90	917(31)		

Stoichiometric UO_2 — 1490°C for 2.25×10^6 sec.
Polycrystal 2 — Calibration: A
Counting time: 13200 sec. — Background: 17 above ch. 80

C	A	C	A	C	A	C	A
5	78(12)	60	175(16)	79	232(18)	90	719(27)
10	80(12)	65	211(17)	80	345(20)	91	804(29)
15	84(12)	70	210(17)	81	311(19)	92	936(31)
20	88(12)	71	208(17)	82	327(19)	93	1220(35)
25	95(13)	72	204(17)	83	373(20)	94	1547(40)
30	95(13)	73	168(16)	84	417(21)	95	2341(49)
35	115(13)	74	257(18)	85	418(21)	96	3625(60)
40	124(14)	75	244(18)	86	480(23)	97	4428(66)
45	135(14)	76	253(18)	87	492(23)	98	2083(46)
50	147(15)	77	275(18)	88	558(24)	99	233(14)
55	159(15)	78	284(18)	89	592(25)	100	6(2)

Stoichiometric UO_2 — 1547°C for 6.912×10^5 sec.
Polycrystal — Calibration: A
Counting time: 17100 sec. — Background: 22 above ch. 80

C	A	C	A	C	A	C	A
5	-	60	52(12)	80	137(14)	91	453(22)
10	-	65	61(12)	81	142(14)	92	551(24)
15	-	70	78(13)	82	145(14)	93	735(28)
20	-	72	93(13)	83	162(14)	94	836(30)
25	15(10)	73	84(13)	84	186(15)	95	1030(32)
30	18(10)	74	70(13)	85	207(16)	96	1221(35)
35	21(10)	75	86(13)	86	208(16)	97	1210(35)
40	25(11)	76	104(14)	87	240(17)	98	644(25)
45	29(11)	77	137(14)	88	273(18)	99	90(9)
50	34(11)	78	118(14)	89	318(19)	100	13(4)
55	42(11)	79	127(14)	90	370(20)		

Stoichiometric UO_2 — 1600°C for 4.32×10^5 sec.
Polycrystal — Calibration: A
Counting time: 84000 sec. — Background: 106 above ch. 80

C	A	C	A	C	A	C	A
35	44(22)	74	172(24)	83	257(22)	92	587(28)
40	52(22)	75	142(24)	84	277(22)	93	756(31)
45	60(22)	76	230(25)	85	279(22)	94	942(34)
50	71(22)	77	206(24)	86	312(23)	95	1132(36)
55	84(22)	78	294(25)	87	339(23)	96	1239(37)
60	99(23)	79	243(23)	88	384(24)	97	918(31)
65	116(23)	80	224(22)	89	422(25)	98	262(16)
70	142(23)	81	226(21)	90	460(26)	99	16(4)
72	150(24)	82	239(21)	91	578(28)	100	9(3)
73	140(24)						

Stoichiometric UO_2 — 1600°C for 2.25×10^6 sec.
Polycrstal 1 — Calibration: A
Counting time: 60000 sec. — Background: 75 above ch. 80

C	A	C	A	C	A	C	A
5	806(33)	60	1784(46)	80	3510(61)	91	6997(85)
10	906(35)	65	2005(48)	81	3470(60)	92	7789(89)
15	988(36)	70	2405(52)	82	3782(63)	93	8968(96)
20	1055(37)	72	2500(52)	83	3894(64)	94	10818(104)
25	1120(38)	73	2652(54)	84	4109(65)	95	13234(116)
30	1192(39)	74	2710(55)	85	4388(67)	96	16092(127)
35	1270(40)	75	2805(56)	86	4457(68)	97	15579(125)
40	1354(41)	76	2946(57)	87	4931(71)	98	6044(78)
45	1422(42)	77	3037(57)	88	5274(74)	99	509(23)
50	1520(43)	78	3068(57)	89	5814(77)	100	110(10)
55	1625(44)	79	3190(58)	90	6196(80)		

Stoichiometric UO_2 — 1600°C for 2.25×10^6 sec.
Polycrystal 2 — Calibration: A
Counting time: 6000 sec. — Background: 7 above ch.80

C	A	C	A	C	A	C	A
5	113(12)	60	267(17)	80	569(24)	91	1741(42)
10	127(12)	65	300(18)	81	533(23)	92	2259(48)
15	138(13)	70	355(20)	82	603(25)	93	3215(57)
20	150(13)	72	367(29)	83	640(26)	94	4506(67)
25	158(14)	73	396(21)	84	701(27)	95	5843(77)
30	168(14)	74	426(21)	85	735(27)	96	5565(75)
35	179(14)	75	438(22)	86	873(30)	97	3056(55)
40	191(15)	76	488(23)	87	889(30)	98	1155(34)
45	205(15)	77	447(22)	88	1092(33)	99	270(16)
50	220(16)	78	485(22)	89	1177(35)	100	43(7)
55	239(16)	79	482(22)	90	1322(36)		

Stoichiometric UO_2 — 1650°C for 5.184×10^5 sec.
Polycrystal — Calibration: A
Counting time: 64100 sec. — Background: 80 above ch. 80

C	A	C	A	C	A	C	A
5	22(18)	60	145(22)	80	317(22)	91	752(30)
10	35(19)	65	169(22)	81	337(22)	92	932(33)
15	46(19)	70	217(23)	82	338(22)	93	1132(36)
20	55(19)	72	228(23)	83	331(22)	94	1425(40)
25	65(20)	73	262(24)	84	375(23)	95	1854(44)
30	74(20)	74	262(24)	85	417(24)	96	2304(49)
35	86(20)	75	265(24)	86	467(25)	97	2103(46)
40	96(20)	76	285(24)	87	494(26)	98	720(27)
45	104(21)	77	251(23)	88	606(28)	99	49(7)
50	116(21)	78	330(24)	89	629(28)	100	3(3)
55	127(21)	79	323(23)	90	693(29)		

Stoichiometric UO_2 — 1584°C for 8.691×10^5 sec.
Single crystal — Calibration: A
Counting time: 60000 sec. — Background: 90 above ch. 80

C	A	C	A	C	A	C	A
77	24(17)	83	42(14)	89	114(17)	95	792
78	32(16)	84	45(15)	90	168(18)	96	533
79	35(15)	85	43(14)	91	256(20)	97	284
80	29(14)	86	51(15)	92	445(25)	98	99
81	46(14)	87	82(16)	93	745(30)	99	9
82	47(15)	88	95(16)	94	850(31)	100	0

Stoichiometric UO_2 — 1620°C for 5.904×10^5 sec.
Single crystal — Calibration: G
Counting time: 66000 sec. — Background: 285 above ch. 68

C	A	C	A	C	A	C	A
63	167	70	495	77	830	84	2186
64	212	71	448	78	931	85	2522
65	275	72	535	79	1065	86	3084
66	339	73	627	80	1215	87	3691
67	399	74	656	81	1350	88	4197
68	413	75	735	82	1545	89	3299
69	518	76	799	83	1803	90	1095

Stoichiometric UO_2 — 1720°C for 2.592×10^5 sec.
Single crystal — Calibration: A

C	A	C	A	C	A	C	A
79	31(15)	85	110(15)	91	532(25)	96	5063(72)
80	49(14)	86	134(16)	92	854(31)	97	5208(72)
81	31(12)	87	156(16)	93	1331(38)	98	4174
82	49(13)	88	205(18)	94	2086(47)	99	352
83	63(13)	89	222(18)	95	3456(59)	100	5
84	66(13)	90	359(22)				

Stoichiometric UO_2 — 1477°C for 6.912×10^5 sec.
Polycrystal — Calibration: B
Counting time: 100600 sec — Background: 36

C	A	C	A	C	A	C	A
55	228(17)	62	275(19)	69	280(19)	75	387(21)
56	214(17)	63	263(18)	70	282(19)	76	378(21)
57	224(17)	64	221(18)	71	312(20)	77	428(22)
58	245(18)	65	280(19)	72	327(20)	78	464(23)
59	221(17)	66	293(19)	73	379(21)	79	489(24)
60	257(18)	67	280(19)	74	365(21)	80	507(24)
61	250(18)	68	277(19)				

Stoichiometric UO_2 — 1600°C for 2.25×10^6 sec.
Polycrystal — Calibration: B
Counting time: 20100 sec. — Background: 7

C	A	C	A	C	A	C	A
60	797(29)	66	976(31)	71	1330(37)	76	1764(42)
61	813(29)	67	1039(32)	72	1340(37)	77	2033(45)
62	888(30)	68	1062(330	73	1492(39)	78	2292(48)
63	933(31)	69	1161(34)	74	1546(40)	79	2500(50)
64	921(31)	70	1248(36)	75	1782(42)	80	2826(53)
65	902(30)						

$UO_{2.001}$ — 1400°C for 4.248×10^5 sec.

Single crystal — Calibration: E

Counting time: 14400 sec. — Background: 40 above ch. 80

C	A	C	A	C	A	C	A
78	50(13)	83	102(14)	88	113(14)	93	754(30)
79	36(12)	84	78 (13)	89	149(15)	94	1452(40)
80	57(12)	85	89(13)	90	189(17)	95	2328(50)
81	83(13)	86	76(13)	91	274(19)	96	1699(42)
82	61(12)	87	99(14)	92	457(24)	97	242 (6)

$UO_{2.001}$ — 1400°C for 1.217×10^6 sec.

Single crystal — Calibration: E

Counting time: 57600 sec. — Background: 160 above ch. 80

C	A	C	A	C	A	C	A
76	104(26)	82	338(27)	88	447(29)	93	1974(50)
77	116(25)	83	332(27)	89	597(31)	94	3686(65)
78	100(24)	84	342(27)	90	631(33)	95	6546(81
79	148(25)	85	331(27)	91	826(36)	96	5033(75)
80	177(25)	86	374(28)	92	1197(41)	97	832(29)
81	252(25)	87	422(29)				

$UO_{2.001}$ — 1400°C for 1.217×10^6 sec.

Polycrystal — Calibration: E

Counting time: 171300 sec — Background: 205 above ch. 80

C	A	C	A	C	A	C	A
5	79(30)	60	440(36)	79	696(35)	90	2544(54)
10	109(30)	65	473(36)	80	891(37)	91	3233(60)
15	143(31)	70	539(37)	81	1036(38)	92	4561(71)
20	174(32)	71	547(37	82	1175(40)	93	7371(88)
25	204(32)	72	597(38)	83	1245(41)	94	13177(116)
30	237(32)	73	555(37)	84	1441(43)	95	15383(125)
35	272(33)	74	594(38)	85	1422(43)	96	5732(76)
40	302(34)	75	632(37)	86	1466(43)	97	435(21)
45	334(34)	76	729(38)	87	1665(46)		
50	366(35)	77	752(38)	88	1830(47)		
55	402(35)	78	695(36)	89	2102(50)		

$UO_{2.01}$ — 1400°C for 3.465×10^5 sec.

Single crystal — Calibration: E

Counting time: 14000 sec. — Back round: 21 above ch,73

C	A	C	A	C	A	C	A
71	8(10)	77	19(8)	83	71(11)	89	428(22)
72	0(9)	78	9(7)	84	71(11)	90	767(28)
73	15(10)	79	7(7)	85	105(12)	91	1470(39)
74	11(10)	80	20(8)	86	109(12)	92	2366(49)
75	12(9)	81	31(8)	87	139(13)	93	1882(43)
76	16(8)	82	60(10)	88	235(17)	94	331(18)

$UO_{2.01}$ (starting as $UO_{2.1}$) 1400°C for 3.465×10^5 sec.
Single crystal
Counting time: 78840 sec.
Calibration: E
Background: 110 above ch. 79

C	A	C	A	C	A	C	A
77	0	82	99(18)	87	292(23)	92	7695(89)
78	0	83	79(17)	88	431(26)	93	7297(86)
79	24(16)	84	136(19)	89	833(32)	94	1461(39)
80	177(20)	85	161(20)	90	1681(44)	95	230(15)
81	54(17)	86	199(20)	91	3771(63)		

$UO_{2.01}$ 1400°C for 4.295×10^5 sec.
Polycrystal 1
Counting time: 51240 sec.
Calibration: D
Background: 50 above ch.80

C	A	C	A	C	A	C	A
5	177(19)	60	445(25)	76	734(30)	87	1897(45)
10	194(20)	65	510(27)	77	697(29)	88	2174(48)
15	212(20)	67	554(27)	78	724(29)	89	2543(51)
20	232(21)	68	539(27)	79	842(31)	90	3251(58)
25	254(21)	69	546(27)	80	860(31)	91	4549(68)
30	273(22)	70	574(28)	81	1002(33)	92	6475(81)
35	296(22)	71	580(28)	82	1077(34)	93	6909(83)
40	317(23)	72	617(29)	83	1130(35)	94	3035(60)
45	341(23)	73	599(28)	84	1273(37)	95	327(18)
50	370(24)	74	584(27)	85	1464(40)	96	14(4)
55	400(25)	75	602(28)	86	1606(41)	97	5(2)

$UO_{2.01}$ 1400°C for 4.295×10^5 sec.
Polycrystal 2
Counting time: 52200 sec
Calibration: D
Background: 52 above ch. 80

C	A	C	A	C	A	C	A
67	209(20)	75	223(20)	83	428(23)	91	3293(58)
68	207(20)	76	285(21)	84	460(24)	92	4905(70)
69	210(20)	77	280(20)	85	544(25)	93	3899(63)
70	232(219	78	332(21)	86	542(25)	94	944(31)
71	236(21)	79	319(21)	87	672(28)	95	39(36)
72	253(22)	80	306(20)	88	865(31)	96	0
73	202(21)	81	350(21)	89	1177(36)		
74	192(20)	82	402(23)	90	1935(45)		

$UO_{2.01}$ 1400°C for 7.931×10^5 sec.
Polycrystal 2
Counting time: 29040 sec.
Calibration: D
Background: 30 above ch. 80

C	A	C	A	C	A	C	A
68	151(16)	76	181(16)	84	350(20)	92	1178(35)
69	169(17)	77	202(17)	85	378(21)	93	1681(40)
70	158(16)	78	181(16)	86	406(22)	94	1952(45)
71	136(17)	79	208(17)	87	465(23)	95	1395(37)
72	188(18)	80	249(18)	88	541(24)	96	366(19)
73	169(17)	81	238(18)	89	620(26)	97	23(5)
74	162(17)	82	283(18)	90	712(28)	98	7(3)
75	161(16)	83	307(19)	91	889(31)	99	1(1)

$UO_{2.01}$ — 1400°C for 7.931×10^5 sec.

Polycrystal 1 — Calibration: D

Counting time: 84720 sec. — Background: 85 above ch. 80

C	A	C	A	C	A	C	A
5	-	60	328(26)	77	454(26)	88	1028(35)
10	237(24)	65	370(27)	78	512(27)	89	1212(37)
15	230(24)	68	367(26)	79	505(27)	90	1523(41)
20	223(24)	69	430(28)	80	586(27)	91	2140(48)
25	221(24)	70	386(27)	81	526(26)	92	3518(61)
30	221(24)	71	481(29)	82	592(28)	93	5535(75)
35	229(24)	72	409(27)	83	632(28)	94	6694(82)
40	245(24)	73	404(27)	84	715(30)	95	4374(66)
45	262(25)	74	430(28)	85	712(30)	96	1187(34)
50	280(25)	75	452(28)	86	818(31)	97	89(9)
55	300(25)	76	354(25)	87	938(33)	98	10(3)

$UO_{2.01}$ — 1400°C for 1.1396×10^6 sec.

Polycrystal — Calibration: E

Counting time: 57600 sec, — Background: 72 above ch. 78

C	A	C	A	C	A	C	A
5	16(16)	60	148(21)	76	301(22)	87	847(31)
10	25(18)	65	167(21)	77	287(21)	88	1055(35)
15	35(18)	67	160(21)	78	342(22)	89	1569(41)
20	45(18)	68	186(22)	79	346(22)	90	2403(50)
25	56(19)	69	203(22)	80	358(22)	91	3455(60)
30	66(19)	70	213(22)	81	412(24)	92	3797(62)
35	79(19)	71	240(23)	82	479(25)	93	2393(49)
40	90(19)	72	220(23)	83	522(26)	94	580(24)
45	102(20)	73	249(23)	84	606(27)	95	36(6)
50	116(20)	74	250(22)	85	673(38)	96	5(2)
55	132(20)	75	265(22)	86	669(38)	97	1(1)

$UO_{2.01}$ — 1450°C for 2.709×10^5 sec.

Single crystal — Calibration: F

Counting time: 92100 sec. — Background: 1800 above ch. 68

C	A	C	A	C	A	C	A
57	428(38)	64	1023(84)	70	1715(72)	76	4393(89)
58	427(88)	65	1904(86)	71	2170(76)	77	4324(89)
59	336(87)	66	1592(80)	72	2360(77)	78	5381(95)
60	0(85)	67	1539(76)	73	2428(78)	79	6590(102)
61	0(85)	68	919(66)	74	3010(81)	80	9826(111)
62	776(89)	69	1725(73)	75	3577(35)	81	12761(126)
63	112(83)						

$UO_{2.01}$ 1450°C for 2.709×10^5 sec.

Polycrystal Calibration: F

Counting time: 72300 sec Background: 200 above ch. 70

C	A	C	A	C	A	C	A
5	344(34)	57	674(38)	68	1273(43)	79	4564(70)
10	345(34)	58	652(38)	69	1383(43)	80	6162(81)
15	358(32)	59	725(39)	70	1595(45)	81	8264(93)
20	367(34)	60	397(39)	71	1758(47)	82	11063(107)
25	380(34)	61	799(40)	72	1956(49)	83	12958(115)
30	389(35)	62	815(40)	73	2216(51)	84	10414(103)
35	410(35)	63	855(41)	74	2397(54)	85	2434(59)
40	443(35)	64	954(42)	75	2614(55)	86	449(22)
45	491(36)	65	1012(42)	76	3102(59)	87	130(11)
50	560(37)	66	1073(42)	77	3469(63)		
55	643(38)	67	1177(42)	78	3982(66)		

$UO_{2.01}$ 1550°C for 1.626×10^5 sec.

Single crystal Calibration: E

Counting time: 243300 sec Background: 450 above ch. 81

C	A	C	A	C	A	C	A
70	32(43)	77	260(42)	84	551(38)	91	1723(51)
71	27(42)	78	340(41)	85	577(38)	92	2073(54)
72	60(43)	79	376(40)	86	912(43)	93	4148(72)
73	85(43)	80	610(41)	87	927(43)	94	6577(85)
74	69(42)	81	429(36)	88	969(43)	95	9916(104)
75	88(43)	82	451(37)	89	1109(45)	96	4486(70)
76	162(43)	83	467(37)	90	1269(47)	97	3612(60)

$UO_{2.01}$ 1550°C for 1.626×10^5 sec.

Polycrystal Calibration: F

Counting time: 15600 sec. Background: 42 above ch. 71

C	A	C	A	C	A	C	A
5	90(16)	60	163(18)	71	219(17)	82	1099(34)
10	94(16)	61	161(18)	72	213(17)	83	996(33)
15	100(16)	62	193(19)	73	228(18)	84	1390(36)
20	106(16)	63	168(18)	74	314(20)	85	1709(42)
25	112(17)	64	199(19)	75	308(20)	86	1508(39)
30	118(17)	65	189(19)	76	459(23)	87	764(28)
35	124(17)	66	209(19)	77	366(21)	88	138(12)
40	132(17)	67	178(18)	78	367(21)	89	6(2)
45	142(18)	68	185(18)	79	411(22)		
50	150(18)	69	167(17)	80	499(24)		
55	163(18)	70	207(17)				

$UO_{2.01}$ 1650°C for 1.89×10^4 sec.

Single crystal Calibration: E

Counting time: 75000 sec. Background: 500 above ch. 82

C	A	C	A	C	A	C	A
75	—	81	186(37)	87	506(39)	93	2207(57)
76	49(45)	82	319(36)	88	528(39)	94	3441(37)
77	152(44)	83	346(37)	89	722(40)	95	5382(78)
78	197(43)	84	468(38)	90	905(44)	96	15894(128)
79	150(41)	85	487(39)	91	1102(46)	97	5343(75)
80	154(39)	86	393(37)	92	1569(51)	98	2215(47)

$UO_{2.01}$ 1650°C for 1.89×10^4 sec.

Polycrystal Calibration: E

Counting time: 86400 sec. Background: 135 above ch.82

C	A	C	A	C	A	C	A
5	129(26)	60	305(29)	79	430(29)	90	691(31)
10	145(26)	65	322(29)	80	380(27)	91	806(33)
15	162(27)	70	337(30)	81	450(28)	92	811(33)
20	180(27)	71	336(30)	82	549(29)	93	911(34)
25	190(27)	72	370(30)	83	569(29)	94	982(35)
30	212(27)	73	326(29)	84	582(29)	95	1195(37)
35	230(28)	74	379(30)	85	572(29)	96	1076(35)
40	245(28)	75	418(31)	86	532(28)	97	979(32)
45	260(28)	76	368(30)	87	575(29)	98	472(22)
50	275(29)	77	425(29)	88	586(29)		
55	290(29)	78	436(30)	89	634(30)		

$UO_{2.01}$ 1650°C for 5.16×10^4 sec.

Single crystal Calibration: E

Counting time: 73500 sec. Background: 275 above ch.81

C	A	C	A	C	A	C	A
70	80(34)	77	245(34)	84	617(34)	91	2823(68)
71	59(34)	78	232(33)	85	706(35)	92	3975(67)
72	50(34)	79	217(31)	86	775(36)	93	5398(77)
73	99(35)	80	266(30)	87	926(38)	94	6704(84)
74	79(34)	81	396(29)	88	1135(41)	95	6827(84)
75	89(35)	82	472(32)	89	1548(46)	96	4770(70)
76	96(33)	83	575(34)	90	2063(51)	97	1579(40)

$UO_{2.01}$ — 1650°C for 5.16×10^4 sec.

Polycrystal — Calibration: E

Counting time: 69180 sec. — Background: 85 above ch.81

C	A	C	A	C	A	C	A
5	388(27)	60	1238(40)	79	2055(48)	90	2370(50)
10	446(28)	65	1450(42)	80	2185(49)	91	2301(50)
15	497(29)	70	1676(45)	81	2375(50)	92	2327(50)
20	545(30)	71	1603(44)	82	2484(52)	93	2190(49)
25	600(31)	72	1755(46)	83	2654(53)	94	2272(49)
30	653(31)	73	1731(45)	84	2753(54)	95	2048(47)
35	713(32)	74	1912(47)	85	2440(51)	96	1792(43)
40	781(34)	75	1864(47)	86	2373(50)	97	1128(34)
45	868(35)	76	1924(47)	87	2374(50)	98	473(22)
50	976(36)	77	2029(47)	88	2299(50)		
55	1095(38)	78	1940(47)	89	2329(50)		

$UO_{2.03}$ — 1500°C for 1.048×10^5 sec.

Polycrystal 1 — Calibration: G

Counting time: 61500 sec. — Background: 200 above ch.66

C	A	C	A	C	A	C	A
5	96	54	504	65	1262	76	2332
10	128	55	539	66	1314	77	2376
15	160	56	612	67	1353	78	2568
20	188	57	608	68	1441	79	2829
25	217	58	656	69	1598	80	2917
30	240	59	708	70	1619	81	3181
35	270	60	731	71	1699	82	3171
40	304	61	864	72	1865	83	3265
45	349	62	878	73	1931	84	3368
50	404	63	1036	74	2056	85	3207
53	488	64	1092	75	2127	86	3044

$UO_{2.03}$ — 1500°C for 1.048×10^5 sec.

Polycrystal 2 — Calibration: G

Counting time: 100140 sec — Background: 330 above ch.76

C	A	C	A	C	A	C	A
5	152	55	652	68	1849	78	3326
10	194	59	880	69	1976	79	3340
15	233	60	919	70	2164	80	3426
20	270	61	1024	71	2336	81	3521
25	316	62	1064	72	2423	82	3295
30	360	63	1107	73	2685	83	3184
35	402	64	1220	74	2702	84	3196
40	452	65	1263	75	2928	85	2885
45	497	66	1454	76	3048	86	2969
50	535	67	1641	77	3300		

$UO_{2.03}$ — 1600°C for 1.74×10^4 sec.

Polycrystal 1 — Calibration: G

Counting time: 22560 sec. Background: 72 above ch.66

C	A	C	A	C	A	C	A
5	101	54	312	65	567	76	1190
10	120	55	339	66	578	77	1324
15	131	56	399	67	611	78	1433
20	147	57	368	68	669	79	1495
25	169	58	396	69	691	80	1740
30	189	59	400	70	781	81	1848
35	195	60	406	71	839	82	1791
40	230	61	434	72	846	86	1898
45	255	62	462	73	927	84	1522
50	273	63	493	74	1014	85	1044
53	260	64	566	75	1040	86	482

$UO_{2.03}$ — 1600°C for 1.74×10^4 sec.

Polycrystal 2 — Calibration: G

Counting time: 75000 sec. Background: 240 above ch.66

C	A	C	A	C	A	C	A
5	162	54	347	65	738	76	1187
10	161	55	328	66	812	77	1297
15	156	56	326	67	751	78	1386
20	159	57	384	68	786	79	1499
25	168	58	420	69	782	80	1692
30	183	59	389	70	758	81	1871
35	199	60	428	71	808	82	2042
40	225	61	495	72	863	83	2342
45	256	62	533	73	970	84	2624
50	286	63	575	74	1018	85	2956
53	268	64	651	75	1128	86	3158

$UO_{2.05}$ — 1400°C for 1.97×10^5 sec.

Polycrystal 1 — Calibration: E

Counting time: 146700 sec. Background: 400 above ch.82

C	A	C	A	C	A	C	A
5	290(43)	60	1250(53)	79	2179(58)	90	4539(73)
10	370(44)	65	1365(54)	80	2459(59)	91	4897(75)
15	447(45)	70	1495(56)	81	2776(62)	92	5386(78)
20	521(46)	71	1742(58)	82	3027(62)	93	5680(80)
25	600(47)	72	1756(58)	83	3295(64)	94	6075(83)
30	675(48)	73	1629(57)	84	3603(66)	95	6201(83)
35	763(49)	74	1799(58)	85	3398(65)	96	5500(78)
40	850(49)	75	1906(59)	86	3426(65)	97	3508(61)
45	942(50)	76	1915(59)	87	3658(67)	98	1840(43)
50	1040(51)	77	2072(59)	88	3824(68)		
55	1155(52)	78	2213(59)	89	4163(70)		

$UO_{2.05}$ 1400°C for 1.98×10^5 sec.

Polycrystal 2 Calibration:E

Counting time: 7?200sec Background:220 above ch.81

C	A	C	A	C	A	C	A
70	306(35)	77	505(35)	84	930(37)	91	1152(40)
71	346(35)	78	528(36)	85	853(36)	92	1175(40)
72	383(36)	79	530(33)	86	844(36)	93	1243(41)
73	366(35)	80	594(33)	87	840(36)	94	1520(43)
74	395(36)	81	719(34)	88	939(37)	95	1424(41)
75	438(36)	82	781(35)	89	949(37)	96	1262(37)
76	464(36)	83	879(36)	90	1007(38)	97	773(28)

$UO_{2.05}$ 1400°C for 3.51×10^5 sec

Polycrystal 1 Calibration:E

Counting time:83520sec Background:100 above ch.77

C	A	C	A	C	A	C	A
5	136(24)	60	778(34	76	1573(43)	87	4671(70)
10	225(25)	65	954(35)	77	1693(44)	88	4629(70)
15	246(25)	67	993(36)	78	1851(45)	89	4491(68)
20	294(26)	68	946(37)	79	2099(48)	90	4397(68)
25	330(27)	69	1024(38)	80	2498(50)	91	3931(64)
30	366(28)	70	1052(38)	81	2709(55)	92	3435(60)
35	412(28)	71	1199(40)	82	3334(59)	93	2327(49)
40	460(29)	72	1140(39)	83	3932(64)	94	701(26)
45	514(30)	73	1302(40)	84	4450(68)	95	57(8)
50	576(31)	74	1355(41)	85	4666(70)	96	21(5)
55	641(32)	75	1580(44)	86	4450(68)		

$UO_{2.05}$ 1400°C for 3.51×10^5 sec

Polycrystal 2 Calibration:E

Counting time:76080sec. Background:90 above ch.77

C	A	C	A	C	A	C	A
67	843(35)	74	1139(38)	81	2554(52)	88	3878(64)
68	831(34)	75	1236(39)	82	2872(55)	89	3696(62)
69	884(35)	76	1332(40)	83	3348(59)	90	3579(61)
70	908(36)	77	1364(40)	84	3829(63)	91	3276(58)
71	976(36)	78	1619(42)	85	3913(64)	92	2739(54)
72	1017(37)	79	1789(43)	86	3800(63)	93	1672(41)
73	1077(38)	80	2101(48)	87	4053(65)	94	401(20)

$UO_{2.1}$ 1400°C for 2.838×10^4 sec

Polycrystal 2 Calibration:C

Counting time:16200sec. Background:24 above ch.68

C	A	C	A	C	A	C	A
61	63(13)	68	80(11)	75	226(17)	82	881(30)
62	75(13)	69	90(12)	76	312(18)	83	63(8)
63	63(18)	70	94(12)	77	445(22)	84	11(3)
64	52(12)	71	132(13)	78	725(28)	85	3(2)
65	61(12)	72	113(13)	79	1155(35)		
66	66(12)	73	148(14)	80	1578(40)		
67	71(11)	74	179(15)	81	1626(41)		

$UO_{2.1}$

Polycrystal 1

Counting time:63000sec.

C	A	C	A
5	59(19)	60	145(22)
10	64(20)	61	138(21)
15	64(20)	62	149(22)
20	67(20)	63	179(22)
25	71(20)	64	165(21)
30	76(20)	65	177(21)
35	85(20)	66	254(22)
40	93(20)	67	241(21)
45	103(21)	68	229(20)
50	117(21)	69	250(20)
55	131(21)	70	310(22)

1400°C for 2.838×10^4sec.

Calibration:C

Background:80 above ch.68

C	A	C	A
71	295(21)	82	1873(44)
72	373(23)	83	2247(16)
73	411(24)	84	49(7)
74	486(25)	85	23(5)
75	634(28)	86	4(2)
76	7773(30)		
77	1094(35)		
78	937(33)		
79	1398(40)		
80	2084(47)		
81	2734(53)		

$UO_{2.1}$

Polycrystal 1

Counting time:83400sec.

C	A	C	A
5	104(22)	60	126(22)
10	100(21)	65	155(23)
15	93(21)	67	144(22)
20	88(21)	68	122(22)
25	84(21)	69	149(22)
30	84(21)	70	170(23)
35	86(21)	71	202(24)
40	88(21)	72	179(23)
45	96(21)	73	220(24)
50	102(21)	74	212(23)
55	112(22)	75	216(22)

1400°C for 1.175×10^5sec.

Calibration:D

Background:90 above ch.77

C	A	C	A
76	245(22)	87	1027(35)
77	300(23)	88	1154(36)
78	335(23)	89	1356(39)
79	394(24)	90	1404(39)
80	434(25)	91	1263(37)
81	498(26)	92	713(27)
82	542(27)	93	147(12)
83	562(27)	94	6(2)
84	679(29)	95	3(2)
85	805(31)	96	1(1)
86	861(32)		

$UO_{2.1}$

Polycrystal 2

Counting time:58260sec.

C	A	C	A
69	194(21)	76	264(22)
70	208(21)	77	290(22)
71	180(20)	78	309(22)
72	201(21)	79	358(20)
73	234(22)	80	397(23)
74	248(22)	81	435(24)
75	244(22)	82	545(26)

1400°C for 1.175×10^5sec

Calibration:D

Background:60 above ch.81

C	A	C	A
83	651(28)	90	1651(42)
84	746(29)	91	1813(44)
85	892(32)	92	1983(46)
86	987(33)	93	1900(45)
87	1118(35)	94	1952(45)
88	1265(37)	95	1824(43)
89	1457(40)	96	1565(40)
		97	864(29)

$UO_{2.1}$ 1400°C for 1.817×10^5 sec.

Single crystal Calibration: D
Counting time: 13560 sec. Background: 28 above ch. 79

C	A	C	A	C	A	C	A
67	12(11)	74	16(11)	81	74(11)	88	336(20)
68	5(11)	75	12(10)	82	104(13)	89	390(21)
69	1(11)	76	23(10)	83	127(13)	90	467(23)
70	5(11)	77	26(10)	84	146(14)	91	479(23)
71	7(11)	78	28(9)	85	211(16)	92	596(23)
72	0(11)	79	44(10)	86	258(18)	93	508(23)
73	4(11)	80	56(11)	87	281(18)	94	421(21)
						95	278(17)

$UO_{2.1}$ 1400°C for 2.012×10^5 sec.

Polycrystal 1 Calibration: D
Counting time: 88500 sec. Background: 92 above ch.78

C	A	C	A	C	A	C	A
5	82(21)	60	217(24)	75	528(28)	86	1740(44)
10	90(21)	65	272(25)	76	619(29)	87	1851(45)
15	95(21)	66	293(26)	77	748(31)	88	1950(46)
20	103(22)	67	294(26)	78	778(31)	89	1990(47)
25	112(22)	68	318(26)	79	892(33)	90	2106(48)
30	121(22)	69	317(26)	80	1003(34)	91	2012(46)
35	131(22)	70	378(27)	81	1100(36)	92	1860(44)
40	145(23)	71	405(28)	82	1224(38)	93	1557(40)
45	156(23)	42	400(28)	33	1440(40)	94	805(28)
50	170(230	73	469(29)	84	1536(41)	95	102(10)
55	189(24)	74	451(27)	85	1619(43)	96	4(2)

$UO_{2.1}$ 1400°C for 2.012×10^5 sec.

Polycrystal 2 Calibration D
Counting time: 73620 sec. Background: 75 above ch. 78

C	A	C	A	C	A	C	A
66	130(21)	73	188(21)	80	345(22)	87	692(29)
67	146(21)	74	219(22)	81	372(23)	88	779(30)
68	172(22)	75	201(21)	82	402(24)	89	873(32)
69	147(21)	76	213(20)	83	475(25)	90	839(31)
70	163(21)	77	268(21)	84	525(26)	91	949(33)
71	229(23)	78	271(21)	85	578(27)	92	903(31)
72	176(22)	79	299(21)	86	645(28)	93	819(29)
						94	398(20)
						95	36(6)

$UO_{2.1}$ 1400°C for 3.617×10^5 sec.

Single crystal Calibration: D

Counting time: 54540 sec. Background: 55 above ch.78

C	A	C	A	C	A	C	A
66	57(17)	74	130(18)	82	390(22)	90	727(29)
67	71(17)	75	190(19)	83	477(24)	91	732(29)
68	60(17)	76	169(18)	84	534(25)	92	699(28)
69	97(18)	77	202(18)	85	588(26)	93	675(26)
70	62(17)	78	246(19)	86	580(26)	94	620(25)
71	94(18)	79	296(20)	87	608(27)	95	444(21)
72	113(18)	80	315(21)	88	703(28)	96	144(12)
73	101(18)	81	341(21)	89	679(28)	97	21(5)

$UO_{2.1}$ 1400°C for 3.829×10^5 sec.

Polycrystal Calibration: D

Counting time: 71400 sec. Background: 72 above ch.78

C	A	C	A	C	A	C	A
5	295(24)	60	351(25)	75	367(24)	86	907(32)
10	287(24)	65	385(26)	76	410(25)	87	906(32)
15	276(24)	66	377(26)	77	497(26)	88	752(30)
20	268(24)	67	383(26)	78	488(25)	89	830(31)
25	267(24)	68	403(26)	79	503(25)	90	734(30)
30	271(24)	69	412(27)	80	555(26)	91	807(30)
35	281(24)	70	405(26)	81	640(26)	92	694(27)
40	291(24)	71	460(27)	82	591(27)	93	469(22)
45	302(24)	72	443(27)	83	662(28)	94	121(11)
50	318(25)	73	456(27)	84	677(29)	95	8(3)
55	331(25)	74	430(26)	704	(29)		

$UO_{2.1}$ 1400°C for 3.812×10^5 sec.

Polycrystal Calibration: D

Counting time: 74460 sec. Background: 75 above ch.78

C	A	C	A	C	A	C	A
66	329(25)	73	618(30)	80	1141(36)	87	1487(41)
67	369(26)	74	643(30)	81	1183(36)	88	1627(42)
68	396(26)	75	970(35)	82	1326(38)	89	1550(41)
69	448(27)	76	779(31)	83	1415(39)	90	1522(41)
70	516(27)	77	882(32)	84	1407(39)	91	1406(39)
71	811(33)	78	980(34)	85	1487(40)	92	1316(37)
72	580(30)	79	1101(35)	86	1516(41)	93	1145(35)
						94	689(26)

$UO_{2.1}$ — 1477°C for 2.79×10^4 sec.

Single crystal — Calibration: E

Counting time: 81600 sec. — Background: 100 above ch. 81

C	A	C	A	C	A	C	A
70	49(21)	77	73(20)	84	270(22)	91	1110(36)
71	60(22)	78	147(21)	85	296(22)	92	1026(35)
72	55(21)	79	191(19)	86	510(27)	93	1190(37)
73	78(22)	80	312(23)	87	386(22)	94	1429(40)
74	63(22)	81	188(20)	88	713(20)	95	1346(39)
75	98(22)	82	208(20)	89	522(27)	96	919(30)
76	136(22)	83	265(22)	90	697(30)	97	288(16)
						98	30(5)

$UO_{2.1}$ — 1477°C for 9.18×10^4 sec.

Single crystal — Calibration: E

Counting time: 139200 sec. — Background: 170 above ch.81

C	A	C	A	C	A	C	A
70	663(37)	77	1244(43)	84	1961(48)	91	1841(47)
71	737(38)	78	1173(41)	85	1907(47)	92	2092(49)
72	752(38)	79	1283(42)	86	1790(46)	93	2407(52)
73	693(37)	80	1490(43)	87	1785(46)	94	3149(57)
74	947(40)	81	1692(45)	88	1837(47)	95	3808(63)
75	1004(41)	82	1734(45)	89	1814(46)	96	3010(56)
76	1070(42)	83	1919(46)	90	1862(47)	97	1057(32)
						98	415(20)

$UO_{2.1}$ — 1477°C for 9.18×10^4 sec.

Polycrystal — Calibration: E

Counting time: 97200 sec. — Background: 115 above ch.82

C	A	C	A	C	A	C	A
71	574(32)	78	913(36)	85	1408(40)	92	1463(41)
72	530(31)	79	934(36)	86	1306(39)	93	1644(43)
73	603(33)	80	1011(36)	87	1290(39)	94	2136(38)
74	620(33)	81	1031(36)	88	1356(40)	95	2538(52)
75	722(34)	82	1244(38)	89	1340(40)	96	2323(48)
76	750(35)	83	1424(41)	90	1364(40)	97	1047(33)
77	849(36)	84	1477(41)	91	-	98	489(22)

$UO_{2.1}$ — 1477°C for 1.026×10^5 sec.

Polycrystal 2 — Calibration: E

Counting time: 89820 sec. — Background: 106 above ch.78

C	A	C	A	C	A	C	A
67	427(29)	74	825(34)	81	1122(36)	88	1003(35)
68	512(30)	75	731(33)	82	1149(37)	89	982(35)
69	529(31)	76	774(32)	83	1211(38)	90	835(32)
70	567(31)	77	828(33)	84	1221(38)	91	811(32)
71	555(31)	78	846(32)	85	1115(36)	92	832931)
72	617(32)	79	908(33)	86	1148(37)	93	434(22)
73	679(33)	80	1014(35)	87	1042(35)	94	162(14)

$UO_{2.1}$ — 1477°C for 1.026×10^5 sec.

Polycrystal 1 — Calibration: E

Counting time: 70020 sec. — Background; 63 above ch.78

C	A	C	A	C	A	C	A
5	127(21)	60	644(32)	76	1481(41)	87	1938(46)
10	149(22)	65	904(34)	77	1593(42)	88	1862(45)
15	174(22)	67	946(36)	78	1646(43)	89	1944(45)
20	199(23)	68	1048(37)	79	1703(43)	90	1780(44)
25	226(24)	69	1036(37)	80	1843(45)	91	1717(43)
30	256(24)	70	1146(38)	81	2026(47)	92	1518(40)
35	293(25)	71	1191(39)	82	2083(47)	93	1065(33)
40	331(26)	72	1267(40)	83	2233(49)	94	414(20)
45	385(27)	73	1258(40)	84	2364(50)	95	55(7)
50	450(28)	74	1284(40)	85	2203(49)	96	12(3)
55	536(29)	75	1423(41)	86	2044(47)		

$UO_{2.1}$ — 1550°C for 1.80×10^4 sec.

Single crystal — Calibration: E

Counting time: 73320 sec. — Background: 104 above ch.81

C	A	C	A	C	A	C	A
70	-	77	105(21)	84	651(29)	91	1483(41)
71	-	78	118(20)	85	722(31)	92	1521(42)
72	0	79	172(21)	86	810(32)	93	1619(43)
73	22(21)	80	197(21)	87	927(34)	94	1687(43)
74	32(21)	81	313(23)	88	1052(35)	95	1414(39)
75	23(21)	82	394(25)	89	1216(38)	96	810(29)
76	87(22)	83	543(27)	90	1400(40)	97	211(15)

$UO_{2.1}$ — 1550°C for 3.42×10^4 sec.

Single crystal — Calibration: E

Counting time: 140100 sec. — Background: 170 above ch.81

C	A	C	A	C	A	C	A
70	198(30)	77	460(32)	84	1323(41)	91	1592(42)
71	197(30)	78	491(32)	85	1229(40)	92	1693(42)
72	215(30)	79	559(32)	86	1227(40)	93	1674(41)
73	232(30)	80	686(33)	87	1350(41)	94	1395(40)
74	309(31)	81	815(34)	88	1432(42)	95	1276(38)
75	318(32)	82	989(36)	89	1446(43)	96	811(30)
76	397(32)	83	1210(39)	90	1451(43)	97	259(16)

$UO_{2.1}$ 1550°C for 1.80×10^4 sec.

Polycrystal Calibration: E

Counting time: 260100 sec. Back round: 308 above ch.81

C	A	C	A	C	A	C	A
5	0(34)	60	217(38)	79	366(34)	90	1467(47)
10	0(34)	65	238(38)	80	493(35)	91	1880(50)
15	0(35)	70	270(39)	81	694(36)	92	2054(52)
20	26(35)	71	265(39)	82	723(37)	93	2335(54)
25	49(36)	72	337(39)	83	781(37)	94	2573(55)
30	73(36)	73	286(39)	84	892(39)	95	2106(49)
35	100(36)	74	376(40)	85	882(39)	96	837(31)
40	119(37)	75	353(40)	86	883(39)	97	162(13)
45	143(37)	76	336(38)	87	1088(41)		
50	164(37)	77	381(37)	88	1231(43)		
55	189(38)	78	351(36)	89	1298(43)		

$UO_{2.1}$ 1550°C for 3.42×10^4 sec.

Polycrystal Calibration: E

Counting time: 106800 sec. Background: 300 above ch.80

C	A	C	A	C	A	C	A
5	30(35)	60	325(39)	78	528(36)	89	1387(45)
10	65(35)	65	355(40)	79	531(35)	90	1463(46)
15	81(36)	69	388(40)	80	661(36)	91	1601(47)
20	112(36)	70	379(40)	81	759(37)	92	1673(48)
25	140(37)	71	362(39)	82	808(39)	93	1736(47)
30	166(37)	72	380(40)	83	954(39)	94	1735(45)
35	196(37)	73	461(41)	84	1081(41)	95	1399(39)
40	220(38)	74	391(40)	85	1101(40)	96	731(27)
45	257(38)	75	528(40)	86	1022(40)	97	110(10)
50	272(38)	76	517(40)	87	1137(42)		
55	300(39)	77	585(39)	88	1281(43)		

$UO_{2.1}$ 1650°C for 4.74×10^3 sec.

Polycrystal Calibration: E

Counting time: 63780 sec. Background: 160 above ch.82

C	A	C	A	C	A	C	A
5	167(30)	60	840(39)	79	2773(57)	90	7442(88)
10	200(30)	65	1080(42)	80	3144(60)	91	6381(82)
15	237(31)	70	1437(46)	81	3840(65)	92	3932(65)
20	272(31)	71	1550(48)	82	3984(66)	93	3623(63)
25	312(32)	72	1668(49)	83	4333(68)	94	3281(60)
30	335(33)	73	1759(50)	84	4620(70)	95	2706(54)
35	395(33)	74	1774(50)	85	4427(69)	96	1795(45)
40	453(34)	75	2057(53)	86	4241(68)	97	343(19)
45	517(35)	76	2263(54)	87	4394(69)	98	131(11)
50	591(36)	77	2434(55)	88	4195(67)		
55	690(37)	78	2528(55)	89	6431(82)		

$UO_{2.1}$

Single crystal

Counting time: 54720 sec.

1650°C for 4.74×10^3 sec.

Calibration: E

Background: 80 above ch.80

C	A	C	A	C	A	C	A
69	198(23)	76	532(30)	83	1565(42)	90	2019(47)
70	200(23)	77	579(30)	84	1720(43)	91	1907(45)
71	230(23)	78	714(30)	85	1716(43)	92	1865(45)
72	265(24)	79	827(32)	86	1790(44)	93	1893(4)
73	377(26)	80	932(33)	87	1829(45)	94	1825(44)
74	385(27)	81	1218(37)	88	1985(46)	95	1634(41)
75	423(27)	82	4444(39)	89	1978(46)	96	1299(36)
						97	804(28)

$UO_{2.12}$

Single crystal

Counting time: 79800 sec.

1400°C for 9.33×10^4 sec.

Calibration: G

Background: 500 above ch.72

C	A	C	A	C	A	C	A
60	84	68	597	76	1338	84	2765
61	105	69	751	77	1574	85	3057
62	151	70	827	78	1677	86	3396
63	230	71	933	79	1798	87	4177
64	244	72	1089	80	2004	88	4524
65	232	73	1155	81	2179	89	4797
66	263	74	1150	82	2315	90	4945
67	404	75	1295	83	2507	91	5137

$UO_{2.12}$

Polycrystal

Counting time: 88080 sec.

1400°C for 9.33×10^4 sec.

Calibration: G

Background: 290 above ch.69

C	A	C	A	C	A	C	A
5	106	57	545	69	1373	80	3561
10	138	58	564	70	1385	81	3795
15	166	59	551	71	1410	82	4165
20	201	60	740	72	1540	83	4477
25	234	61	651	73	1706	84	4592
30	266	62	603	74	1893	85	5087
35	300	63	689	75	1958	86	5342
40	336	64	885	76	2302	87	5564
45	375	65	904	77	2738	88	5779
50	405	66	1033	78	2919	89	5792
55	495	67	1160	79	3239	90	5674
56	489	68	1189				

$UO_{2.15}$ 1400°C for 3.45×10^4 sec.

Single crystal Calibration: E

Counting time: 74400 sec. Background: 105 above ch.82

C	A	C	A	C	A	C	A
71	77(22)	78	318(26)	85	658(29)	92	917(34)
72	305(27)	79	323(25)	86	662(30)	93	1000(35)
73	158(24)	80	377(25)	87	699(30)	94	975(34)
74	166(24)	81	405(25)	88	699(30)	95	1078(35)
75	167(24)	82	478(26)	89	780(31)	96	982(33)
76	234(25)	83	595(28)	90	1171(37)	97	1027(33)
77	223(25)	84	686(30)	91	966(34)	98	621(25)

$UO_{2.15}$ 1400°C for 3.45×10^4 sec.

Polycrystal Calibration: E

Counting time: 97980 sec. Background: 260 above ch.83

C	A	C	A	C	A	C	A
5	282(36)	60	690(42)	80	1255(45)	91	2365(54)
10	324(37)	65	728(42)	81	1307(45)	92	2638(56)
15	367(38)	70	760(42)	82	1695(48)	93	2655(56)
20	412(38)	72	1027(45)	83	1658(47)	94	-
25	451(39)	73	961(45)	84	1946(50)	95	2859(58)
30	488(39)	74	910(44)	85	1878(49)	96	3046(59)
35	539(40)	75	970(45)	86	1833(48)	97	3080(58)
40	559(40)	76	1047(46)	87	2266(53)	98	2125(48)
45	594(40)	77	-	88	1953(50)		
50	625(41)	78	-	89	2118(51)		
55	660(41)	79	1261(46)	90	2235(52)		

$UO_{2.15}$ 1400°C for 5.28×10^4 sec.

Single crystal Calibration: E

Counting time: 266700 sec. Background: 320 above ch.79

C	A	C	A	C	A	C	A
68	0	75	151(34)	82	311(31)	89	744(38)
69	0	76	65(32)	83	341(31)	90	899(39)
70	0	77	39(30)	84	459(33)	91	1043(41)
71	0	78	78(29)	85	477(34)	92	1387(43)
72	0(35)	79	167(28)	86	456(33)	93	1559(43)
73	30(36)	80	177(29)	87	536(34)	94	1315(39)
74	115(36)	81	288(30)	88	664(36)	95	466(22)

$UC_{2.15}$ 1400°C for 5.28×10^4 sec.

Polycrystal Calibration: E

Counting time: 93300 sec. Background: 112 above ch.79

C	A	C	A	C	A	C	A
68	133(24)	75	236(25)	82	346(24)	89	403(25)
69	135(25)	76	218(24)	83	358(24)	90	392(25)
70	153(25)	77	207(22)	84	384(25)	91	414(23)
71	156(25)	78	245(22)	85	389(25)	92	494(26)
72	186(25)	79	250(22)	86	354(24)	93	501(25)
73	197(29)	80	274(22)	87	307(23)	94	423(22)
74	209(23)	81	329(24)	88	375(24)	95	137(12)

$UO_{2.15}$ 1400°C for 9.12×10^4 sec.

Polycrystal Calibration: E

Counting time: 237600 sec. Background: 630 above ch.82

C	A	C	A	C	A	C	A
5	735(57)	60	4000(81)	79	7374(96)	90	7903(96)
10	930(59)	65	4730(85)	80	7708(97)	91	7967(96)
15	1120(59)	70	5560(89)	81	8286(99)	92	7985(96)
20	1324(62)	71	5865(91)	82	8881(101)	93	7654(94)
25	1535(64)	72	5804(91)	83	9605(104)	94	7132(91)
30	1740(65)	73	6174(87)	84	9790(107)	95	6683(87)
35	1830(66)	74	6362(94)	85	9144(102)	96	5056(75)
40	2220(69)	75	6501(95)	86	8607(99)	97	2490(50)
45	2660(72)	76	6792(97)	87	8272(98)	98	889(30)
50	2960(74)	77	6888(95)	88	8442(99)		
55	3410(77)	78	7064(96)	89	8328(98)		

$UO_{2.15}$ 1450°C for 2.88×10^4 sec.

Single crystal Calibration: F

Counting time: 87300 sec. Background: 300 above ch.70

C	A	C	A	C	A	C	A
59	678(43)	66	1249(47)	73	2197(53)	80	3767(66)
60	756(44)	67	1338(47)	74	2323(54)	81	4104(69)
61	763(44)	68	1465(48)	75	2483(55)	82	4681(73)
62	942(46)	69	1662(49)	76	2725(58)	83	5429(76)
63	929(46)	70	1763(49)	77	2932(59)	84	5227(74)
64	1046(47)	71	1914(50)	78	3047(60)	85	2382(50)
65	1197(48)	72	2125(52)	79	3160(61)	86	396(20)

$UO_{2.15}$ 1450°C for 2.88×10^4 sec.
Polycrystal Calibration: F
Counting time: 61800 sec. Background: 168 above ch.71

C	A	C	A	C	A	C	A
5	858(39)	60	1704(49)	71	2403(51)	82	4511(69)
10	927(40)	61	1765(49)	72	2522(53)	83	4721(71)
15	994(41)	62	1862(50)	73	2557(55)	84	4695(70)
20	1054(42)	63	1942(51)	74	2677(55)	85	3382(60)
25	1106(42)	64	1982(52)	75	2770(56)	86	1615(41)
30	1164(43)	65	2047(52)	76	2969(57)	87	309(17)
35	1215(43)	66	2078(52)	77	3049(58)	88	57(8)
40	1272(44)	67	1963(50)	78	3211(60)		
45	1332(45)	68	1968(50)	79	3388(61)		
50	1416(46)	69	2063(50)	80	3643(63)		
55	1553(47)	70	2260(50)	81	4133(67)		

$UO_{2.15}$ 1350°C for 9.84×10^4 sec.
Single crystal Calibration: F
Counting time: 234900 sec. Background: 700 above ch.70

C	A	C	A	C	A	C	A
59	538(58)	66	1202(60)	73	3012(66)	80	5711(84)
60	740(59)	67	1453(60)	74	3173(68)	81	6866(91)
61	776(60)	68	1712(60)	75	3250(68)	82	7684(95)
62	870(61)	69	1901(60)	76	3400(69)	83	9077(100)
63	936(61)	70	2244(60)	77	3914(72)	84	7310(90)
64	922(61)	71	2397(61)	78	4662(77)	85	2745(56)
65	1177(61)	72	2567(61)	79	4812(79)	86	456(22)

Th in stoichiometric UO_2 1620°C for 5.904×10^5 sec.
Polycrystal Calibration: G
Counting time: 63600 sec. Background: 609 above ch.66

C	A	C	A	C	A	C	A
5	123	52	207	63	657	74	2301
10	131	53	271	64	746	75	2563
15	131	54	183	65	749	76	2810
20	131	55	285	66	913	77	3116
25	139	56	288	67	998	78	3271
30	150	57	317	68	1077	79	3047
35	159	58	266	69	1197	80	3137
40	175	59	353	70	1332	81	2883
45	191	60	331	71	1483	82	2474
50	189	61	356	72	1828		
51	215	62	531	73	2129		

Th in $UO_{2.01}$ — 1600°C for 5.574×10^4 sec.

Single crystal — Calibration: G

Counting time: 21600 sec. Background: 175 above ch. 66

C	A	C	A	C	A	C	A
55	169	64	500	73	931	82	5208
56	239	65	478	74	1059	83	5724
57	213	66	607	75	1095	84	6577
58	275	67	589	76	1261	85	6071
59	286	68	608	77	1534	86	1133
60	277	69	683	78	1831		
61	261	70	628	79	2302		
62	338	71	778	80	2884		
63	400	72	857	81	3783		

Th in $UO_{2.1}$ — 1620°C for 5.7×10^3 sec.

Polycrystal 1 — Calibration G

Counting time: 133200 sec. Background: 400 above ch. 66

C	A	C	A	C	A	C	A
5	244	52	903	63	2083	74	5862
10	285	53	850	64	2435	75	6581
15	321	54	986	65	2522	76	7016
20	360	55	1114	66	2719	77	7711
25	399	56	1272	67	2880	78	8123
30	440	57	1202	68	3073	79	8161
35	498	58	-	69	3347	80	8389
40	561	59	1443	70	3752	81	8259
45	666	60	1603	71	4164	82	7533
50	792	61	1734	72	4724		
5.	855	62	1982	73	5299		

Th in $UO_{2.1}$ — 1620°C for 5.7×10^3 sec

Polycrystal 2 — Calibration: G

Counting time: 78800 sec. Background: 136 above ch. 66

C	A	C	A	C	A	C	A
5	61	52	295	63	732	74	2396
10	80	53	312	64	775	75	2861
15	94	54	346	65	880	76	3204
20	104	55	378	66	911	77	3628
25	118	56	381	67	1002	78	3870
30	144	57	402	68	1144	79	4182
35	154	58	466	69	1143	80	4401
40	185	59	450	70	1313	81	4423
45	221	60	477	71	1488	82	4121
50	265	61	603	72	1964		
51	280	62	626	73	2072		

ThO_2 Air (commercial pellet) 1584°C for 4.071×10^5 sec.
Counting time: 5400 sec. Background: 220

C	A	C	A	C	A	C	A
56	55	62	146	68	249	74	997
57	48	63	119	69	423	75	1305
58	78	64	138	70	380	76	1557
59	64	65	164	71	396	77	1857
60	72	66	325	72	628	78	2129
61	79	67	240	73	584	79	1376

ThO_2 H_2 1625°C for 2.349×10^5 sec.
Counting time: 18660 sec. Background 380

C	A	C	A	C	A	C	A
56	126	63	638	70	1868	77	3826
57	158	64	669	71	2134	78	4219
58	245	65	814	72	2267	79	4508
59	229	66	965	73	2672	80	4630
60	316	67	1164	74	2925	81	5151
61	361	68	1347	75	3247	82	5585
62	478	69	1529	76	3555	83	6497
						87	9018

ThO_2 H_2 1640°C for 2.214×10^5 sec.
Counting time: 27660 sec. Background: 450

C	A	C	A	C	A	C	A
56	103	63	290	70	788	77	2030
57	138	64	368	71	867	78	2364
58	141	65	415	72	1034	79	2945
59	149	66	405	73	1210	80	3846
60	165	67	527	74	1391	81	4134
61	230	68	594	75	1490	82	4695
62	273	69	566	76	1722	83	4816

ThO_2 CO/CO_2 1640°C for 4.383×10^5 sec.
Counting time: 82500 sec. Background: 1600

C	A	C	A	C	A	C	A
59	103	65	344	71	549	77	1612
60	91	66	305	72	621	78	2013
61	144	67	396	73	772	79	2156
62	218	68	366	74	924	80	2073
63	199	69	419	75	1081	81	177
64	264	70	491	76	1285	82	0

ThO_2 Air (pellet 1) 1650°C for 2.494×10^5 sec.
Counting time: 65700 sec. Background: 1200

C	A	C	A	C	A	C	A
53	141	60	392	67	663	74	891
54	106	61	460	68	745	75	989
55	174	62	448	69	836	76	1081
56	262	63	547	70	844	77	1276
57	274	64	536	71	833	78	1243
58	283	65	614	72	977	79	1183
59	296	66	636	73	971	80	940

ThO_2 Air (pellet 2) 1650°C for 2.494×10^5 sec.
Counting time: 65700 sec. Background; 1200

C	A	C	A	C	A	C	A
58	46	65	181	72	531	79	1004
59	79	66	364	73	602	80	1209
60	124	67	270	74	584	81	1322
61	174	68	326	75	681	82	1498
62	181	69	399	76	711	83	1285
63	138	70	469	77	791	84	1088
64	163	71	482	78	930	85	553

ThO_2 H_2 1600°C for 8.94×10^4 sec.
Counting time: 53800 sec. Background: 500

C	A	C	A	C	A	C	A
62	14	68	95	74	999	80	3932
63	40	69	190	75	1199	81	4119
64	50	70	320	76	1637	82	4197
65	93	71	431	77	1963	83	4295
66	121	72	540	78	2614	84	1856
67	93	73	711	79	3003	85	0

ThO_2 H_2 (pellet 1) 1670°C for 1.548×10^5 sec.
Counting time: 53700 sec. Background: 750

C	A	C	A	C	A	C	A
53	46	61	267	69	1081	77	2432
54	117	62	304	70	1137	78	3065
55	102	63	338	71	1294	79	3746
56	194	64	500	72	1512	80	4707
57	159	65	626	73	1665	81	5468
58	153	66	704	74	1799	82	5631
59	211	67	819	75	2026	83	4992
60	249	68	943	76	2239	84	2335

ThO_2 H_2 (pellet 2) 1670°C for 1.548×10^5 sec.

Counting time: 16800 sec. Background: 240

C	A	C	A	C	A	C	A
59	107	66	308	73	615	80	1644
60	131	67	309	74	774	81	1703
61	105	68	318	75	830	82	1740
62	175	69	342	76	916	83	1404
63	202	70	436	77	1001	84	565
64	176	71	531	78	1157		
65	202	72	627	79	1296		

ThO_2 H_2 1720°C for 9.432×10^4 sec.

Counting time: 74460 sec. Background: 1200

C	A	C	A	C	A	C	A
52	118	60	301	68	687	76	2225
53	127	61	292	69	758	77	2624
54	148	62	414	70	911	78	3276
55	231	63	423	71	1047	79	4180
56	183	64	451	72	1116	80	4015
57	187	65	546	73	1428	81	4850
58	277	66	516	74	1559	82	3124
59	273	67	688	75	1923	83	0

ThO_2 Vacuum 1825°C for 6.18×10^4 sec.

Counting time: 39120 sec. Background: 950

C	A	C	A	C	A	C	A
55	85	63	353	71	923	79	1877
56	77	64	418	72	1084	80	2136
57	195	65	492	73	1246	81	2392
58	168	66	583	74	1357	82	2714
59	224	67	610	75	1378	83	3129
60	288	68	738	76	1468	84	3832
61	263	69	826	77	1642	85	4363
62	333	70	949	78	1769	86	4290

ThO_2 Vacuum 1890°C for 3.282×10^4 sec.

Counting time: 88060 sec. Background: 1400

C	A	C	A	C	A	C	A
63	75	69	164	75	487	81	1842
64	153	70	241	76	585	82	2166
65	137	71	294	77	656	83	2338
66	141	72	305	78	784	84	2639
67	137	73	490	79	1042	85	1105
68	288	74	476	80	1271	86	0

ThO_2 Vacuum (pellet 1) 2069°C for 1.398 x 10^4 sec.

Counting time: 72900 sec. Background: 1200

C	A	C	A	C	A	C	A
62	56	67	196	72	413	77	977
63	15	68	231	73	470	78	1177
64	119	69	262	74	591	79	1052
65	120	70	280	75	660	80	750
66	170	71	343	76	837	81	0

ThO_2 Vacuum (pellet 2) 2069°C for 1.398 x 10^4 sec.

Counting time: 158700 sec. Background: 3000

C	A	C	A	C	A	C	A
62	344	67	708	72	1734	77	4548
63	372	68	890	73	1996	78	4322
64	412	69	991	74	2561	79	3905
65	642	70	1251	75	3084	80	2008
66	697	71	1473	76	3830	81	0

REFERENCES

1. McNamara,P., Ph.D. Thesis, London, (1963).

2. Auskern,A.B., and Belle, J., Jounal of Nuclear Materials (J.N.M.) 3 (1961) 267-76.

3. Lindner, R., and Schmitz,F., Zeitschrift fur Naturforsch., 16a (1961) 1373-8.

4. Schmitz,F., Thesis, Braunschweig.

5. Nagels,P., Van Lierde,W., De Batist,R., Denayer,M., De Jonghe,L., and Gevers,R., I.A.E.A."Thermodynamics" (1966) SM66/46.

6. Mobius, Witzman, Gerlach, Z.Chem. 4 (1964) 154-5.

7. Rhodes,W.H., and Carter,R.E., Journal of the American Ceramic Society (J.A.Cer.S.) 49 (1966) 244-9.

8. Ure,R.W., J.Chem.Phys. 26 (1957) 1363-73.

9. Matzke,Hj., J.N.M. 11 (1964) 344-7.

10. Belle,J., ed., "UO_2": Properties and Nuclear Applications U.S.A.E.C.(1961).

11. Thermodynamic and Transport Properties of UO_2 and Related Phases, Tech.Rept.Series No.39, I.A.E.A., Vienna (1965).

12. Yust,C.S., and Morgan,C.S., ORNL-3870 pp.38-43.

13. Kelly,R., and Matzke,Hj., J.N.M. 17 (1965) 179-91.

14. Johnson,J.R., and Curtis,C.E., 2nd. U.N.Conf.Peaceful Uses Atomic Energy P/559.

15. Herring,C., J.Appl.Phys. 21 (1950) 437.

16. Nabarro,F.R.N., Rept.Conf.Strength of Solids.(London Phys. Soc.) (1947) 47.

17. Coble,R.L., and Burke,J.E., Prog.Cer.Sci. 3 (1963).

18. Shuttleworth,R., and Mackenzie,J., Proc.Phys.Soc. 62B (1949) 833.

19. Carrol,R.M., Am.Soc.Testing Mater., Spec.Tech.Publ. No.306 (1961) 110-22.

20. Felix,F., Lagerwall,T., Schmelling,P., and Zimen,K.E., 3rd.U.N.Conf.Peaceful Uses P/472.

21. Lewis,W.B., AECL-1402 (1961).

22. Armstrong,W.H., and Irvine,W.R., J.N.M. 9 2 (1963).

23. Christie,G., and Williams,J., J.N.M. 5 (1962) 1-4.

24. Amato,I., Colombo, R.L., and Protti,A.M., Energia Nucl. 11 3 (1964) 121.

25. Hall,A.R., Scott,R., and Williams,J., J.N.M. 1 (1959) 39.

26. Amato,I., Colombo,R.L., and Protti,A.M., J.A.Cer.S. Aug. (1963).

27. Lindner,R., Proc.Int.Symp.Reactivity Solids, Amsterdam, (1960) 467-74.

28. Roberts,L.E.J., and Walter,A.J., AERE-R3345.

29. Martin,A.E., and Edwards,R.K., J.Phys.Chem. 69 5 (1965) 1788.

30. Aitken,E.A., Brassfield,H.C., and Fryxell,R.E., I.A.E.A. Conf. (1965) SM66/83.

31. Amato,A., Colombo,R.L., and Balzari,A.M.P., J.N.M. 15 2 (1965) 125-8.

32. Cohen,I., and Berman,R.M., J.N.M. 18 (1966) 77-107.

33. Heslop,R.B., and Robinson,P.L., "Inorganic Chemistry", Elsevier, (1960).

34. Willis,B.T.M., Proc.Roy.Soc.(London) Series A274 (1966) 122-44.

35. Steeb,S., and Mitsch,P., J.N.M. 15 2 (1965) 81-7.

36. Nagels,P., et al., 3rd. U.N.Conf.Peaceful Uses P/444.

37. Rouse,K.D., Valentine,T.M., and Willis,B.T.M., AERE-4414.

38. Dawson,J.K., and Lister,M.W., J.Chem.Soc. (1950) 2177-81.

39. Arrott,A., and Goldman,J.E, Phys.Rev. 108 (1957) 948-53.

40. Haraldsen,H., and Bakken,R., Naturwiss. 28 (1940) 127.

41. Roberts,L.E.J., and Markin,T.L., to be published Brit. Cer.Soc.

42. Hoch,M., ibid.

43. Lidiard,A.B., J.N.M. 19 1 (1966) 106.

44. Crank,J., "Mathematics of Diffusion", Oxford Univ. Press.

45. Jost,W., "Diffusion", Academic Press.

46. Barrer,R.M., "Diffusion in and through Solids", Univ.Press Cambridge, (1951).

47. Turnbull,D., in "Atom Movements" ASM., Cleveland, Ohio, (1950) 129.

48. Fisher,J.C., J.Appl.Phys. 22 1 (1951) 74.

49. Whipple,R.T.P., Phil.Mag. 45 (1954) 1225.

50. Wood,V.E., et al., J Appl.Phys. 33 12 (1962) 3574-9.

51. Levine,H.S., and MacCullum,C.J., J.Appl.Phys. 31 (1960).

52. Suzuoka,T., Trans.Japan Inst.Metals 2 1 (1961) 25
Ibid. 2 3 (1961).

53. Wuttig,M., J.A.Cer.S. 49 2 (1966) 112.

54. Wahl,A.C., and Bonner,N.A., "Radioactivity applied to Chemistry", J.Wiley & Sons(1957) 66-68.

55. Carter,R.E., Ph.D. Thesis, London (1953).

56 Bethe,H.A., Reviews of Mod.Phys 22 2 (1950).

57. Alcock,C.B., Hawkins,R.J., Hills,A.W.D., and McNamara,P., I.A.E.A.Conf. SM66/36. (Includes work from this thesis).

58. Schmitz,F., I.E.E.A.Conf."Thermodynamics" 2 (1966) 188 and J.N.M. 17 (1965) 259-69.

59. Yajima,S., Furuya,H., and Hirai,T., J.N.M. 20 (1966) 162.

60. Belle,J., and Lustman,B., USAEC WAPD-184(1957).

61. Slifkin,L., and Williams,G.T., Acta Met. 11 (1963).

62. Wajda,E.S., Acta Met., 2 (1954) 184.

63. Marin,J., et Michaud, ., Compt.Rend.Acad.Sci. 261 (1965).

64. Hart,E.W., Acta Met., 5 (1957) 597.

65. Taylor,J.M., "Semiconductor Particle Detectors" Butterworths (1963).

66. Salmon,P G., and Allsworth,F.L., AERE-R4122.

67. Fray,D., Ph.D. Thesis, London (1965).

68. Harman, B.L.M., Private communication.

69. Fano,U., Phys.Rev. 70 (1946) 44.

70. Van Lierde,W., Strumane,R., Smets,E., and Amelinckx,S., J.N.M. 5 (1962) 250-3.

71. Scott,K.T., and Harrison,K.T., J.N.M. 15 4 (1965) 310-1.

72. Auskern,A.B., and Belle,J., J.N.M.,3 (1961) 267-76.

73. Thorn,R.J., and Winslow,G.H., I.A.E.A.Conf.(1965) SM66/82

74. Kantan,S.K., et al., 2nd. U.N.Conf. P/1705.

75. Allred,V.D., Buxton,S.R., and McBride,J.P., J.Phys.Chem. 61 (1957) 117.

76. Hurst,R., and Glover,K.M., AERE C/M 100.

77. Rand,M.H., and Kubachewski,O., "The Thermodynamic Properties of Uranium Compounds", Oliver and Boyd (1963).

78. Ackermann,R.J., Thorn,R.J., and Gilles,P.W., J.A.Chem.S. 78 (1956) 1767.

79. Jackson.N., AERE C/R 2767.

80. Sood,D., Indian Atomic Energy, Private communication.

81. Gibbs,B.M., and Rawson,H., Trans.Brit.Cer.Soc. 60 (1961) 345-7.

82. Seddon,B.J., Reactor Materials, 8 4 (1966).

83. Markin,T.L., and Bones,R.J., AERE-R4178.

84. Aukrust,E., Førland,T., Hagemark,K., I.A.E.A.Conf. (196) SM26/9.

85. Anthony,A.M., Kiyoura,R., and Sata,T., J.N.M. 10 8 (1963).

86. Aronson,S., and Belle,J., J.Chem.Phys. 29 (1958) 151.

87. Kiukkola,K., and Wagner,C., J.Electrochem.Soc. 104 (1957) 379-87.

88. Peters,H., and Mobius,H.H., Z.phys.Chem. 209 (1958) 298.

89. Mitchell,A., Nature 201 4917 (1964) 390-1.

90. Elliott,J.F.,ed., "The Physical Chemistry of Steelmaking" Conf. (1956).

91. Franklin,A.D., Harwell.

92. Zener,C., J.Appl.Phys. 22 (1951) 372.

93. Shewmon,P.G., "Diffusion in Solids", McGraw-Hill (1963).

94. Matzke,Hj., AECL.

95. Anderson,J.S., I.U.P.A.C. "High Temperature Technology", (1964).

96. Ramke,W.G., "Thorium Oxide", ASD-TDR-63-635 July (1963).

97. Carter,R.E., and Richardson,F.D., Trans.A.I.M.E. 200 (1954) 1244.

98. Himmel,C., Birchenall,C.E., and Mehl,R.F., Trans.A.I.M.E. 197 (1953) 827.

99. Roth,W.L., J.Appl.Phys.Suppl. 30 (1959) 303.

100. Condit,R.H., and Birchenall,C.E., Met.Rept., March (1960) AFSOR TN 60-245, A.S.T.I.A. Virginia.

101. Steele,B.C.H., Ph.D.Thesis, London (1966).

102. Federer,J.I. and Padgett,R.A., J.N.M. 17 (1965).

103. Roberts,J.P., and Wheeler,C., Trans.Farad.Soc. 56 4 (1960) 570-80.

104. Wuensch,B.J., and Vasilos,T., J.A.Cer.S. 47 2 (1964) 63.

105. Paladino,A.E., and Kingery,W.D., J.Chem.Phys. 37 (1962) 957.

106. Leipold,M.H., J.A.Cer.S. Sept., (1966) 502.

107. Laurent.F., et Benard,J., Compt.Rend. 241 (1955) 1204.

108. Kingery,W.D., and Berg,M., J.Appl.Phys. 26 10 (1955) 1205-12.

109. Johnson,D.L., and Cutler,I.B., J.A.Cer.S. 46 11 (1963) 541-50.

110. Howard,R.E., and Lidiard,A.B., Rept.Prog.Phys. 27 (1964) 161-135.

111. Cowan,R.E., WAD-TM-73 (1957).

112. Ram,P., Godiyar,H.S., and Jena,P.K., J.Less Common Metals, 10 3 (1966) 185-9.

113. Scott,R., Hall,A.R., and Williams,J., J.N.M. 1 (1959) 39-48.

114. Paladino,A.E., and Coble,R.L., Symp.Kinetics Ceramic Reactions, No. 3-28-62.

115. Darken,L.S., and Gurry,R.W., "Physical Chemistry of Metals" McGraw-Hill (1953).

116. Williams,J., Barnes,E., Scott,R and Hall,A., J.N.M. 1 (1959) 28-38.

117. Cottrell,A.C.H., "Dislocations and Plastic Flow in Crystals", Oxford Univ.Press, (1953).

118. Coble,R.L., and Guerard,Y.H., J.A.Cer.S. July (1963).

119. Chang,R., J.Appl.Phys. 31 3 (1959) 484-7.

120. Armstrong,W.H., Irvine,W.R., and Martinson,C.H., J.N.M. 7 2 (1962) 133-41 and J.N.M. 9 2 (1963).

121. Armstrong,W.H., Causey,A.R., and Sturrock,W.R., J.N.M. 19 1 (1966) 42.

122. Christie,G., and Williams,J., J.N.M. 5 (1962) 1-4.

123. Amato,I., Colombo,R.L., and Balzari,A.F., J.N.M. 18 (1966) 252-60.

124. MacEwan,J.R., J.A.Cer.S. 45 (1962) 37-46.

125. Felix,F., Lagerwall,T., Schmelling,F., and Zimen,K.E., 3rd. U.N.Conf. P/472.

126. MacEwan,J.R.,and Stevens,W.H., J.N.M. 11 1 (1964) 77-93.

127. Childs,B.G., J.N.M. 9 (1963) 217.

128. Carroll,R.M., and Sisman,O., J.N.M. 17 (1965) 270.

129. Cornell,R.M., and Williamson,G.K., J.N.M. 13 (1964) 278 and J.N.M. 17 2 (1965) 200.

130. Foex,M., Bull.Soc.Chim.(France) 16 55 (1949) 231.

131. Bailey,W.E., Danko,J.C., and Ferrari,M.M., A.Cer.S.Bull. 41 (1962) 768-72.

132. Kopal,Z., "Numerical Analysis", Chapman and Hall, pp.347 and 523.

ACKNOWLEDGEMENTS

The author wishes to thank his supervisor, Professor C. B. Alcock, for the provision of research facilities and for advice and encouragement during the course of this work.

Thanks are also due to the author's colleagues in the Ceramic and Nuclear Materials Group and the Nuffield Research Group, in particular Dr. A. W. D. Hills and Mr. D. Sood, for many valuable discussions, and to Dr. P. S. Rogers and Miss B. L. M. Harman for reading and commenting on the thesis.

In addition, the author would like to thank Mr. J. Butler for maintaining the alpha-ray spectrometer in working order, and to express appreciation for the kind co-operation shown by the permanent staff at Imperial College.

The author is indebted to the United Kingdom Atomic Energy Authority Research Establishment, Harwell, for their financial support of this work, and for materials and facilities granted to him through Dr. L. E. J. Roberts.

R. J. Hawkins